INFORMATION TO USERS

This manuscript has been reproduced from the microfilm master. UMI films the text directly from the original or copy submitted. Thus, some thesis and dissertation copies are in typewriter face, while others may be from any type of computer printer.

The quality of this reproduction is dependent upon the quality of the copy submitted. Broken or indistinct print, colored or poor quality illustrations and photographs, print bleedthrough, substandard margins, and improper alignment can adversely affect reproduction.

In the unlikely event that the author did not send UMI a complete manuscript and there are missing pages, these will be noted. Also, if unauthorized copyright material had to be removed, a note will indicate the deletion.

Oversize materials (e.g., maps, drawings, charts) are reproduced by sectioning the original, beginning at the upper left-hand corner and continuing from left to right in equal sections with small overlaps. Each original is also photographed in one exposure and is included in reduced form at the back of the book.

Photographs included in the original manuscript have been reproduced xerographically in this copy. Higher quality 6" x 9" black and white photographic prints are available for any photographs or illustrations appearing in this copy for an additional charge. Contact UMI directly to order.

UMI

A Bell & Howell Information Company
300 North Zeeb Road, Ann Arbor MI 48106-1346 USA
313/761-4700   800/521-0600

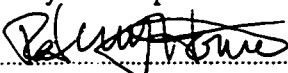# HARVARD UNIVERSITY

THE GRADUATE SCHOOL OF ARTS AND SCIENCES

THESIS ACCEPTANCE CERTIFICATE

The undersigned, appointed by the

Division   of Engineering and Applied Sciences

Department

Committee

have examined a thesis entitled

"A Viscoelastic Model of the Human Fingerpad
and a Holistic Model of Human Touch"

presented by Dianne Tanya Victoria Pawluk

candidate for the degree of Doctor of Philosophy and hereby
certify that it is worthy of acceptance.

Signature ....

Typed name Professor R. Howe

Signature ....

Typed name Professor T. McMahon

Signature ....

Typed name Professor R. Kronauer

Date May 14, 1997

A Visocelastic Model of the Human Fingerpad and a Holistic Model of Human Touch

A thesis presented

by

Dianne Tanya Victoria Pawluk

to

The Division of Engineering and Applied Sciences
in partial fulfillment of the requirements
for the degree of
Doctor of Philosophy
in the subject of
Engineering Sciences
Harvard University
Cambridge, Massachusetts

May 1997

UMI Number: 9733376

UMI
300 North Zeeb Road
Ann Arbor, MI 48103

ii

Abstract

The main intent of this thesis is to develop an engineering model describing the response of the human peripheral tactile system when an object dynamically contacts the fingerpad. In developing such a model, it is only possible to measure the system at two points: mechanically at the surface of the skin and neurophysiologically as the resulting nerve signal heads toward the brain. We first consider the dynamic mechanical interaction between the fingerpad and a prototypical object (i.e., a flat indentor) applied normal to the fingerpad. Experimentally we applied controlled position trajectories to the fingerpad and measured the resulting force and spatially distributed pressure response. We will show that these experimental results can be explained by an analytical model consisting of a quasi-linear viscoelastic model of tissue combined with a Hertzian contact model. The contact mechanics also create stresses and strains within the tissue, which are then transduced through the mechano-electrical components of the peripheral mechanoreceptive units, resulting in a nerve fiber response. We have, in addition, considered the transmission of the signal through these components by developing a '1-D' model which relates the input applied to the surface of the skin to the resulting nerve fiber response. Using existing neurophysiological data, we have shown that the response of the mechanoreceptive units to '1-D' stimuli can be modeled by simple linear mechanical components combined with the Hodgkin-Huxley equations.

Contents

Acknowledgements

I would like to thank my advisor, Rob Howe, for his support and guidance, particularly in teaching me how to build experimental equipment. I would also like to thank my committee members Tom McMahon and Richard Kronauer for their insight and knowledge about physiological systems and how to model them, which they provided me both in their courses and throughout my Ph.D. experience. In addition, I would very much like to thank Roland Johansson and his group, including Göran Westling, Per Jenmalm and Anders Bäckström, at Umeå University, Sweden for providing me with their unpublished data. The data were truly invaluable to the completion of my thesis.

I would also like to thank my fellow labmates for their help and encouragement. In particular, I am indebted to Eric Dunn for not only designing and constructing some of my equipment, but for the help and knowledge he provided on so many occasions with the experimental set-up. I am also grateful to Jae Son, Parris Wellman and Bill Peine for their design and construction of my tactile array sensor, especially Parris for his many attempts to build me the perfect sensor; and I very much appreciated the helpful discussions with both Bill and Parris on the distributed pressure model. I would further like to thank Aram Hajian for his help with the pilot work on the bulk fingerpad response. And finally, I would like to thank Dimitri Kontarinis and Danny Sanchez for their help on occasion with the experimental set-up. Furthermore, I would like to thank all my labmates, both past and present, for their camaraderie.

In addition, I would like to thank my family for their support.

And finally I would like to thank Professor Jones for lending me his electronics rack.

Chapter 1

Introduction

Anyone who has tried to search for their keys on a cold, moonless winter's night can appreciate the difficulty of not having the sense of touch. Touch is important in determining object properties which are unavailable to other senses. It is needed when vision is unavailable, such as in searching for a light switch in the dark; or even in the simple act of reaching to grasp an object, when our hand occludes our view of the very object on which we are concentrating. Other properties, such as texture and surface finish, are difficult to perceive by other senses, but are readily apparent when we scan our finger across an object. In addition, touch is important for dexterous grasping and manipulation even when vision is present. This has been revealed by the difficulty people have in manipulating objects when the tactile receptors are anesthetized [54].

The main intent of this thesis is to develop an engineering model of the transduction processes involved in the human sense of touch. The purpose is to determine which aspects of the transduction mechanism are fundamental, in terms of being necessary and sufficient, to describe the peripheral tactile system. In developing such a model, it is only possible to measure the system at two points: mechanically at the surface of the skin and neurophysiologically as the resulting nerve signal heads toward the brain. The goal of this thesis is to understand the relationship between the input applied to the surface of the skin and the

outputs which can be measured at these two points. More specifically, our aim is to:

1. develop an experimentally based model which captures the primary relationship between the displacement and velocity of indentation of an object and the resulting spatially distributed pressure response on the fingerpad; and

2. use existing neurophysiological data to determine the fundamental components needed to relate prototypical indentations to the resulting nerve response.

Determining the essential parameters to which the tactile receptors respond is important for our basic understanding of human touch and motor control. Developing such models can further be used as an exploratory tool for the design of experimental protocols.

The information gained also has direct application to the development of hand-arm prostheses. The fact that child amputees often prefer to use their remaining stub, which retains some somatosensory sensation over the use of their prostheses (which allow minimal sensory feedback) is indicative of the importance of tactile sensing for this application. Mimicking the human tactile system is unwieldy due to the complexity of the system, the large number of receptors (17,000 in the human hand [27]), and the significant degradation of the sensors with time. However, understanding the underlying principles is expected to be of significance in designing an effective interface. These principles can also provide insights for the design of dexterous robotics.

Understanding the human sense of touch also has applications to the design of teleoperational and virtual reality interfaces. In the absence of being able to perfectly replicate the environment at the subject's fingertips, we must be able to select the necessary and sufficient components to reproduce. In addition, developing a mechanical model of the interaction of the fingerpad with an actual environment is important for the simulation of the interaction in a virtual environment and in the replication of a remote environment during teleoperations to a human operator.

1.1 System

The system we are interested in examining is the response of the peripheral tactile system when an object dynamically contacts the fingerpad (Figure 1-1). There are two major components which we need to consider. First we must consider the mechanical interaction between the object and the fingerpad on contact. We then must consider what is happening beneath the surface of the skin. This is a complicated system consisting of the mechanics of the fingerpad, the mechanics of the specialized ending associated with each nerve fiber, as well as the properties of the nerve fibers themselves. This system is described in more detail below. The mechanical properties of the fingerpad are not only important in the transmission of the stimuli signal deeper into the tissue, but are also reflected in the interaction with the object at the contact surface.

1.1.1 Biomechanics of the Fingerpad

The nonhairy, or glabrous skin, of the human fingerpad is highly structured and consists of two interdigitating layers: the epidermis on the surface and the dermis beneath (see Figure 1-1:Right). The epidermis consists of a layer of several cells, the most superficial of which are keratinized. Most of the dermis is densely packed, primarily composed of collagen fibers (approximately 75% of the dry weight) and elastin fibers (about 4%) in a hydrophilic gel referred to as ground substance. Beneath the skin is a layer of subcutaneous tissue, containing fat cells, which is loosely attached to the dermis above and to muscle and bone below. All of these layers are expected to contribute to the nonlinear, viscoelastic properties of the fingerpad. In addition, there are blood vessels and capillaries, sweat ducts and nerves running through both the dermal and subcutaneous layers of the fingerpad [12, 33, 38].

Structurally, the skin of the fingerpad has two ridge systems. The primary ridges (i.e., the fingerprint ridges) are apparent on the surface of the skin. In addition, the epidermis projects into the dermis in another ridge system consisting of a regular series of pegs. The

3

shallower pegs, or limiting ridges, are firmly attached to the dermis and the deeper pegs, or intermediate ridges, are relatively free-floating [33]. The complexity of the ridge system has led to frequent speculation as to their purpose, but will not be considered here.

1.1.2 Mechanoreceptors in the Glabrous Skin of the Hand

There are four types of mechanoreceptive units found in the glabrous skin of the human hand: the SAI, SAII, FAI and FAII units. Each unit consists of a primary axon with one or more associated specialized endings, or end organs. The types are named according to their classification in terms of speed of adaptation, either fast (no static response) or slow (static response present), and by the size of their receptive fields, either type I (small, sharp borders) or type II (large, obscure borders). Figure 1-1 shows a cross-section of the skin and the location of the end organs thought to be associated with each mechanoreceptive unit. The Meissner corpuscles (Mr) are the end organs which are associated with the FAI units, and to which afferent fibers branch both within (unmyelinated) and between (myelinated). The Merkel cell complexes (Ml) are the end organs which are associated with the SAI units, and which have branching myelinated fiber structures also both within and between end organs. The Ruffini endings (R) and Pacinian corpuscles (P) each are connected to only a single myelinated fiber, and are associated with the SAII units and FAII units respectively.

The receptive fields of the FAI and SAI units on the surface of the skin are approximately circular or oval in shape, with a typical diameter between 2 − 8 mm. The sensitivity of these units is relatively uniform throughout the receptive field and very steep at the edges. However, several zones of maximal sensitivity are apparent within the receptive field and most likely correspond to the location of the end organs associated with each mechanoreceptive unit. This suggests that there are approximately 12 − 17 end organs associated with each FAI unit and 4 − 7 end organs associated with each SAI unit. The FAII and SAII units, in contrast, have only a single zone of maximum sensitivity, corresponding to their single end organ. The size of the receptive fields of these units are very large,

4

typically covering a whole finger or part of the palm [27].

1.2 Thesis Overview

In considering the system we would like to analyze, we first must consider the contact interaction between the fingerpad and the object. In Chapter 2 we will consider the dynamic bulk mechanical interaction between the fingerpad and a flat object, such as frequently used during manipulation tasks. We will present experimental results and show that a standard quasi-linear viscoelastic model of soft tissue is able to successfully explain the data. Furthermore, to examine the ergonomic implications of our model, we will use it to calculate the maximum forces and energy dissipation for the transient and steady state response to repetitive displacement trajectories.

In Chapter 3 we will present experimental measurements of the dynamic distributed pressure response and a model which is capable of explaining these results. We will furthermore show that it is consistent with our previous analysis of the lumped fingerpad response. In addition, we will consider the extension of our model to objects of varying curvature and compliance, and relate our analysis to the response of the SAI units to varying curvature obtained by Goodwin and his colleagues [13].

We will then consider, in Chapter 4, what is happening beneath the surface of the skin. For our analysis we will restrict ourselves to a one dimensional model considering the response of the peripheral tactile system to temporal stimuli. In Chapter 5 we will discuss the implications of the results of this model in relation to our previous biomechanical analysis. In addition, we will discuss the future direction of this work.

5

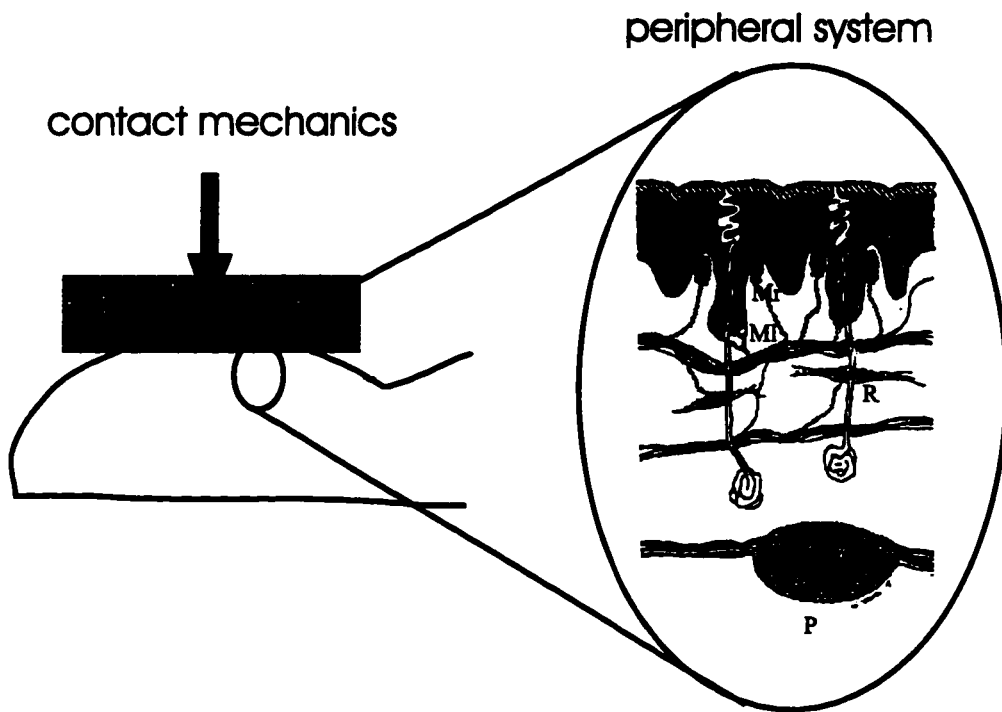Figure 1-1: Peripheral mechanoreceptive system of the human fingerpad. Left: object contact with the fingerpad creates stresses within the skin which can be measured by the pressure distribution at the contact interface. Right: enlargement of a small area beneath the surface of the skin. Cross-section illustrating the skin structure and the location of the four types of nerve terminals. From [27].

Chapter 2

Bulk Fingerpad Response

2.1 Introduction

The fleshy pad at the tip of the human finger mediates many of our mechanical interactions with the world. Because it acts as a coupling element between the hand and grasped objects, a complete explanation of precision manipulation must include the role of fingerpad deformation. Fingerpad mechanics are also a major factor in tactile sensory response, which is an essential component of dexterity [28, 54]. Dynamic properties are particularly important in this context, as several of the specialized mechanoreceptors in the fingertip respond only to changing mechanical stimuli [28]. Fingerpad dynamics are also important in practical applications like the ergonomic design of vibrating tools [35] and in the analysis of repetitive tasks like keyboard typing [48, 49].

Previous Work.

Many researchers have examined the viscoelastic properties of skin. Much of this work is aimed at determining mechanical properties under tension loading (e.g. [32, 36, 37, 53]), although Lanir and colleagues have examined the skin on the forehead under compressive loads [31]. These results are of limited use in analyzing mechanical interactions with the

7

fingerpad, because the loading is compressive and the relevant anatomy includes both skin and subcutaneous tissue. For ergonomic and rehabilitation purposes, a few researchers [35, 52], have measured the mechanical impedance of the fingerpad as a function of vibration frequency (20 Hz to 10 kHz) over a variety of preload forces (0.5 to 5.6 N). For similar ergonomic purposes, Serina, Mote and Rempel [48] examined fingerpad displacement as subjects applied low frequency force sinusoids (0.25 to 3 Hz) to a flat plate at a contact angle of 45 degrees. Serina [47] further developed a quasi-static model of the fingerpad as an ellipsoidal membrane, inflated by an internal pressure and compressed between two infinite, parallel plates.

Gulati [15] and Gulati and Srinivasan [16] have more extensively measured the lumped response of the fingerpad to variously shaped indentors (point, cylinder and flat plate) applied in position ramp and hold (0.5 - 32 mm/sec) and sinusoidal (0.125 - 16 Hz) trajectories. In addition, Gulati proposed separate models of the lumped fingerpad for the different indentor shapes, each consisting of a series of five linear Kelvin models acting at different depths.

This chapter presents both experimental results and an experimentally-based model that describes the lumped response of the fingerpad to dynamic displacements. Our model is based on a standard model of soft tissue: Fung's quasi-linear viscoelastic theory [12]. Fung's model assumes that the tensile stress on a tissue of constant cross-sectional area can be described by two components: an elastic response, which is a nonlinear function of position, and the reduced (i.e., normalized) relaxation function, which is dependent on time. These two components are then combined in a similar manner to linear viscoelastic theory. This standard model has been successfully applied to many different tissues including tendons and ligaments [55]. Here, we will show that it applies equally well to the compression of the fingerpad *in vivo* despite the changing contact area.

In our experiments, a flat probe indents the finger at a 20 to 40 degree angle, a con-

figuration used in many manipulation operations like grasping a flat-sided box. Controlled displacements are applied to the fingerpad that result in forces between 0 and 3 N. Forces in this range are the most relevant for examining the response of the fingerpad during grasping [54] and are also the typical forces in typing [49]. By using a fast indentation ramp followed by a constant-position hold, the position-dependent stiffness and time-dependent viscoelastic response are independently determined. The resulting model is then verified with novel data from sinusoidal indentation trajectories. It is further used to consider the maximum forces and energy dissipation for repetitive inputs, of relevance for ergonomic design [35, 49, 52]. This lumped element model also forms the basis for an explanation of the dynamic distributed pressure response across the fingerpad, which is the subject of Chapter 3.

2.2 Methods

2.2.1 Experimental Apparatus

A flat-tipped, motorized indentor (see Figure 2-1) applied controlled displacements normal to the fingerpad of the index finger. The subject's hand was supported in a plastic mold closely fitted to the dorsum of the hand with the index finger raised at a 20-40° angle with respect to the axis of the distal phalange. The hand and forearm were constrained using athletic tape, and the fingernail was glued to the mold to preclude fingerpad movement.

A two-axis strain gauge force sensor (RMS noise $\approx$ 3 mN) measured the forces applied normal to the fingerpad and in one tangential direction; the tangential force signal served only to confirm the absence of significant shear forces. The signals were filtered with a two-pole analog low-pass filter with a 1 kHz cutoff frequency. A magneto-resistive position sensor located on the motor shaft measured the position of the indentor (RMS noise $\approx$ 3 μm). A 4.5 gram, low impedance piezoelectric accelerometer measured the acceleration of the indentor tip (RMS noise $\approx$ 90 mm/sec^2, resonant frequency $=$ 22 kHz). The

data were recorded using a 16-bit analog-to-digital converter at a sampling rate of 10 kHz; the quantization levels were below the RMS noise of the sensors.

2.2.2 Experimental Procedure

Experiment 1: Time scale determination - Constant velocities. Trajectories of constant velocity (0.2, 8, 16, 32, 48, 64 and 80 mm/sec) were applied to the fingerpad to a force level of 2-3 N. The velocities were presented in a pseudo-random order for a total of 28 trials (4 at each level). Six healthy subjects (1 female, 5 male; ages 24-36) voluntarily participated in this study. Slower speeds (1, 0.5, 0.2 and 0.1 mm/sec) were also examined for two subjects (1 female, 1 male).

Experiment 2: Identification - Ramp-and-hold. The fingerpad response was identified by applying a fast ramp at 60 mm/sec to approximately 2-3 N, followed by a 5-7 sec hold phase at the endpoint position. The objective was to examine time-independent effects with the fast ramp, and time-dependent effects with the hold phase [12]. 60 mm/sec was chosen for the ramp as only small differences were found above this speed in Experiment 1. The duration of the hold phase was chosen by determining when the measured force essentially stopped decreasing.

Experiment 3: Verification - Sinusoids. The system response to more general, but easily interpretable inputs, was investigated using sinusoidal trajectories. These trajectories were a 20 mm/sec position ramp to a set operating point, followed by 5 cycles of either a 2, 4, 8 or 16 Hz position sinusoid which spanned a force range from close to 0 N to approximately 2 N.

The second experimental protocol combined trials for experiments 2 and 3. Four trials of the fast ramp-and-hold were followed by a pseudo-random presentation of four trials each of the four different types of sinusoidal trajectories (16 trials), and then four trials, again, of the fast ramp-and-hold. The latter four trials were intended to verify stationarity of the system. Four healthy subjects (1 female, 3 male; ages 20-28) voluntarily participated.

10

General Considerations. During all experiments, the fingerpad was allowed to recover from any viscoelastic effects for a minimum of 14 seconds between each trial. This was verified by determining the repeatability among the four trials of the fast ramp and hold experiment: repeatability of the peak force response was within 3.5% and there were no ordering effects ($\eta = 0.17$). However, the effective mass of the probe tip in front of the force sensor did affect the response significantly at high accelerations. In the case of the fast ramp and hold, it was necessary to adjust the force response by measuring the acceleration and compensating for inertial effects by subtracting the inertial forces due to deceleration of the probe tip. For all experiments, coupling of the force to directions perpendicular to the indentation was below 4%.

2.3 Experimental Results

Experiment 1: Time scale determination - Constant velocities. Data from the response of a typical fingerpad to indentations of constant velocities are shown in Figure 2-2. In general, the force increases exponentially for all indentation velocities with the slope increasing in steepness for increasing speed. The response saturates for speeds above approximately 60 mm/sec (Figure 2-2), and below approximately 0.2 mm/sec (slower speeds not shown). The maximum speed case corresponds to the instantaneous stiffness before the viscoelastic response begins, and the minimum case corresponds to the steady state stiffness after the viscoelastic response has died out. In between, viscoelastic effects contribute to the force response.

Experiment 2: Identification - Ramp-and-hold. The experimental data from all subjects for the system identification protocol showed an exponentially increasing force response to the fast position ramp, similar to the faster speeds in Figure 2-2. For the position hold phase, subjects showed an exponentially decaying force response which approached a non-zero steady state value within 5-7 seconds (Figure 2-3). A small artifact, due to the rapid

11

deceleration of the indentor at the end of the ramp, is visible near 0.01 sec. Also during this latter phase, the effects of subjects' blood pressure variations at the pulse frequency (approximately 1 Hz) were clearly seen.

Experiment 3: Verification - Sinusoids. The responses to sinusoidal displacement trajectories of differing frequencies exhibited the same general characteristics as the previous data. A response to a 4 Hz sinusoid is shown in Figure 2-4. The increasing stiffness of the fingerpad with increasing indentation is visible in the distorted force response within each cycle. The relaxation of the force over time is, in part, discernible by comparing the peaks between cycles.

2.4 Analysis

2.4.1 Model

Model Structure. The model we propose to use to describe the force response is based on Fung's quasi-linear viscoelastic model of tissue [12]. It consists of two components: (1) an instantaneous elastic response, $T^{(e)}$, which is the instantaneous force response of the fingerpad to a step change in position, x; and (2) the reduced relaxation function, $G(t)$, which is the normalized, time varying response of the fingerpad following the position step. Our system identification protocol, consisting of a fast position ramp followed by a position hold phase, was used to identify these two components, separately.

Examining the force response as a function of position for the fast position ramp (Figure 2-2) suggested that the elastic response, $T^{(e)}$, can be modeled as an exponential function of position, analogous to tissues of constant cross-sectional area

$$T^{(e)}(x) = \frac{b}{m}[e^{m(x-x_0)} - 1] \tag{2.1}$$

where b and m are constants to be determined from the experimental measurements.

12

Fung suggests that in general the reduced relaxation function includes an infinite number of time constants. Plotting the natural logarithm of the force response of the fingerpad during the hold phase as a function of time (Figure 2-3) suggests that the reduced relaxation function, $G(t)$, can be reasonably approximated as a sum of three dominant time constants: one below 10 msec, another between 10-100 msec and a third much slower term. In addition, a nonzero steady state term is clearly required. $G(t)$ is then represented by

$$G(t) = \frac{c_0 + \sum_{i=1}^{3} c_i e^{-v_i t}}{\sum_{i=0}^{3} c_i} \qquad (2.2)$$

where c_i are the proportion each term contributes to the force relaxation response and v_i are the time constants.

The resulting force response, $P(t)$, to an arbitrary applied displacement trajectory, $x(t)$, is then described by the convolution

$$P(t) = \int_{-\infty}^{t} G(t - \tau) \frac{\partial T^{(e)}[x(\tau)]}{\partial x} \frac{\partial x(\tau)}{\partial \tau} d\tau. \qquad (2.3)$$

Parameter Fit. We can quantify the two components of the model by fitting the results of Experiment 2. As there is relatively little change in the force response above the speed chosen for the fast ramp (see Figure 2-2), it is a good approximation to the instantaneous response, $T^{(e)}(x)$, and can be used to characterize it. Because the two components are linearly combined in the model, the reduced relaxation function, $G(t)$, can be parameterized by the hold phase at a single position.

The instantaneous response, $T^{(e)}(x)$, could be determined by obtaining a least squares fit of the data to Equation 2.1 for the parameters m, b and x_0. However, this form of the response is difficult to parameterize, as allowing all three parameters to vary may prevent the solution from converging to realistic values. Determining x_0 directly from the experimental records, to define it a priori and reduce the search space, is also problematic due to the

13

near-zero slope of the response at low forces and the inevitable presence of noise in the sensor signals.

These issues can be avoided if we differentiate Equation 2.1 with respect to position and obtain stiffness as a function of force:

$$k = \frac{dT^{(e)}}{dx} = mT^{(e)} + b \qquad (2.4)$$

This form is more reliable to parameterize as it is insensitive to the value of x_0, and requires a simpler, linear fit to m and b.

The stiffness for the experimental data was calculated by first smoothing the position and force trajectories with a 9 point symmetric moving average (0.9 msec width). Then the force was numerically differentiated with respect to position using a 5 point interpolating polynomial for unequally spaced points [1]. Plotting the calculated stiffness as a function of force (Figure 2-5) shows that the stiffness increases linearly with force, in accord with Equation (2.4).

The resulting linear least squares fit of Equation (2.4) to the responses for all subjects are shown in Figure 2-5; the corresponding parameters are given in Table 2.1. The variation of the stiffness accounted for by Equation (2.4), r_k^2, was very significant (on average, 97%), confirming the choice of the functional form for $T^{(e)}$. However, the large variation of the parameters m and b across subjects ($\approx$ 2:1) for this small sample suggests that we cannot make *quantitative* generalizations to the general population.

The force response to the hold phase was fit to Equation (2.2) to determine the parameters c_0, and c_i and v_i, $i = 1$ to 3, of the reduced relaxation function, $G(t)$. Four trials were fit by a simplex method using MATLAB. The resulting least squares fits for all subjects are given in Table 1 and shown for subject p.w. in Figure 2-3. The variation of the force relaxation accounted for by the model ($r^2_{G(t)}$) was, on average, 87%. However, this somewhat underestimates the model's accuracy. Note that although the parameter fit

14

for this subject had the lowest variance accounted for ($r^2_{G(t)} = 0.77$), the fit appears to be much better; most of the remaining variance is probably due to blood pressure variations at the pulse frequency. These variations are clearly visible in Figure 2-3, and were present for other subjects as well.

It would be useful to correlate the fitted parameters for both $T^{(e)}$ and $G(t)$ with easily measured variables, such as the width and thickness of the fingerpad. This might permit prediction of the fingerpad dynamics without the need to perform biomechanical measurements. In Table 2.1 we include the measured thickness (t) and width (w) of the finger at approximately the middle of the contact area. The slope of the instantaneous response, m, was significantly negatively correlated with both the thickness and width of the fingerpad ($r_{mt} = -0.81$, $r_{mw} = -0.79$). This suggests that thicker and wider fingers are also softer. Correlations with other model parameters were less clearly interpretable due to their smaller variation between subjects. It should also be noted that the parameters obtained for $G(t)$ are not necessarily unique due to the process of fitting a sum of exponentials [12]. In addition, due to the small sample size, it is difficult to draw conclusions for the general population.

Model Prediction And Confirmation. The model was verified using the force responses to the sinusoidal position trajectories of Experiment 3. This data was not used to parameterize the model and its form is distinct from the ramp-and-hold, although it is sufficiently simple that interpretation is straightforward. The predicted force output, $P(t)$, was calculated from the measured position input, $x(t)$, using Equations (2.1), (2.2) and (2.3), with the parameters determined from the fast ramp and hold experiments (Table 1).

In addition to the parameters that had been previously determined, the initial starting point of the response, x_0, was needed. As it was difficult to estimate x_0 directly from the experimental results (see above), it was obtained by performing a least squares fit of Equation (2.1) to the fast ramp data; x_0 was the fitted parameter, with the values of m

and b given in Table 1 used as constants. Using the resulting values of x_0 for the calculated predictions of the force response to the sinusoidal inputs produced a good fit to the data. The model response was calculated using the actual experimental displacement input applied and then filtered using a two-pole digital filter with a cut-off frequency of 1 kHz to replicate the effects of the analog filter on the force sensor. The average mean squared error (mse) was 7%, where the mse was calculated by

$$mse = \frac{\sum_{i=0}^{n}(P(i)_{measured} - P(i)_{model})^2}{\sum_{i=0}^{n}(P(i)_{measured} - \overline{P(i)}_{measured})^2} \times 100\%. \tag{2.5}$$

The maximum error typically occurred at the peaks of the sinusoidal inputs and was, on average, 18%. Although the error was larger at the peaks, it was comparable to the variation in the peaks between repeated trials in the actual experimental results, which was approximately 12%.

These model predictions can be improved upon by taking into account the small finger movements which were discernible in the data. The average change in position variation at a measured force of 0.05 N was 80μm. The value for x_0 used in predicting the force response was therefore allowed to vary in the fitting algorithm within a range of 80μm between trials for each subject. In addition, variations were correlated in size and direction with the positional change determined at 0.05 N. The average mse of the new predictions improved to 4.5%; the error at the peaks decreased to 10%. A representative comparison between the predicted model output and the experimental data is given in Figure 2-4; the mean squared error (mse) was 4%.

Limitations of the Model. Valid model predictions are limited to trajectories which remain in contact with the fingerpad; breaking contact during retraction produces erroneous results. However, the calculation of the model response to sinusoidal data showed that the model is successful in predicting both loading and *unloading* of the fingerpad even at low forces.

The ability to predict the instant when contact is broken in dynamic interactions may be of use in designing tactile sensing experiments [4].

Comparison to Data Outside the Range of the Model. It is of interest to compare the predictions of our model to experimental results outside the range which we used to develop it. Lundström [35] and Thompson and his colleagues [52] have collectively examined the point (linearized) impedance of the fingerpad over a large range of frequencies (20-10,000 Hz) and force preloads (0.5-5.6 N). The method by which they measured the impedance was to apply small sinusoidal displacements superimposed on static force levels which defined the operating point. The impedance was measured as the RMS of the dynamic force signal divided by the RMS of the velocity signal. During the experiments, Thompson and his colleagues held the amplitude of the velocity constant, while Lundström held the amplitude of the acceleration constant.

Comparison of their data to the predictions of our model suggests that our model is capable of describing the magnitude of the force response to sinusoidal inputs as high as 200 Hz and for preloads up to 5.6N. However, it becomes increasingly less accurate in modeling the phase response, and subsequently the response to more general inputs, for frequencies above 30 Hz. The inability to model the response at higher frequencies is probably due to the mass of the fingerpad, which is not included in our model. In addition, it may be due to an underestimation of the fastest time constant of the force relaxation function (which corresponds, on average, to a −3 dB breakpoint of 37 Hz) because of the finite time response of the indentor; the peak acceleration limits of the indentor used in these experiments limited the ability to approximate an input step function.

In more detail, we can determine the point impedance predicted by our model by first linearizing Equation 2.3 about point $x(t)$. This results in

$$P(t) = \int_{-\infty}^{t} G(t - \tau) K_x \frac{\partial x(\tau)}{\partial \tau} d\tau. \tag{2.6}$$

Assuming a steady state response to the preload, P_0, is reached by $t = 0$, we can then represent the force response by

$$P(t) = P_0 + \int_0^t G(t - \tau)K_x \frac{\partial x(\tau)}{\partial \tau}d\tau. \tag{2.7}$$

Furthermore, as we are only interested in the dynamic force response, we can ignore P_0. We can now take the Laplace Transform to obtain

$$P(s) = sG(s)K_x X(s) \tag{2.8}$$

from which the impedance is

$$Z(s) = \frac{P(s)}{sX(s)} = K_x G(s). \tag{2.9}$$

By nondimensionalizing the impedance at a point with respect to K_x (i.e., considering only $G(s)$) we can obtain how it is expected to vary with frequency. The magnitude and phase of $G(t)$ for a typical subject are shown in Figures 2-6 and 2-7, respectively. The magnitude response suggests that we would expect the impedance at a point to decrease with increasing frequency with a slope of approximately -20 dB/decade, where

$$dB = 20 \log_{10} Z(s). \tag{2.10}$$

To see how the frequency response scales with force preload, we can take the logarithm of Equation 2.9

$$log \mid Z(s) \mid = log(K_x) + log \mid G(s) \mid \tag{2.11}$$

18

We furthermore can relate the stiffness at a point to the force preload by

$$K_x = mP_0 + b'. \tag{2.12}$$

If we assume that b' is relatively small and hence ≈ 0, which appears to be a reasonable assumption from our data, then it follows that

$$log \mid Z(s) \mid = log(m) + log(P_0) + log \mid G(s) \mid, \tag{2.13}$$

from which we would expect that the preload only contributes a constant offset to the $log \mid Z(s) \mid$. This offset is also expected to increase linearly with preload.

We can compare these predictions to the results of Thompson and his colleagues [52] who experimentally measured the impedance of the fingerpad for frequencies from 30 Hz to 1 kHz and using preloads of 0.5 to 5.6 N. Their measurement of the magnitude of the impedance (see Figure 2-7) is consistent with our predictions. The frequency responses until approximately 200 Hz is relatively linear with a slope of approximately -20 dB/decade at all preloads. The responses at differing preloads are reasonably parallel to each other, as would be expected if the nonlinear stiffness only contributes to the offset. Furthermore, the offset seems to approximately increase linearly with preload.

The one notable discrepancy between our model and the data of Thompson (cf. Figures 2-8 and 2-9) is in the phase response of the impedance. Our model is consistent with Thompson's data in showing that the phase response at 30 Hz is around $-70°$ to $-90°$. However, our model also shows that the phase response begins to decrease after this point, consistent with our experimental observation that the force response varied little with increasing velocities higher than approximately 60 mm/sec (Figure 2-2). This is in contrast to the data of Thompson and his colleagues which show the phase response continuing to increase. The discrepancy is probably due to the mass of the fingerpad, which was not

19

considered in our model and would be expected to contribute a +180° phase shift to the phase response at higher frequencies. With this caveat in mind, our model appears to be applicable to a broader input range than was initially examined.

2.4.2 Human Motor Control Considerations

The qualitative form of the experimental results, as elucidated by our model, shows several desirable properties for human motor control. At low forces, the fingerpad is very compliant. This facilitates initial grasping of an object by avoiding large forces that might disturb the object before its position is precisely determined. However, highly compliant fingers would make manipulation difficult due to the uncertainty of the object's position as measured by the proprioceptors. This problem is corrected passively by the increasing stiffness of the fingerpad as the grasp force is incremented. Furthermore, damping increases in proportion to the stiffness (because the reduced relaxation function is linear) thereby maintaining stability with increasing force.

In addition, high stiffness at high grip forces is useful for rejecting disturbances. The stiff coupling between the finger and object lessens relative displacements as forces are applied to the object in the course of a manipulation task. Preservation of this relationship is also aided by the relatively low stiffness of the joints of the finger. The effective tip stiffness of the index finger in extension at 2 N is over an order of magnitude less than the fingerpad in compression (0.14 vs. 4.4 kN/m) and increases more slowly (40 vs. 2100 m^{-1}) [17]. Therefore, if forces are applied to the object, the fingertips remain in contact and the joints accommodate the disturbance, minimizing the change in contact force.

2.4.3 Ergonomic Considerations

The properties of the lumped response of the fingerpad have important implications for the ergonomic design of vibrating tools and the analysis of repetitive tasks. High fingertip forces have been cited as a factor contributing to musculoskeletal disorders during typing [49], and

20

the ability of the fingerpad to absorb and dissipate energy has been assigned both beneficial [52] and detrimental [35] properties. It is therefore of interest to examine the magnitude of the force response and the energy dissipation under different loading conditions, similar to real tasks.

One parameter describing the difference between tasks is whether a transient input, such as a tap during typing, or a steady state repetitive input, such as the vibration of a power tool, is used. Three other parameters are the frequency content of the task, the offset displacement of the input and the maximum amplitude variation. To gain some insight into the effect of these variables, we simulated the response of our model (using the estimated parameters for subject a.h.) to a 100 mm/sec ramp followed by position sinusoidal inputs. Peak-to-peak amplitudes of 0.14 mm and 0.28 mm were superposed on offset levels of 1.5 mm and 3.0 mm.

The magnitude of the force response was examined for driving frequencies between 1 and 128 Hz and, the energy dissipated for frequencies between 1 and 30 Hz. An input duration of eight seconds allowed transient effects to relax to a steady state response. For actual tasks, the resulting values are somewhat underestimated as the model is based on measurements that include the effect of the tissue between the bone and the nail, while in manipulation only tissue between the bone and the fingerpad skin is involved [46]. However, the conclusions should show the correct qualitative behavior.

Forces. The force responses appeared as distorted sinusoids following an exponential decay envelope (as in Figure 2-4), which reduced the forces typically by a factor of two from the initial transient to the steady state. Since the envelope is produced by the linear temporal response to the offset value, it had a similar effect on all input amplitudes and offsets. Changes in the input frequency were also temporal and, therefore, linear: for all input amplitudes and offsets, the peak-to-peak force response in the steady state increased with increasing frequency by a factor of approximately two. In general, the force responses range

from values close to the steady state elastic response to those approaching the instantaneous elastic response (a factor of approximately four).

The nonlinear stiffness produced large changes in the output due to changes in the input amplitude and offset values. The offset value of the input obviously had a nonlinear effect on the mean force output. For example, the mean value of the steady state response to a 16 Hz, 0.28 mm peak-to-peak sinusoid was 0.48 N for an offset of 1.5 mm, compared to 11.2 N at an offset of 3.0 mm. (If the system was linear, we would expect the mean force level at an offset of 3.0 mm to be only 2 times that at 1.5 mm, i.e., 0.96 N.) However, in addition, the offset of the input also had a nonlinear effect on the peak-to-peak force resulting from the superposed sinusoid. For the above example, the steady state peak-to-peak force was 0.93 N for an offset of 1.5 mm and 21 N (instead of 1.86 N, as in a linear system) for an offset of 3.0 mm. The amplitude of the sinusoidal input also had a nonlinear effect due to the nonlinear stiffness.

Energy Dissipation. There are many ways to characterize the dissipative effects of a viscoelastic element; here we calculated: (1) the power dissipation,

$$\dot{W} = \frac{W(loading) + W(unloading)}{\Delta t(loading) + \Delta t(unloading)} \tag{2.14}$$

and (2) the fractional energy dissipated,

$$\%\Delta W = \frac{W(loading) + W(unloading)}{W(loading)} \times 100\% \tag{2.15}$$

where the work, W was calculated numerically from the applied displacement and force response as

$$W = \int P dx \tag{2.16}$$

and Δt is the time duration of the given phase. Loading refers to the portion of the sinusoidal cycle when displacements are increasing, and unloading refers to the portion when displacements are decreasing. The dissipation measures were calculated over the first half sinusoid as an estimate of the initial transient, and over the last full sinusoid to estimate the steady state results.

As shown in Figure 2-10 (a), the power dissipation is about 1.5-3 times greater during the initial transient than in the steady state, although the fractional energy dissipated remained approximately the same. The extreme case of a transitory input is perhaps a rapid tap, which is a simple approximation to typing. During the loading phase, more work is done due to the initial transient response to the d.c. offset. During the unloading phase, the finger may break contact with the object because of the finite time response of the tissue. (In these simulations, amplitudes were chosen to always maintain contact.) In the extreme case contact breaks immediately when the direction reverses and no work is done during the unloading phase; all the work done during contact is therefore dissipated ($\%\Delta W = 100\%$).

Viscous effects also dissipated more energy at higher frequencies, both in terms of absolute and fractional quantities. This was partly obscured in the transient response presumably due to the dominance of the response to the offset value, which was much larger than the amplitude of the superposed sinusoid.

Figure 2-10 (b) shows the effects of changes in the offset value and in the amplitude of the sinusoidal input. Not surprisingly for this nonlinear system, the amount of power dissipated increased considerably with both an increase in the offset value and in amplitude. The relatively constant fractional energy dissipated with large changes in the offset value was unexpected; however, this is a direct consequence of assuming an exponential form for the instantaneous stiffness. If we consider a point x_i, we can note that by differentiating the instantaneous response (Equation 2.1) we obtain

$$\frac{\partial T^{(e)}(x_i)}{\partial x} = be^{mx_i}.$$

(2.17)

23

If we then consider a variation about this point, Δx

$$\frac{\partial T^{(e)}(x_i + \Delta x)}{\partial x} = be^{m(x_i + \Delta x)} \tag{2.18}$$

$$= be^{mx_i}e^{m\Delta x}. \tag{2.19}$$

Similarly for a series of variations (such as a superimposed sinusoidal displacement input), the resulting stiffness can be considered a product of the contribution of the offset (e^{mx_i}) and of the variation ($e^{m\Delta x(t)}$). As the contribution of the offset is independent of time, it only contributes a scaling factor to the resulting force output

$$P(t) = \int_{-\infty}^{t} G(t-\tau)\frac{\partial T^{(e)}[x(\tau)]}{\partial x}\frac{\partial x(\tau)}{\partial \tau}d\tau \tag{2.20}$$

$$= be^{mx_i}\int_{-\infty}^{t} G(t-\tau)\frac{e^{m\Delta x(\tau)}}{\partial x}\frac{\partial x(\tau)}{\partial \tau}d\tau. \tag{2.21}$$

Consequently, it will only contribute a scaling factor to the resulting work calculation. Since the fractional energy dissipated is a ratio of the total work done to the work done on the loading phase, the constant factor due to the offset is canceled out. Therefore, the offset value is not expected to affect the fractional energy dissipated.

The ergonomic ramifications of these energetic calculations is complex. For example, energy dissipation in the fingerpad may lessen the loading on more proximal tissues such as the tendons and joints of the finger, which may be beneficial in transient tasks like typing. The effects on the fingerpad itself, however, may be harmful, as the high dynamic force levels that dissipate energy may also interfere with blood flow and lessen tactile sensitivity [35]. The model developed here can provide a quantitative basis for detailed ergonomic analyses of these factors in specific tasks.

2.5 Discussion

The model presented here works well in predicting the functional form of the lumped force response of the fingerpad. Although the estimated parameter values fell within a fairly narrow range, the small sample size makes it difficult to *quantitatively* generalize parameter values to the entire population. These parameters are also expected to be affected by several other variables. The elementary mechanical properties of the biomaterial constituting the fingerpad change with hydration and temperature. Structurally, the underlying bone is modified significantly toward the tip, enlarging into a disk at the end. Also, the curvature of the finger in the distal direction alters the contact area as the angle between the finger and the surface changes, which we will show in Chapter 3 to influence the lumped elastic response.

The efficacy of Fung's quasi-linear viscoelastic model is noteworthy, given that it was developed for tissues of constant cross-sectional area in tension. Here we considered a biomaterial of changing cross-sectional area in compression. In Chapter 3, we show why this result is not surprising despite the significant change in the contact area with indentation amplitude: the dynamic contact distribution combines the localized tissue responses to produce the lumped response in a manner that retains the functional form of the underlying tissue. One possible explanation for the model's success for compression as well as tension is that as the fingerpad is compressed, the collagen fibers may bow out and stretch as in tissues under tension.

In general, our experimental results are consistent with those obtained by Gulati and Srinivasan [16] and Serina and colleagues [48], who have examined the response of the fingerpad in similar force and frequency ranges. The model which we have developed is comparable in accuracy to that developed by Gulati [15]. However, our model builds upon well-developed biomechanical theory that has been widely validated for other tissues [55]. In addition, in Chapter 3 we demonstrate that this model is easily extended to successfully

describe the distributed pressure response of the fingerpad. This includes experimental results and an analytical model which describe the spatiotemporal variation of the pressure distribution across the contact area as a function of the applied displacement.

Subject	w (mm)	t (mm)	m (mm^{-1})	b (N/mm)	V.A.F.$_k$	c$_0$	c$_1$	c$_2$	c$_3$	v$_1$ (sec^{-1})	v$_2$ (sec^{-1})	v$_3$ (sec^{-1})	V.A.F.$_{G(t)}$
d.p.	12	9.5	3.2	0.092	0.98	0.22	0.45	0.15	0.18	253	14	0.66	0.99
d.s.	14	11.5	1.6	0.28	0.97	0.29	0.4	0.19	0.13	183	11	0.77	0.85
a.h.	14	10	2.1	0.18	0.98	0.25	0.4	0.19	0.16	224	14	0.63	0.88
p.w.	17	13	1.6	0.22	0.96	0.29	0.38	0.20	0.13	264	22	0.69	0.77
means	14	11	2.1	0.19	0.97	0.26	0.41	0.18	0.15	231	15	0.69	0.87

Table 2.1: Model parameters for individual subjects.
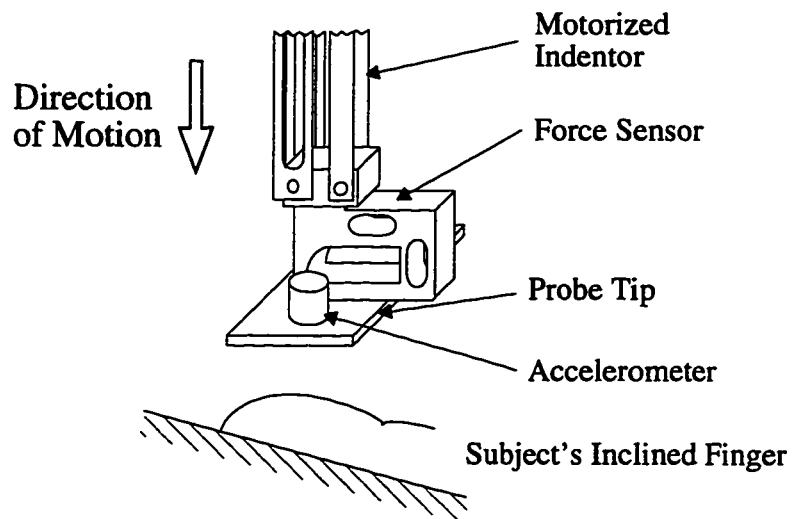
Figure 2-1: Side view of the tip of the experimental apparatus. Sensors at the tip measured the force and acceleration. A joint sensor on the motor shaft measured the position.
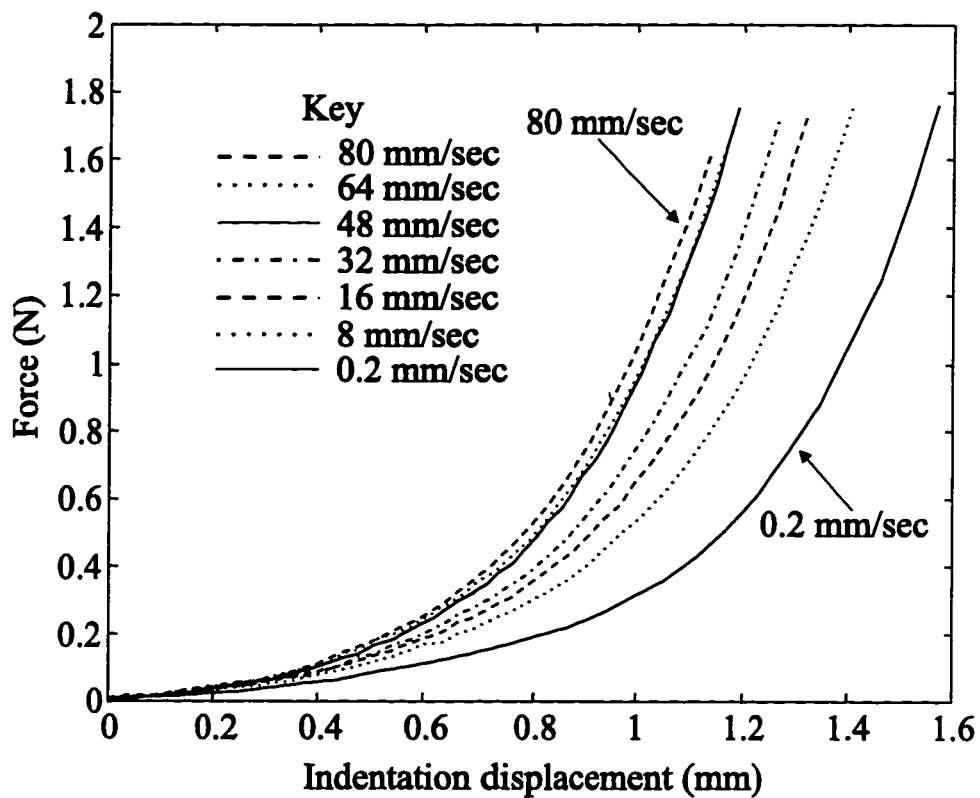
Figure 2-2: Response of the fingerpad of a typical subject to indentations of constant velocities. Data at each speed are from four trials which were geometrically averaged.
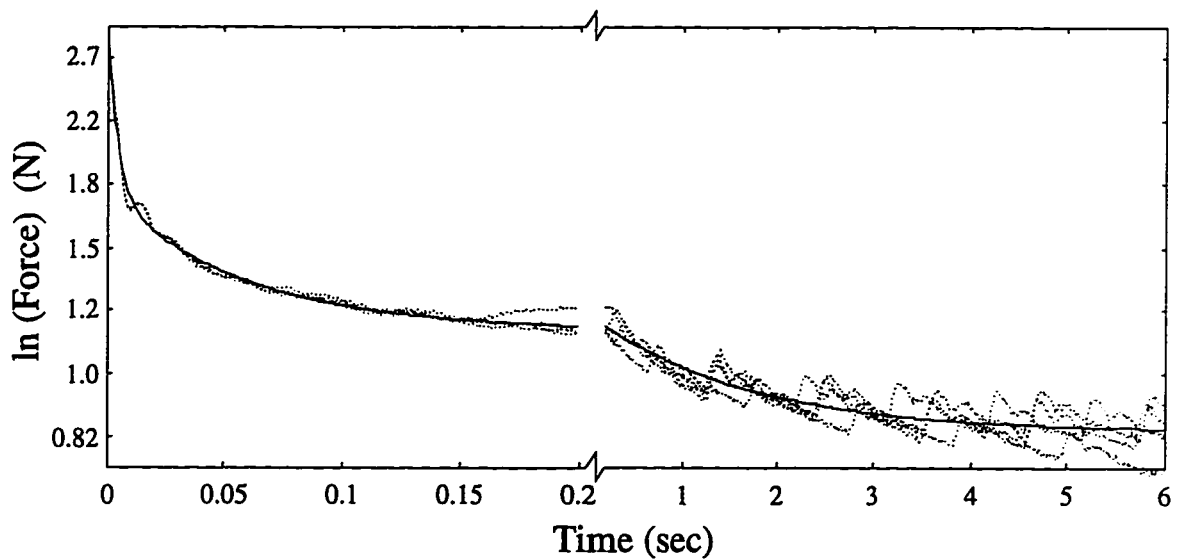
Figure 2-3: Force relaxation of the fingerpad of subject p.w. Dotted lines are four experimental trials; the solid line is the model fit. Blood pressure variations at the pulse frequency are clearly visible.
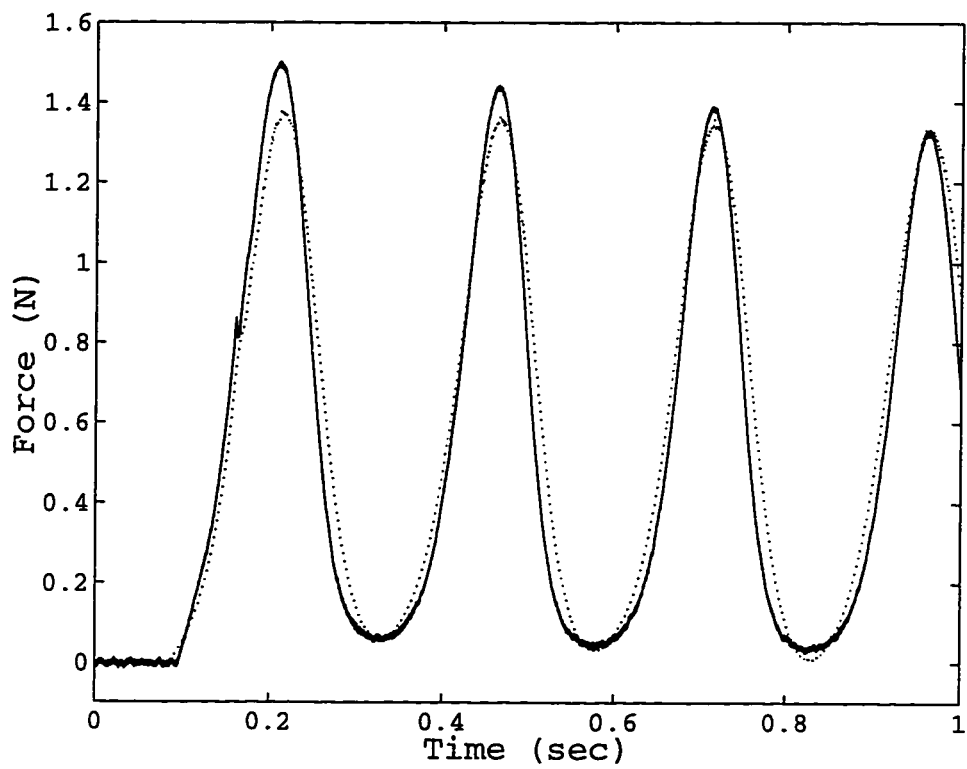
Figure 2-4: Response to a 20 mm/sec position ramp followed by a position sinusoid at 4 Hz. The solid line is the experimental data for a typical trial and the dotted line is the model prediction.
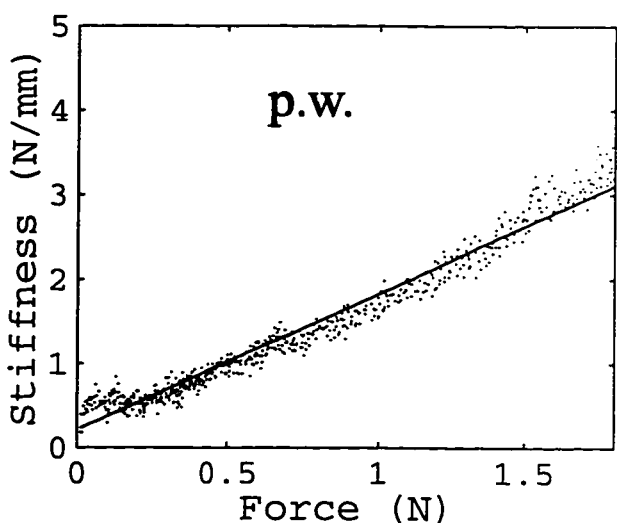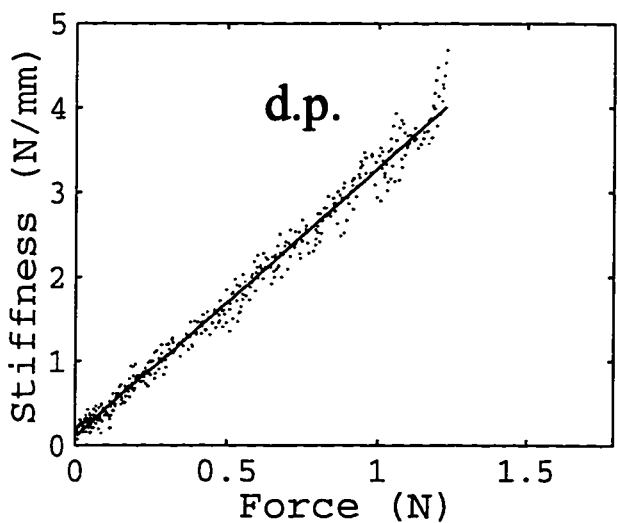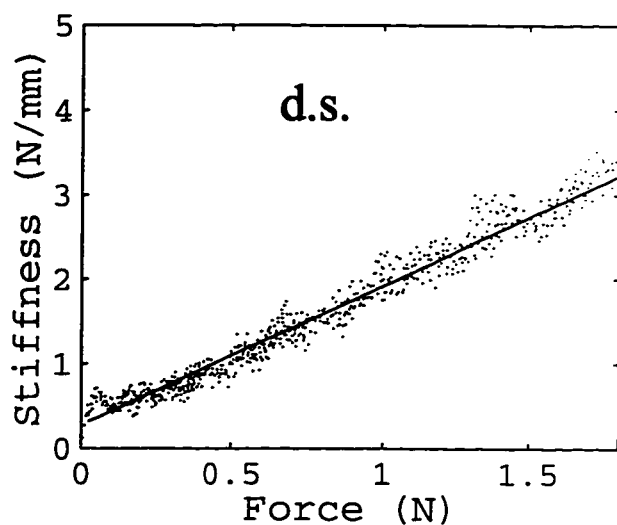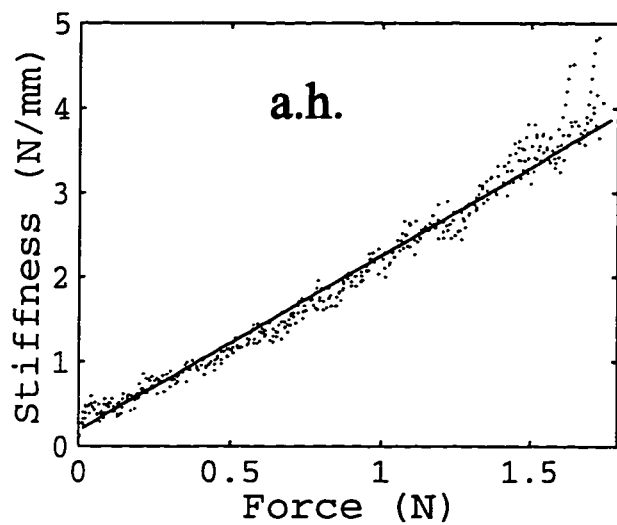
Figure 2-5: Elastic response of the fingerpad for all four subjects. Calculated stiffness as a function of force. Dotted lines are experimental data for 4 trials; the solid line is the model fit.
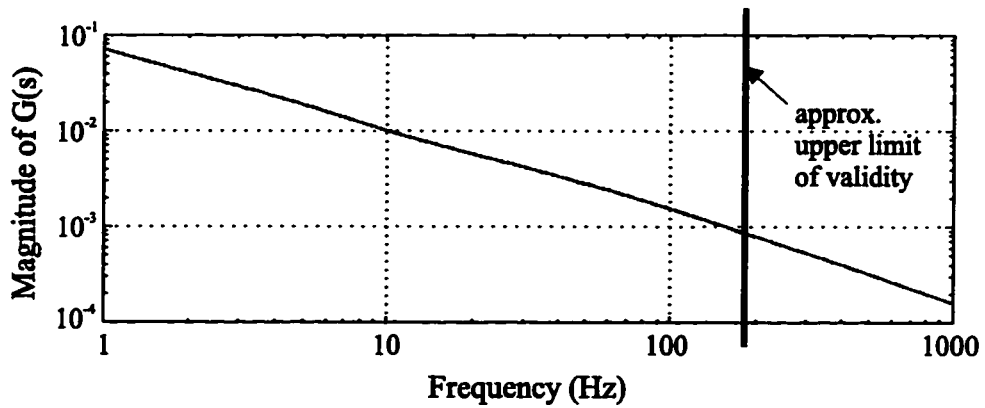
Figure 2-6: Mechanical impedance spectrum of the force relaxation function of the fingerpad model for a typical subject. Note that for multiple preloads this would form parallel lines as in the figure below (see text for details).
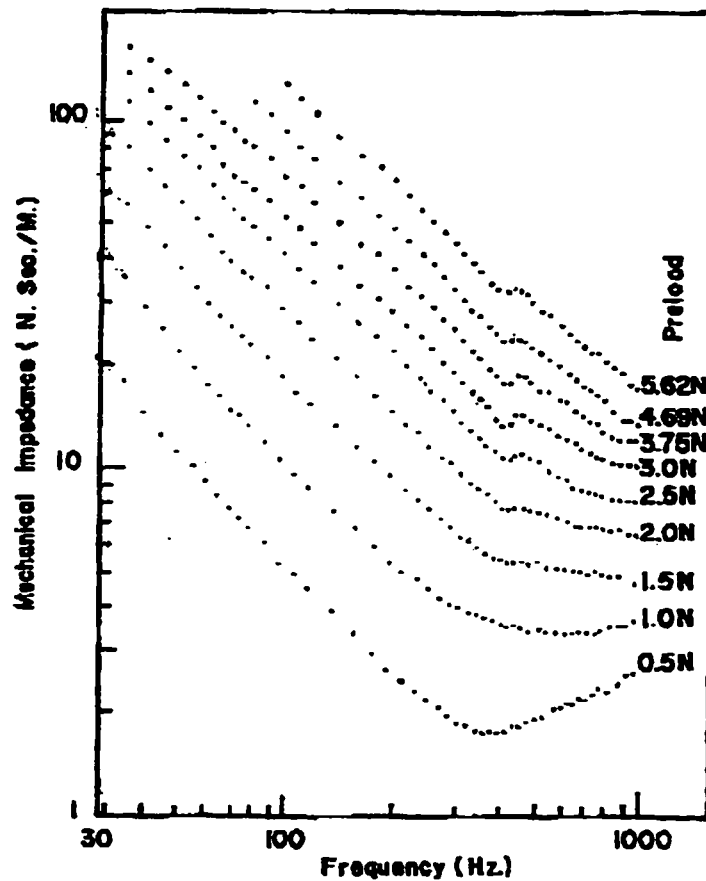

Figure 2-7: Mechanical impedance spectrum of the human fingerpad at various preloads (average of 16 subjects). Reprinted from [52] with kind permission from Kluwer Academic Publishers.
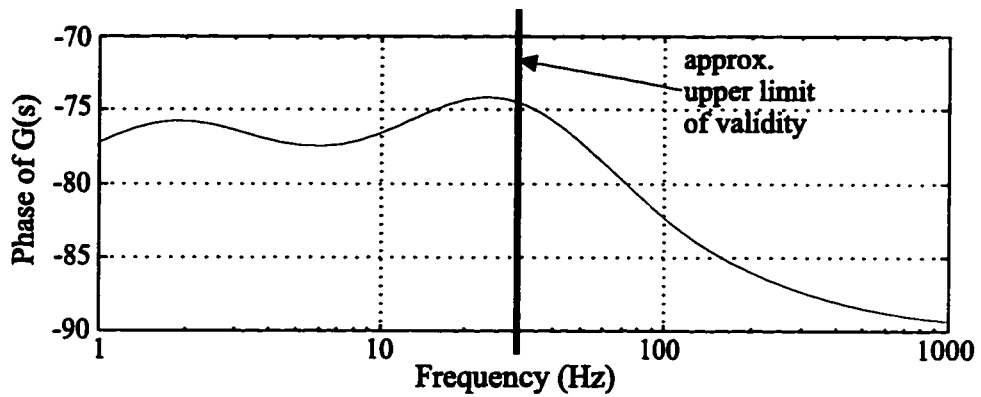
Figure 2-8: Impedance phase-angle spectra of the force relaxation function of the fingerpad model for a typical subject.
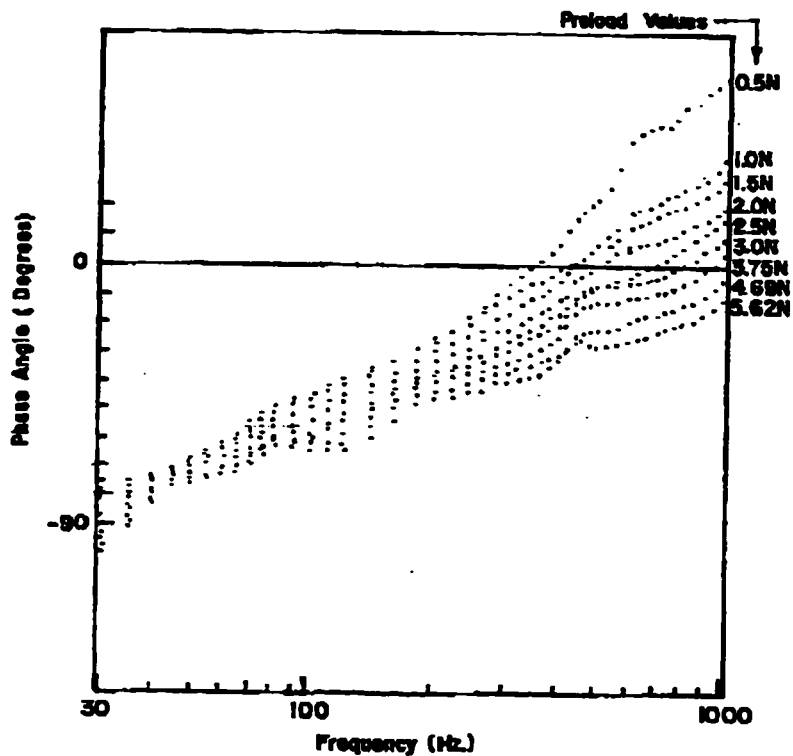

Figure 2-9: Impedance phase-angle spectra of the human fingerpad at various preloads (average of 16 subjects). Reprinted from [52] with kind permission from Kluwer Academic Publishers.
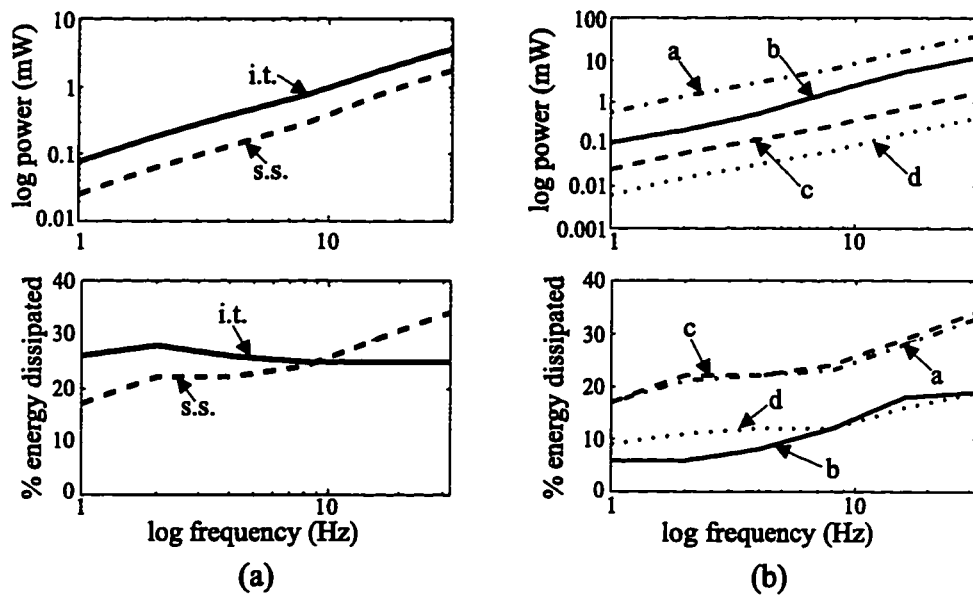
Figure 2-10: Estimated power dissipation and fractional energy dissipation. (a) Comparison of initial transient (i.t.) and steady state (s.s.) responses for a 0.28 mm peak-to-peak sinusoidal displacement input (A) superposed on a 1.5 mm offset ($\bar{x}$). (b) Comparison for different input amplitudes in the steady state: a. $\bar{x} = 3.0$, $A = 0.28$, b. $\bar{x} = 3.0$, $A = 0.14$, c. $\bar{x} = 1.5$, $A = 0.28$, and d. $\bar{x} = 1.5$, $A = 0.14$.

Chapter 3

Spatially Distributed Fingerpad Response

3.1 Introduction

As a finger touches a rigid object, the skin contact area begins as a small spot, then expands to subtend much of the fleshy pad at the fingertip. The resulting pressure distribution across the skin is an important determinant of the mechanical behavior of the hand-object system in manipulation. For example, rotational sliding between the finger and the object is largely governed by the size of the pressure distribution: for a given net force and pressure pattern, the torsional friction about the fingertip is proportional to the contact radius [22]. An understanding of the fingerpad pressure distribution can help explain the mechanical basis of human dexterity.

The distributed pressure response also provides information about the local mechanical conditions at the surface of the skin to which the tactile mechanoreceptive afferents respond [27]. This is important not only for the understanding of tactile perception, but also due to the importance of tactile information during manipulation tasks. Previous experiments have shown that without the sense of touch, precision manipulation skills are severely diminished

34

even though the motor aspects are fully functional [28]. This may be in part because information about the contact pressure distribution is absent.

By correlating the resulting pressure distributions with the responses of the mechanoreceptive afferents, we may begin to comprehend the population response of these units. Combining our understanding of the distributed responses with system models of the mechanoreceptive units (see Chapter 4) will allow us to examine the population response quantitatively. Determining the essential mechanical parameters to which these populations respond is important for the development of neural prostheses, as well as providing insights for dexterous robotics.

Another application, for which it is important to understand the mechanical interaction between the fingerpad and an object, is in providing tactile feedback in teleoperations and virtual reality [42]. In these systems, tactile information sensed at the remote site is conveyed through tactile display devices to recreate the tactile stimulus directly on the operator's fingertip. In order to do this realistically, we must understand how the finger would have interacted with the remote object if it was in direct contact.

In this investigation, we are interested in determining the general shape and trends in the pressure distribution upon contact, rather than developing an exact model. For tactile perception we are interested in determining the average local conditions at the surface above a mechanoreceptive unit, which has a typical receptive field of approximately $3-4$ mm. For tactile display systems, we are interested in providing realistic pressures to the operator's fingerpad using actuators spaced at approximately 2 mm intervals [42].

Practically, we are also interested in developing a tractable analytical model of the response. This is essential for providing tactile feedback in teleoperational and virtual displays, where an efficient model is needed which can be realistically implemented with a real-time controller. In addition, the computational efficiency of such a model will facilitate the investigation of the distributed mechanical response, as well as the mechanoreceptors' population response.

35

As the mechanoreceptive afferents respond to dynamic stimuli, the pressure distribution characterization must include the effects of indentation velocity. Examining the effects of velocity is also needed as motion is an inherent component in tactile exploration, as well as grasping and manipulation. Chapter 2 investigated the dynamic, lumped element response of the human fingerpad *in vivo* to a compressive load. Here, we examine the dynamic, spatially distributed response.

Previous Work.

Several distributed, linear, elastic models have been proposed to relate the application of a stimulus on the surface of the skin to neural responses of the mechanoreceptive units in the skin. Phillips and Johnson [43] used a homogeneous isotropic semi-infinite half-plane model to relate predicted subsurface stresses and strains to experimental responses of the mechanoreceptor units. Dandekar [6] developed a detailed 3-D finite element model which took into account the precise geometry of the fingertip, as well as the layered structure of the skin. He also compared his model to the mechanoreceptor responses for various stimuli, as well as to bulk fingerpad measurements obtained by Gulati and Srinivasan for different indentor shapes [16].

Another model, developed by Van Doren [7] for the investigation of the psychophysical detection of spatiotemporal sinusoids, has considered the fingertip as a viscoelastic medium. This model treated the fingerpad as a linear Voigt body and included the finite depth of the skin. Although the model was based on estimates of the material properties of skin, Van Doren did not compare his model to experimental data.

In fact, there has been little experimental work examining the distributed response of the fingerpad. Srinivasan [50] has examined the surface deformation of the fingerpad to a static line load delivered by a sharp wedge by measuring the deflection of the skin surface photographically. In addition, he proposed a model of the fingertip as a fluid-filled membrane under plane strain conditions to explain the results. Both Westling and

Johansson [54] and Serina [47] have examined the growing contact area during quasi-static indentations of a flat probe by ink staining the fingerpad. Serina further proposed a model of the fingerpad as an ellipsoidal fluid filled membrane to explain the increase in contact area. We are unaware of previous experimental work that examined the distributed response to more complex or dynamic stimuli.

This chapter presents both experimental results and an experimentally based model which describes the distributed pressure response of the fingerpad to dynamic stimuli within the force ranges of 0 - 2 N. Forces in this range are the most relevant for examining the response of the fingerpad during grasping and for considering the response of the mechanoreceptive units [54]. In these experiments, a flat probe indents the finger at a 20 to 40 degree angle, a configuration used in many manipulation operations like grasping a flat-sided box. Several types of displacement trajectories are applied to the fingerpad. The experimentally derived model includes the significant viscoelastic and nonlinear stiffness components of the skin plus the mechanics of contact.

3.2 Methods

3.2.1 Experimental Apparatus

As for the lumped response, a flat-tipped, motorized indentor applied controlled displacements normal to the fingerpad of the index finger. The subject's hand was supported in a plastic mold closely fitted to the dorsum of the hand with the index finger raised at a 20-40° angle with respect to the axis of the distal phalange. The hand and forearm were constrained using athletic tape, and the fingernail was glued to the mold to preclude fingerpad movement.

In addition to the position, acceleration and two axes of force, the pressure distribution was also measured. To record the pressure distribution across the fingerpad, we used a

capacitive tactile array sensor [9], a device developed for robotics applications. This device has two crossed layers of copper strips separated by silicone rubber spacers (see Figure 3-1), which forms parallel plate capacitors at each of the cross points. Applying pressure to the sensor's upper surface forces the top and bottom copper strips closer together, increasing the capacitance at these points. The change in the measured capacitance corresponds to the local pressure above the cross-point [9]. We will refer to a cross-point as an array element.

We used a flat 8 element by 8 element sensor array, shown in Figure 3-1 and described in detail in Appendix A. The elements were spaced 2 mm apart, giving a total sensor area of 256 mm^2. The noise of the sensor was gaussian with a standard deviation of 0.5 kPa ($\approx$ 1.2 g). Temporally, the responses of the array elements reached within 80% of their final value in less than 5 msec. Spatially, summation occurred across an element and coupling between adjacent elements; the coupling between adjacent elements was less than 11%. The spatial impulse function was similar for all elements and can be closely approximated by

$$f_{spatial}(r) = \frac{1}{2\pi\sigma^2}e^{\frac{-1}{2}(\frac{r^2}{\sigma^2})}$$
(3.1)

where $\sigma = 0.96$ mm and r is the radial distance from the center of the element. Details of the calibration procedures can be found in Appendix A.

As the array sensor has some compliance ($E_a = 1$ MPa), its potential effect on the measurements should be considered. For the force range of interest (0 − 3 N) applied by a flat indentor, the estimated elastic modulus of the fingerpad, E_f, is in the worst case (i.e., at the very peak force levels for the fast ramps) typically 234 kPa. However, on average, the error is typically less than 5% with a maximum error on most trajectories (i.e., at the peak force levels of all but the fast ramps) less than 10 %. We have, therefore, chosen to ignore the compliance of the array sensor and assume that it is rigid.

The tactile array elements were sequentially sampled at a rate of 13 kHz, which created a time skew between the response of the individual elements; the maximum time skew,

between the first and last element sampled, was about 5 msec. This skew had a significant effect on the recorded pressure distribution for fast displacement inputs. To avoid the error introduced by this effect, all other measurements (i.e., bulk force, position and acceleration) were sampled with each tactile element (i.e., at 13 kHz), and the response was modeled using the individual data associated with each element at its time of measurement.

The center of contact was aligned with the center of the array by calculating the pressure centroid at a net force of about 2-3 N for the given finger position, and iteratively moving the finger closer to the center of the array. The centroid was calculated by:

$$x_{centroid} = \frac{\sum_{i=1}^{8} \sum_{j=1}^{8} x_{ij} p_{ij}}{\sum_{i=1}^{8} \sum_{j=1}^{8} p_{ij}} \tag{3.2}$$

$$y_{centroid} = \frac{\sum_{i=1}^{8} \sum_{j=1}^{8} y_{ij} p_{ij}}{\sum_{i=1}^{8} \sum_{j=1}^{8} p_{ij}} \tag{3.3}$$

for which x_{ij} and y_{ij} are the position of the center of the element in the ith row and j^{th} column, so -7 mm $\leq x_{ij}, y_{ij} \leq 7$ mm, and p_{ij} is the pressure measurement at that element.

3.2.2 Experimental Design

Protocol. Two different input trajectories were used to identify the system. First, the elastic response of the system was examined using a quasi-static indentation trajectory to obtain a densely sampled response. A 0.2 mm/sec (quasi-static) position ramp was applied to the fingerpad to approximately 2-3 N; 0.2 mm/sec was chosen as the force response did not differ appreciably from that at slower speeds (see Chapter 2). Also, as in Chapter 2 (refer to Chapter 2 for details), a fast ramp at 60 mm/sec was applied to approximately 2-3 N, followed by a 5-7 second hold phase at the end point position. The objective of this component of the analysis was to examine time-independent effects (the instantaneous elastic response) with the fast ramp, and time-dependent effects (the relaxation function)

with the hold phase [12].

The system response to more general, but easily interpretable inputs, was investigated using sinusoidal trajectories. These trajectories were a smooth position ramp to a set operating point, followed by 5 cycles of either a 2, 4, 8 or 16 Hz position sinusoid which spanned a force range from close to 0 N to approximately 2 N.

The protocol applied four trials of the quasi-static ramp, followed by four trials of the fast ramp and hold, then a pseudo-random presentation of four trials each of the four different types of sinusoidal trajectories (16 trials) and, finally, four trials, again, of the fast ramp and hold. The latter four trials were to verify stationarity of the system. Four healthy subjects (1 female, 3 male; ages 20-28) voluntarily participated.

Additional Considerations. The center of contact with the fingerpad, determined by the force centroid, was aligned with the center of the tactile array before the protocol was executed. This allowed at least most, if not all, of the contact area to be measured by the tactile array sensor. In addition, because of its importance in modeling the contact distribution, the exact force centroid was recorded both before and after the experiment.

During the experiment, the fingerpad was allowed to recover from any viscoelastic effects for a minimum of 14 seconds between each trial; the adequacy of this interval was previously verified in Chapter 2. To minimize the effect of any drift in the sensors, the data just before contact in each trial was used as a baseline for the force, acceleration and distributed pressure measurements. For all experiments, generation of forces in directions perpendicular to indentation was below 4 %. Friction was minimized by using a thin layer of petroleum jelly on the surface of the sensor.

3.3 Experimental Results

Quasi-static ramp. The pressure responses of individual elements to the quasi-static ramp (Figure 3-2) appeared to show an exponential response, as did the net force response.

40

The element responses were found to be smaller in size for increasing distance away from the center of contact. It was interesting that both the element responses and the net force response were exponential, as the sum of the element responses must equal the net force. This implies that the contact distribution (i.e., the profile of the pressures) must be consistent with this constraint.

To characterize the form of the contact distribution, the quasi-static data is plotted in Figure 3-3. These plots show the distributed response, with increasing force, as isobars of constant pressure; as shown in the figure, the contact area grew significantly with the increase in force. Although the distribution was symmetric about the medial line of the finger, there was a clear asymmetry in the longitudinal (proximal-distal) direction of the fingerpad. These differences are probably due to differences in curvature of the finger, which is higher in the distal portion in the longitudinal direction and also increases in the lateral direction toward the tip.

Pressure profiles (as a function of radial distance from the center of contact) are shown in Figure 3-4. Because of the proximal-distal asymmetry, the left side of the figure indicates the proximal half of the fingerpad above the lateral line through the center, and the right side indicates the distal half of the fingerpad below this line. The profiles at all force levels were similar, appearing parabolic in shape. The small non-zero values of pressure at large values of radial displacement (i.e., the 'tails'), which all profiles exhibited, can be attributed to the spatial response of the tactile array sensor used to measure the pressure distribution (see Appendix A).

Fast Ramp-and-hold. In conformance with the results in Chapter 2, the lumped response of the fingerpad for all subjects showed an exponentially increasing response (as a function of position) to the fast position ramp and an exponentially decaying force response (as a function of time) to the position hold phase. The pressure responses of all of the individual array elements also roughly showed these characteristics. The response of several elements,

41

as well as the lumped force response, to the position hold phase is shown in Figure 3-5; all elements showed an exponentially decaying force response which approached a non-zero steady state value within 5-7 seconds. The response magnitudes were, again, smaller for increasing distance away from the center of contact.

However, the peaks of the measured pressure element responses (with time) also varied as a function of the sampling order of the array elements due to the time skew (5 msec) between elements. This made it difficult to determine the form of the contact distribution. The sampling limitation for an individual element (i.e., 200 Hz) also made it difficult to determine the details of the form of both the instantaneous response and the force relaxation. Although, together, the quasi-static and fast ramp-and-hold results suggest that the pressure response can be described by a nonlinear stiffness and linear force relaxation.

Sinusoids. In order to determine whether the nonlinear stiffness and linear force relaxation of the pressure responses held for more general inputs, we examined the responses to sinusoidal trajectories. We were also able to examine the contact distribution during the slower frequencies. The measured responses exhibited the same general characteristics of the previous data. The distributed response to a 4 Hz sinusoid is shown in Figure 3-6; the size of the response was smaller for increasing distance away from the center of contact (but was not affected by the sampling skew). The increasing stiffness of the fingerpad with increasing indentation is visible in the distortion from "sinusoidal" of the measured pressures within each cycle. The relaxation of the pressures over time is in part discernible by comparing the peaks between cycles.

3.4 Analysis

3.4.1 Model

Previous Model of the Lumped Response. In Chapter 2, we showed that a model based on Fung's quasi-linear viscoelastic theory of tissue [12] can describe the lumped response of the fingerpad. It consisted of two components: (1) an instantaneous elastic response, $T^{(e)}(x)$, which is the instantaneous force response of the fingerpad to a step change in the position, x; and (2) the reduced relaxation function, $G(t)$, which is the normalized, time varying response of the fingerpad following the position step. The instantaneous elastic response, $T^{(e)}(x)$, can be described by

$$T^{(e)}(x) = \frac{b}{m}[e^{m(x-x_0)} - 1] \tag{3.4}$$

where b and m are constants to be determined from the experimental data, and the reduced relaxation function, $G(t)$, by

$$G(t) = \frac{c_0 + \sum_{i=1}^{3} c_i e^{-v_i t}}{\sum_{i=0}^{3} c_i} \tag{3.5}$$

where the c_i's and v_i's are also constants to be determined from the data. The resulting force response, $P(t)$, to an arbitrary, applied displacement trajectory, $x(t)$, is then described by the convolution

$$P(t) = \int_{-\infty}^{t} G(t - \tau) \frac{\partial T^{(e)}[x(\tau)]}{\partial x} \frac{\partial x(\tau)}{\partial \tau} d\tau \tag{3.6}$$

Distributed Pressure Response. Our model of the distributed pressure response is based on the observation that Fung's quasi-linear viscoelastic model was developed for specimens of tissue of constant cross-sectional areas. (The fact that it models the fingerpad response was

43

surprising, given the changing area of contact.) We therefore assumed that an individual small area of the fingerpad in contact with the applied object can be described by a quasi-linear model. This is supported by Figures 3-2 and 3-5 which show that individual pressure elements (with a small area of contact) exhibit both a nonlinear elastic response and significant force relaxation. More general responses of the pressure elements (e.g., Figure 3-6) also show this nonlinear stiffness behavior as well as force relaxation: this is shown by the distortion with increasing indentation within a sinusoidal cycle and the decay between cycles, respectively.

However, we cannot simply treat each small area of skin as an independent tissue specimen because it is coupled to adjacent areas and continuity must be maintained throughout the medium. We thus combined the quasi-linear tissue model with a description of the contact mechanics. For simplicity we will assume radial symmetry, which is shown in Figure 3-3 to be approximately true.

To determine an appropriate contact model, we first examined the densely sampled quasi-static case. Figure 3-4 shows the resultant pressure distributions at three different indentation values. One plausible model is to use the Hertzian theory that describes two frictionless elastic solids of revolution in contact [29]. Although the fingerpad has a nonlinear elastance, for a given rigid body indentation position, x_i, we can approximate the response as locally linear. For Hertzian contact, the pressure, $p(r, x_i)$, at a distance r outwards from the center is given by

$$p(r, x_i) = \frac{8}{\pi R} \mathcal{G}_i [a^2 - r^2]^{\frac{1}{2}} \tag{3.7}$$

where $\mathcal{G}_i$ is the shear modulus of the fingerpad at x_i (assuming incompressibility), a is the radius of the contact circle described by

$$a = [Rx]^{\frac{1}{2}} \tag{3.8}$$

44

and $(1/R)$ is the relative curvature of the fingerpad and the contact probe which is given by

$$1/R = (1/R_{fingerpad} + 1/R_{probe}).$$ (3.9)

For our experiments the probe was flat, and therefore the relative curvature is defined by the curvature of the fingerpad: $R = R_{fingerpad}$.

We would predict from this model that the pressure distribution at a given indentation value, x_i, would be parabolic in shape. This appears to be a plausible form for the distribution at all indentation depths in our data, although there is a noticeable top-bottom asymmetry on the fingerpad. For simplicity, we will ignore the asymmetry. In general, the results suggest that the Hertz model can be used to describe the contact mechanics.

Now we must combine the quasi-linear viscoelastic model of biological tissue with the Hertz model of contact. As with the lumped response, the model of the pressure on a small area, A, determines the response by two components: the instantaneous response and the reduced relaxation function. However, we now describe the instantaneous response as a function of both the instantaneous elasticity of the tissue *and* of the contact mechanics. If we assume separability of the tissue stiffness and the contact mechanics, we can describe the instantaneous response of the pressure distribution, $p(r, x)$, by

$$p(r, x) = t^{(e)}(u) \cdot c(r, x)$$ (3.10)

where $t^{(e)}(u)$ is the instantaneous stiffness of the center of the contact distribution, given by

$$t^{(e)}(u) = \frac{b}{m}[e^{m(u-u_0)} - 1].$$ (3.11)

Here u is the deformation at the point of maximum indentation on the fingerpad, and b and

m are constants to be determined by the data. For contact with rigid objects, such as in our experiment, u is equal to the rigid body motion, x. [1]

The contact distribution, $c(r, x)$, is described by Hertzian contact, Equations (3.7)-(3.9) normalized with respect to $2\mathcal{G}$ (i.e., for $2\mathcal{G} = 1$). By doing this, in essence we are replacing the constant shear modulus, $\mathcal{G}$, by a nonlinear expression. However, in analogy to linear viscoelastic theory [29], we have chosen to replace $2\mathcal{G}$ in Equation 3.7 with the nonlinear material component $t^{(e)}(u)$.

In describing the viscoelastic properties of the material composition of the fingerpad, we will assume that we can describe the reduced relaxation function, $G(t)$, for the material by

$$G(t) = \frac{\sum_{i=0}^{n} c_i e^{-v_i t}}{\sum_{i=0}^{n} c_i} \tag{3.12}$$

where the c_i's and v_i's are constants to be determined by the data. As in Fung's model for tissues of constant cross-sectional area, we assume we can combine the instantaneous response and the reduced relaxation function in a linear manner. By analogy to linear viscoelastic theory [29], the dynamic pressure distribution is given by

$$p(r, t) = \int_0^t G(t - \tau) \frac{\partial p(r, x)}{\partial x} \frac{\partial x}{\partial \tau} d\tau. \tag{3.13}$$

Relation between the distributed and lumped responses. The distributed pressure response, $p(r, t)$, can be related to the lumped force, $P(t)$, by integrating the pressure distribution over the contact area. For the assumption of radial symmetry, this implies integrating over

---

[1] Although in our experiments, $x = u$, this distinction is important when trying to extrapolate to indentation of compliant objects. This modification is due to Bill Peine and is based on his observations during work on indenting compliant objects with rigid inclusions.[41].

46

the contact circle with radius a, or:

$$P(t) = \int_0^{2\pi} \int_0^a p(r,t) \cdot r\,dr\,d\theta \tag{3.14}$$

Substituting Equation (3.13) for $p(r,t)$, integrating over the angle and rearranging the order of integration yields

$$P(t) = \int_0^t G(t-\tau)\{\int_0^a \frac{\partial p(r,x)}{\partial x} \cdot 2\pi r\,dr\}\frac{\partial x}{\partial \tau}d\tau. \tag{3.15}$$

This is equivalent to Equation (3.6) with

$$T^{(e)}(x) = \int_0^a p(r,x) \cdot 2\pi r\,dr. \tag{3.16}$$

So the lumped instantaneous response equals the integral of the instantaneous pressure distribution. This relates the distributed model directly to the lumped fingerpad equations (3.4)-(3.6).

One consequence of this result is that the reduced relaxation function, $G(t)$, is expected to be the same for the lumped force and distributed pressure responses. This is shown to be qualitatively true in Figure 3-5; the differences are most likely due to the significantly lower sampling rate for the pressure element responses (i.e., 200 Hz cf. 13 kHz) which precludes capture of the fast transients.

3.4.2 Parameter fit

Ideally, we can characterize the distributed response with a fast position ramp followed by a constant position hold using the bulk position and the tactile array data. The instantaneous response, $p(r,x)$, can be determined by the fast ramp phase, and the reduced relaxation function, $G(t)$, by the hold phase. However, this does not work well in practice because of the sampling limitation on the individual elements of the tactile array sensor (i.e., 200 Hz)

47

which is unable to capture the fast changes in the signal.

Since in our model the reduced relaxation function for the distributed response is equivalent to that for the lumped response, $G(t)$ was determined by fitting Equation (3.5) to the force sensor data (which was sampled at 13 kHz). The force response to the hold phase was fit to Equation (2.2) to determine the parameters c_0, and c_i and v_i, $i = 1$ to 3, of the reduced relaxation function, $G(t)$. Four trials were fit by a simplex method using MATLAB. The resulting least squares fits for all subjects are given in Table 3.1. The variation of the force relaxation accounted for by the model ($r^2_{G(t)}$) was, on average, 83%. The increased error in the fit from that obtained in Section 2 was primarily due to the increased variability in the data itself.

To determine the instantaneous response, $p(r, x)$, we first note that for the steady state elastic response, $p_{ss}(r, x)$, the reduced relaxation function, $G(t)$, becomes equivalent to its steady state value, c_0, and the distributed pressure response, $p(r, t)$ (Equation (3.13)) becomes

$$p_{ss}(r, x) = \frac{c_0}{\sum_{i=0}^{n} c_i} \cdot p(r, x). \tag{3.17}$$

Consequently, the instantaneous response can be determined from the steady state response, which is more densely sampled.

We fit the distributed pressure data to the model of $p_{ss}(r, x)$ taking into account the spatial impulse response of the array sensor elements (Equation 3.1) as described in Appendix A. The predicted measured pressures are then the convolution of the actual pressure distribution at the surface of the sensor with the sensor's impulse response. Hence,

$$p_{predicted}(r) = p_{ss}(r, x) * f_{spatial}(\rho). \tag{3.18}$$

In order to determine the parameters, the initial starting point of the response, x_0, was

needed. It was determined by examining each trial in reverse order to obtain the first zero crossing. The resultant x_0 was the average of those of the four trials.

The integral square error was minimized using a simplex search on R, $c_0 b$ and m over the entire displacement contact trajectory. The resulting least squares fits for all subjects are given in Table 3.2. Figure 3-4 shows the fit for a typical subject. The mean squared error of the fit for all subjects was, on average 9.6%. Most of the error in the fit is due to the top-bottom asymmetry of the distribution, as discussed below.

3.4.3 Model Verification

The model was verified using the distributed pressure responses to the sinusoidal position trajectories of the third experiment. These data were not used to parameterize the model and their form is distinct from the ramp-and-hold and the quasi-static ramp. However, the data are sufficiently simple that interpretation is straightforward. The predicted distributed pressure response, $p(r, t)$, was calculated from the measured position input, $x(t)$, using the model with the parameters determined from the system identification (Tables 3.1 and 3.2). The initial starting point, x_0, was assumed to be the same as in the quasi-static trials.

The model response was calculated using the actual experimental displacement input applied to the fingerpad, subsampled at 2500 kHz. Note that this rate is significantly higher than the experimental sampling rate of each of the individual elements. This was necessary in order to avoid numerical error due to quantization of the rapid force relaxation response. In order to take into account the spatial effects of the array sensor, the model was then spatially filtered using Equation 3.1 for comparison with the data.

The variance accounted for by the model (v.a.f.) was, on average, 75%.[2] A representative comparison between the model output and the experimental data is given in Figure 3-6. As shown in the figure, the model fit is typically very good at the center of the contact

---

[2]For one subject, the estimate was significantly poorer than for the other subjects. If we were not to include this subject in the average, the variance accounted for would be 80%.

distribution, and increases in error towards the edges of the contact area. This is not unexpected as we have assumed radial symmetry for simplicity when clearly the fingerpad is not radial symmetric (see Figure 3-3). In the distal direction, because of this assumption, we would expect to overestimate the width of the distribution and underestimate the rate of pressure decrease with distance from the center of contact. In the proximal direction we would expect the converse to be true: the width would be underestimated and the rate of pressure decrease, as a function of distance away from the center of contact, would be overestimated. As shown in Figure 3-6, this is indeed what happens. In fact, most of the error in the fit is believed to be due to the fingerpad asymmetry.

The model predicted behavior similar to the data in showing a nonlinear increasing stiffness with amplitude and increasing peak forces with frequency due to damping. However, the damping appeared to be somewhat underestimated for all subjects. This error was possibly due to inaccuracy in measuring the force relaxation function, as a result of the finite time response of the indentor and the compliant rubber coating of the sensor.[3]

3.4.4 Limitation of the Model and Experimental Method

The primary limitation of the model itself is in the assumption of radial symmetry of the fingerpad; as shown in Figure 3-3, the pressure responses of the actual data were clearly asymmetric. However, by assuming symmetry, we believe that we have captured the essence of the response behavior while providing a tractable analytical model. It was also observed that the amount of asymmetry varied with contact angle, although no effort was made to control this angle precisely. In future experiments, it may be of interest to more precisely control the contact angle to quantify this effect. This may be of interest in grasp analysis where issues like the size and centroid of contact area are important considerations for contact stability. Nonetheless, the fundamental behavior is expected to be the same despite

---

[3]The damping is, in turn, expected to affect the estimate of the instantaneous stiffness response from the quasi-static case. This explains why the model always underestimated the response at higher frequencies rather than overestimate the response at lower frequencies.

variations in angle.

Another limitation of the model, as with the lumped fingerpad response, is that it is limited to trajectories which remain in contact with the fingerpad. Breaking contact during retraction produces erroneous results. However, the calculation of the model response to the sinusoidal data suggests that the model can successfully explain the unloading as well as the loading phase of a trajectory. This was unexpected as Lee and Radok have shown that the extension of Hertzian contact to general *linear* viscoelastic theory in the manner we have paralleled for our quasi-linear model only holds if the contact area is increasing throughout [29].

The primary experimental limitation was with the spatial and temporal resolution of the array sensor itself. The limitation of the temporal resolution of the array sensor prevented us from measuring the force relaxation and instantaneous stiffness of the individual pressure elements directly to identify the system. Instead, we had to rely on the model theory to estimate these parameters. However, except for one subject, these estimates quantitatively predicted the response of the fingerpad to sinusoidal indentations. (The response of the subject in question showed all the correct trends; but it appeared that the stiffness of the fingerpad was overestimated, possibly due to the indirectness of the measurement.)

The array sensor was also limited in its spatial accuracy due to the width of an element's spatial impulse function. Preliminary results by Johansson and his colleagues [25] suggest that the contact distribution is flatter in the center with a sharper fall-off in the distal direction. This is not inconsistent with our results due to the limited spatial resolution of our sensor. However, limited resolution does not invalidate our results as our intent is to determine the mean pressure response above the mechanoreceptive units; the smallest receptive fields (with a relatively uniform sensitivity and consisting of multiple end organs) range between 2 − 8 mm in diameter [27]. This is typically larger than the resolution of our sensor. In addition, basing the model on Hertz contact provides it with a simple and well-developed analytical framework.

51

3.5 Extension of the Model

One desirable property of the model which we have developed is that because it is based on Hertz contact, it is simple to extrapolate the distributed pressure response to spherical objects of different sizes. This will be important not only in understanding the tactile system's sensitivity to local curvature, but also due to the importance of this information during manipulation of more complex objects. This extension requires only the inclusion of the radius of the probe in the calculation of the relative radius of contact

$$1/R = (1/R_{fingerpad} + 1/R_{probe}). \tag{3.19}$$

The analysis can also be extended further to ellipsoidal probes by using the more general (although more complicated) version of the Hertz theory of contact [29].

Our model can also be extended to predict the pressure distribution upon contacting compliant surfaces. This extension is most easily performed by linearizing about the indentation position of interest, x_i, for which the instantaneous pressure distribution can be described as

$$p(r, x_i) = \frac{2E^*}{\pi R}[a^2 - r^2]^{\frac{1}{2}} \tag{3.20}$$

where the modulus of elasticity, E^*, is described by

$$\frac{1}{E^*} = \frac{1 - \nu_1^2}{E_1} + \frac{1 - \nu_2^2}{E_2}. \tag{3.21}$$

E_1 is the modulus of elasticity of the fingerpad at x_i, ν_1 (assuming incompressibility) is 0.5, E_2 is the modulus of elasticity of the object and ν_2 is its Poisson's ratio (assuming a homogeneous object).

From this analysis, it can be shown that the curvature of the object and its compliance

affect the distributed response in different manners when indented as a function of displacement. A change in curvature will affect both the magnitude of the pressures as well as the width of the contact area, whereas a change in compliance will only change the magnitude of the pressure, albeit in a complicated manner.

3.6 Comparison to Mechanoreceptor Neural Firing

Recently, Goodwin and his colleagues [13] have examined the neural response of the SAI type mechanoreceptors to rigid spheres of differing curvature applied to the fingerpad. It is of interest to use the extended version of our model, taking into account object curvature, to predict the distributed pressure on the fingerpad. Although it is important to consider the whole system when examining the final neural output (see Chapter 4), we hope to gain some insight as to the contribution of the skin mechanics by correlating the predicted pressure distribution with the neural response.

As the stimulus examined was relatively slow, we will ignore viscous effects in our consideration of the response.[4]. In addition, as the force was varied over a relatively small range (i.e., 10 − 20 g wt), we will assume, for simplicity, that the modulus of elasticity, E^*, can be assumed constant. As a result we will compare a linearized, quasi-static version of our model (i.e., Hertz contact itself) to the neural responses measured by Goodwin and his colleagues.

Figure 3-7 shows the normalized neural response of the SAI units to stimuli of differing curvature applied to the center of the receptive field. The expected local pressure above the center of the receptive field of the mechanoreceptive unit, according to Hertz contact [29], can be described by

$$p_0 = (\frac{6PE^{*2}}{\pi^3 R^2})^{1/3} \tag{3.22}$$

---

[4]The actual response was a 20 mm/sec ramp followed by a constant force hold phase at 10, 15, and 20 g wt for 1 second

where P is the applied force, E^* is the modulus of elasticity of the fingerpad, and R is defined by Equation 3.19. Assuming E^* to be constant, we would therefore expected p_0 to vary as a function of the curvature and applied force as:

$$p_0 \propto P^{1/3}(C_{fingerpad} + C_{probe})^{2/3} \tag{3.23}$$

where $C_{fingerpad}$ is the curvature of the fingerpad (assumed to correspond to a typical finger-pad radius of 15 mm) and C_{probe} is the curvature of the probe (ranging from 0 to 700 m^{-1}). The normalized response is shown in Figure 3-8 and can be compared to the neural data in Figure 3-7. The predicted response of the biomechanical model is similar to that of the neural data in that it starts at a comparable nonzero value (≈ 0.3), increases with increasing curvature as some decelerating function and 'fans out' with increasing applied force. Part of the discrepancy in the results can be attributed to assuming a constant modulus of elasticity; thereby ignoring the variation of the modulus of elasticity *with object curvature* which exists in our model. If we consider the response of the complete model, we would expect the 'fan out' to increase.

It is also of interest to correlate the actual pressure distribution predicted by the biomechanical model to neural data. Unfortunately, presumably because of practical experimental constraints, Goodwin and his colleagues did not obtain population responses of the afferent units to stimuli applied at a fixed contact point. They did obtain response profiles of single afferent units to stimuli applied at varying distances of the receptive field; however, this allows the radius of curvature of the fingerpad to vary. We therefore are unable to correlate the response at zero probe curvature to our biomechancal data and model. Nevertheless, if we assume this variation is small compared to the curvature of the objects being contacted (which is probably a reasonable assumption for the more curved objects), then we can use these single afferent profiles as an approximate representation of the population response.

Examining the profiles of the neural responses (see Figure 3-9), we can see that they

look approximately parabolic in shape, as would be expected from our model. It is also interesting to note that the neural profiles exhibit spatial 'tails' (cf. to a parabola) similar to that of the spatial profile of the biomechanical response (due to the spatial filtering effects of the tactile array sensor), suggesting that the mechanical and/or neural components of mechanoreception also have a spatial averaging effect on the response.

Another parameter which we can consider is the change in the contact radius as a function of increasing curvature. As shown in Figure 3-9, the radius over which the neural population responds decreases for increasing curvature until some limit. This can be predicted by the simplified version of our model (i.e., Hertz contact [29]), where a, the contact radius, is described by

$$a = (\frac{3PR}{4E^*})^{1/3}.$$ (3.24)

For a constant force, and assuming E^* constant,

$$a \propto (C_{fingerpad} + C_{probe})^{-1/3}$$ (3.25)

The change in the contact radius predicted by our model is shown in Figure 3-10 and appears to be a plausible description of the changes found in the neural data.

These results suggest that our model plausibly describes the variations of the neural population responses to statically indented objects of differing curvature. However, a wider range of contact forces and a more quantitative analysis is needed to confirm this initial success. In addition, the response to more dynamic stimuli need to be used to more completely examine this issue.

3.7 Discussion

The distributed model presented here appears to work relatively well in explaining the measured data. Although the results are limited in accuracy by the spatial resolution of the distributed pressure sensor, it is sufficient to obtain a reasonable estimate of the average pressure above a mechanoreceptive unit. The model also can be extended to predict the response of the fingerpad to spheres of differing curvature and compliance. Correlating the changes in the pressure distribution for spheres of differing curvature with the results of Goodwin and his colleagues [13] suggests that the model can conceivably be used to explain the population response of the SAI units to curvature. This initial success in extending the predictive power of the model and the inherent simplicity of its analytical form, further suggests it as a plausible method for providing realistic tactile feedback of curvature and compliance for teleoperations and virtual reality [40, 41].

Subject	c_0	c_1	c_2	c_3	v_1 (sec^{-1})	v_2 (sec^{-1})	v_3 (sec^{-1})	V.A.F.$_{G(t)}$
d.p.	0.33	0.44	0.13	0.10	163	2.8	0.31	0.89
d.s.	0.33	0.42	0.16	0.08	256	9.7	0.91	0.83
a.h.	0.29	0.47	0.13	0.10	226	8.6	0.61	0.89
p.w.	0.33	0.42	0.16	0.08	238	20.5	0.79	0.67
f.c.	0.29	0.49	0.11	0.10	175	8.2	0.59	0.87
means	0.31	0.45	0.14	0.09	212	10.0	0.64	0.83

Table 3.1: Model parameters of the normalized force relaxation for individual subjects.

Subject	R (mm)	m (mm^{-1})	b (kPa/mm)	m.s.e.
d.p.	15	2.1	2.3	8.0 %
d.s.	12	1.1	6.1	9.6 %
a.h.	14	1.9	1.9	14 %
p.w.	17	1.1	3.6	9.0 %
f.c.	15	1.7	3.8	7.6 %
means	14	1.6	3.5	9.6 %

Table 3.2: Model parameters of the quasi-static indentation for individual subjects.
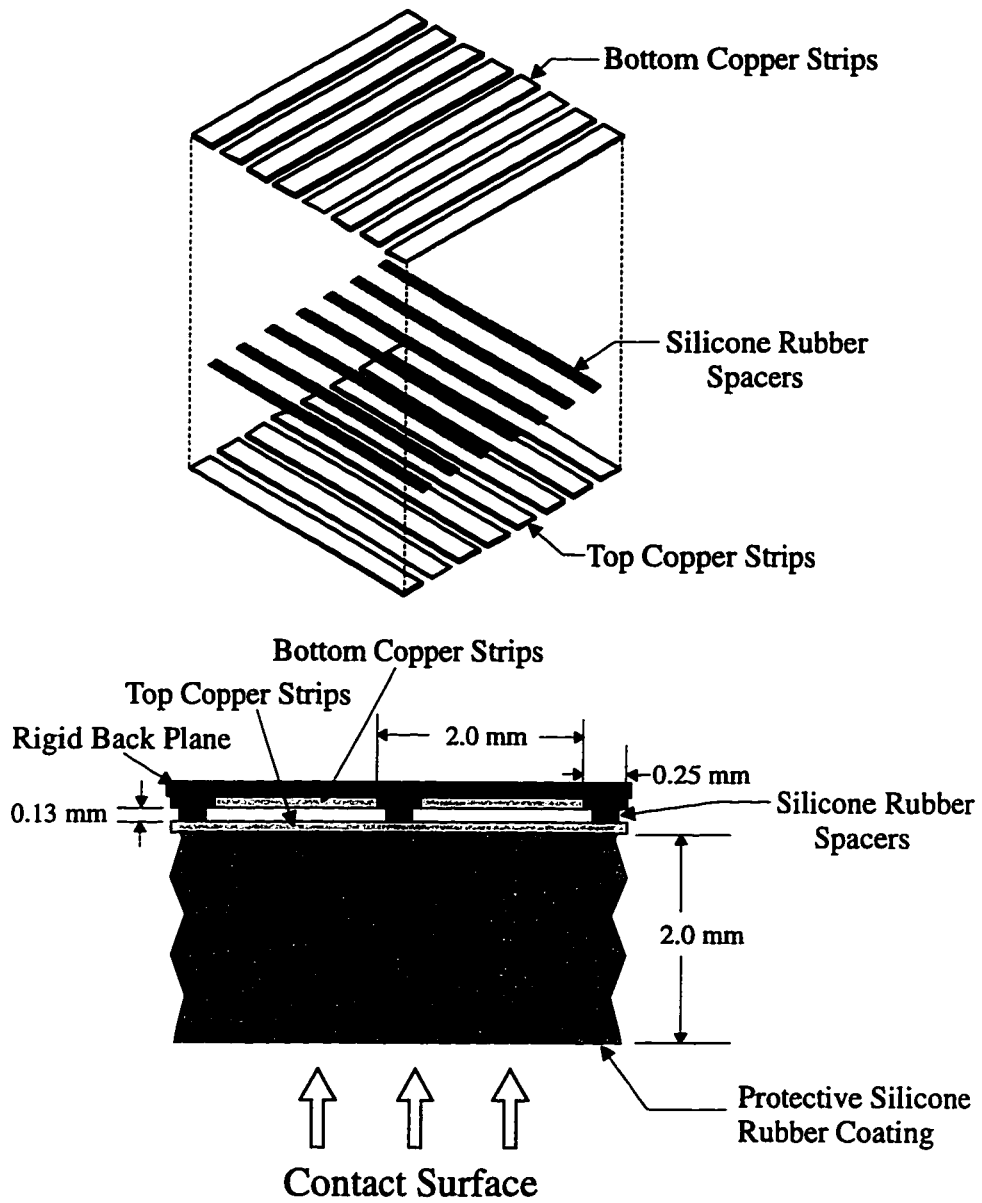
Figure 3-1: Tactile array sensor. Left: side view showing the two layers of copper strips separated by silicone rubber spacers. Right: exploded view showing sensor construction.
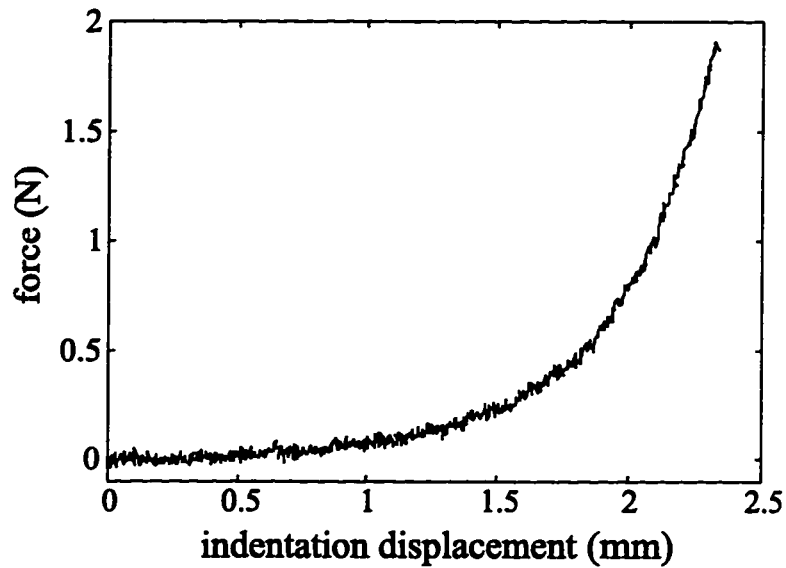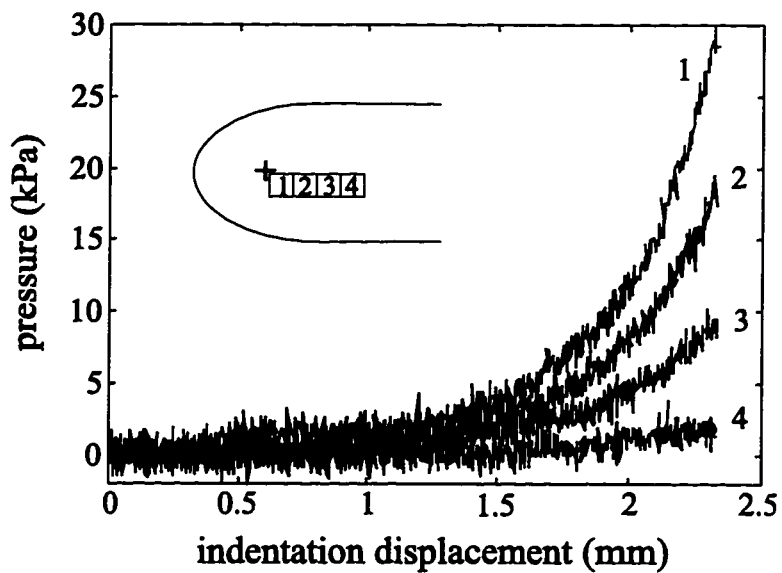
Figure 3-2: Quasi-static response. One experimental trial of a typical subject. (a) Lumped response found by summing all of the pressure array elements. (b) Distributed response. Pressures measured by four individual tactile array elements along the line indicated in the insert. Responses decrease for elements further away from the center of contact (indicated by the cross).
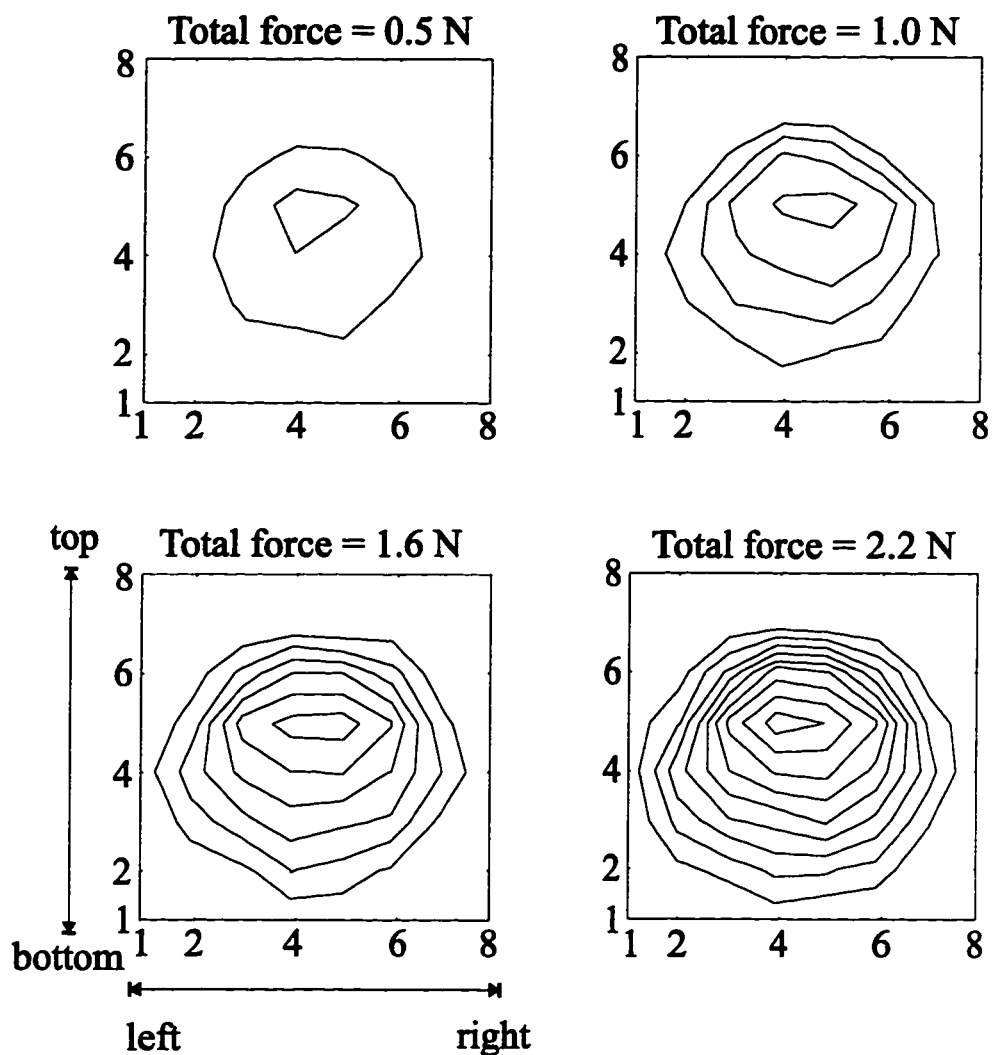
Figure 3-3: Contour plots of the distributed pressure responses to a quasi-static indentation. One experimental trial of a typical subject. Contours indicate increasing pressure levels of 4 kPa. Orientation of the array sensor with respect to the fingerpad is indicated in the lower left hand corner. The axes indicate the row and column number of each array element, which were spaced 2 mm apart.
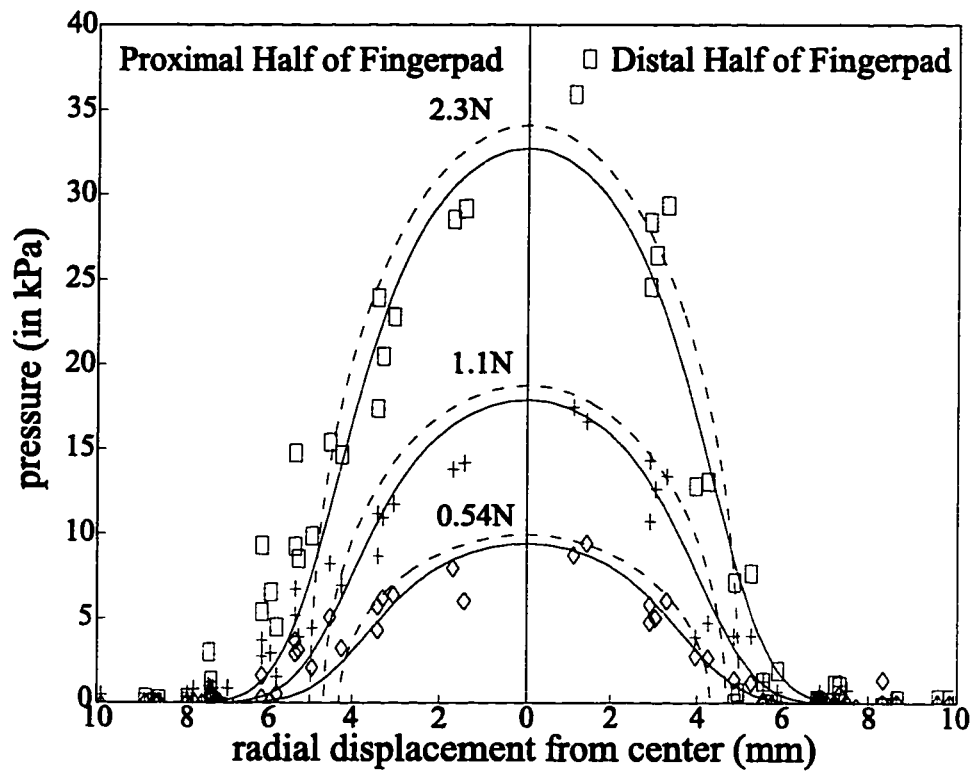
Figure 3-4: Pressure profiles in response to a quasi-static indentation at increasing net force values of 0.54 N, 1.1 N and 2.3 N. Measured pressures are indicated by symbols, the width and height of which indicate the error in the measurement. Left plot indicates array elements in the bottom half of the fingerpad; right plot indicates elements in the top half. Solid lines are the model fit, which also accounts for the spatial response of the distributed pressure sensor. Dashed lines are the estimated behavior at the surface of the fingerpad.
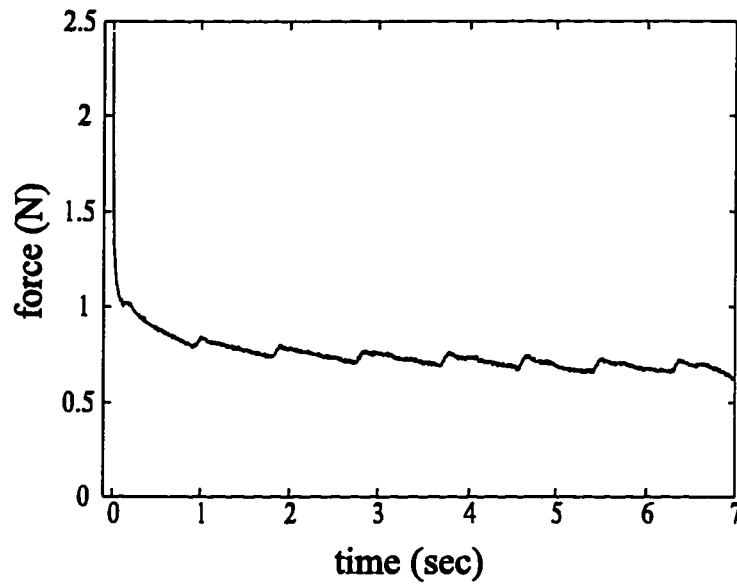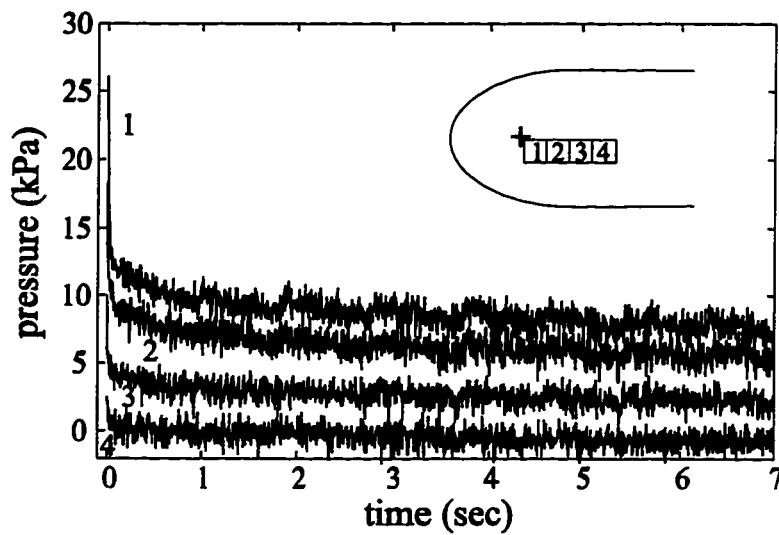
Figure 3-5: Force relaxation. One experimental trial of a typical subject. (a) Lumped response. (b) Distributed response. Pressures measured by four individual tactile array elements along the line indicated in the insert. Responses decrease for elements further away from the center of contact (indicated by the cross).
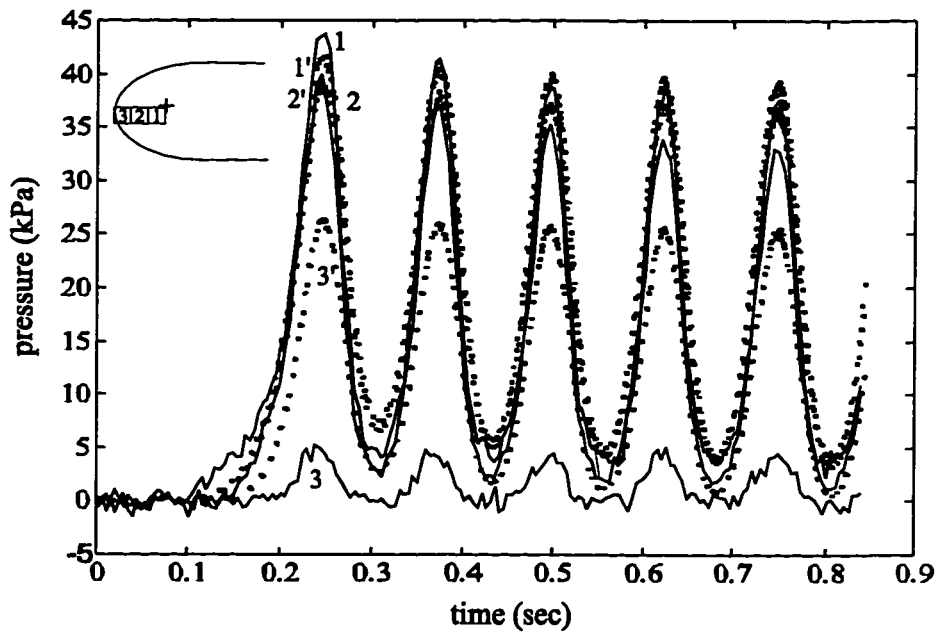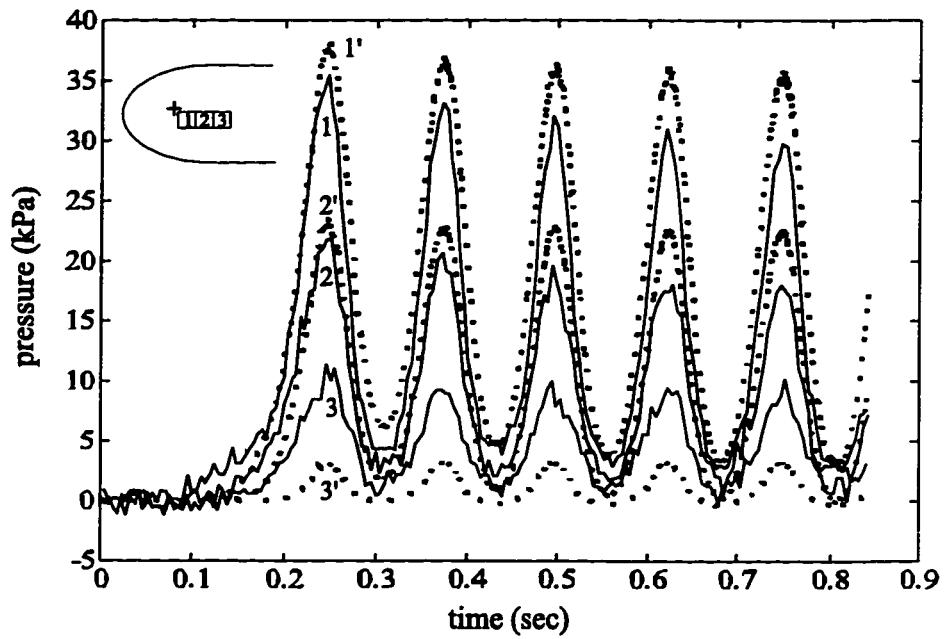
Figure 3-6: Distributed response to a 8 Hz sinusoidal displacement input. Pressures measured by six individual tactile array elements along the lines indicated in the inserts. Top: proximal half of fingerpad. Bottom: distal half of fingerpad. Responses decrease for elements further away from the center of contact (indicated by the cross). Note that the two halves are not symmetric as the center of contact was not in the center of the array. Solid lines are the experimental data. Dotted lines are the model fit.

63
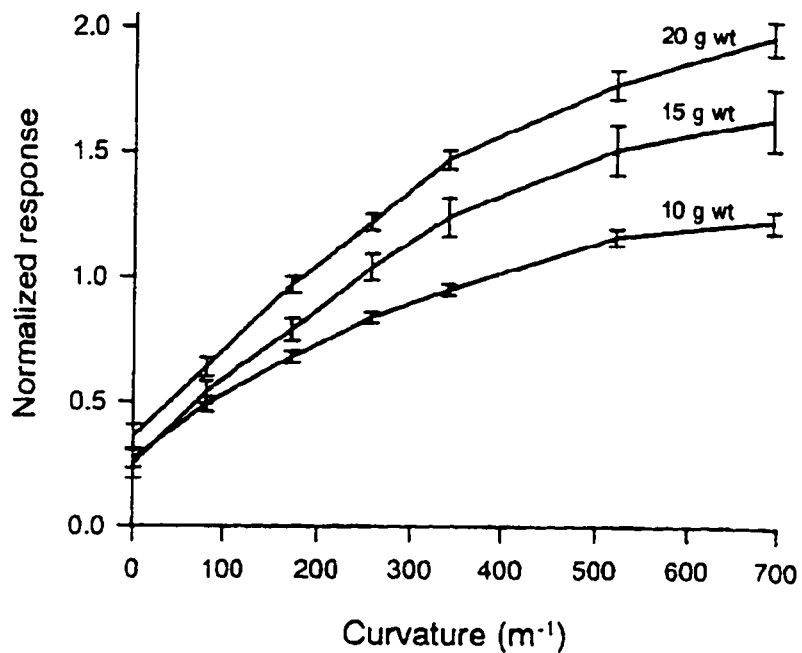
Figure 3-7: Normalized responses of the SAIs to stimuli at the center of the receptive field. Each fiber has a single normalization factor for the entire data set. For 10 and 20 gm wt, $n = 16$, for 15 gm wt, $n = 11$. Reprinted with permission from [13].
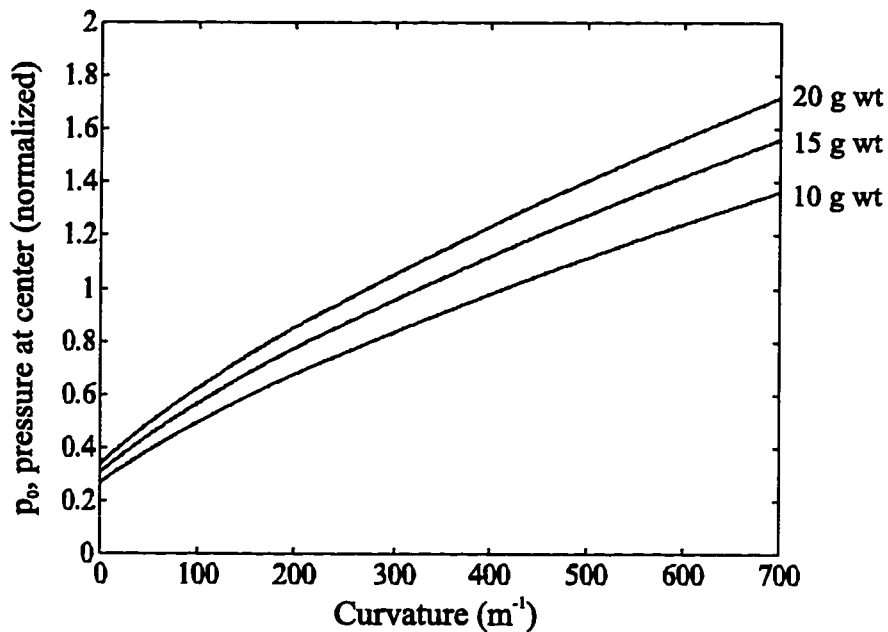
Figure 3-8: Normalized pressure response of the center of contact for the distributed biomechanical model, assuming E^* is approximately constant.
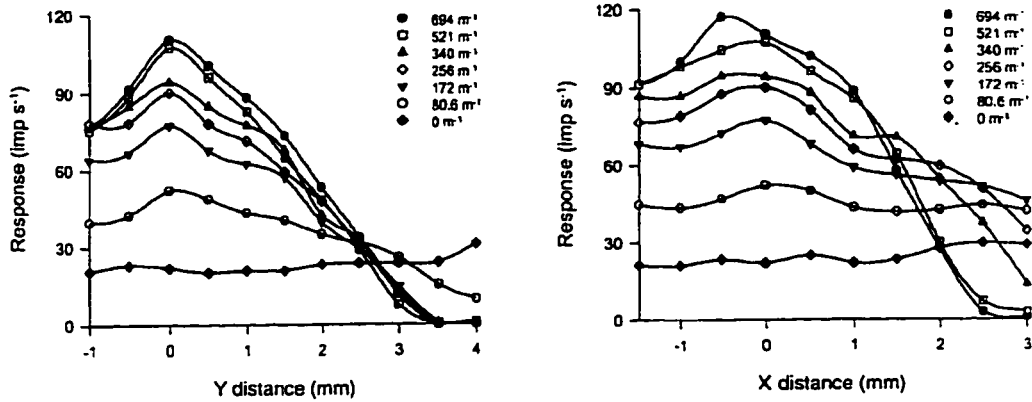
Figure 3-9: Responses of an SAI to curved spheres as a function of distance from the receptive field center. The y-axis is the center line along the longitudinal axis. The x-axis is the center line in the lateral direction. Reprinted with permission from [13].
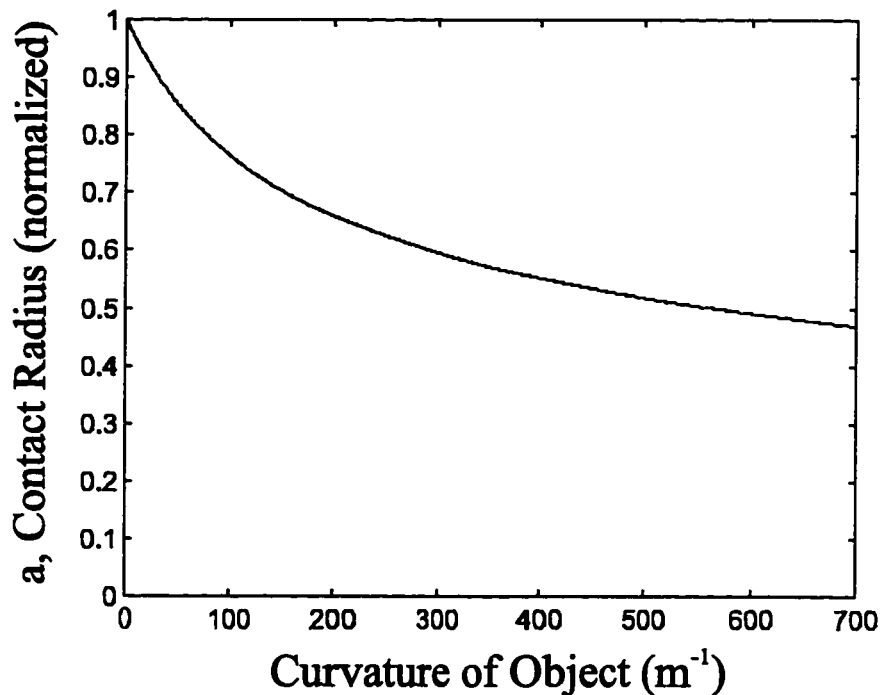
Figure 3-10: Contact radius as a function of curvature for the distributed biomechanical model, assuming E^* is approximately constant.

65

Chapter 4

Holistic Model of Human Touch

4.1 Introduction

The peripheral mechanoreceptive system in the skin consists of several functional compo-nents: the mechanical response of the skin, the mechanical response of the end organ, the creation of the generator potential, the initiation of an action potential, and (for some units) the branching structure of the afferent fibers [30]. Except for one of the receptor types, experimentally only the stimulus applied to the surface of the skin and the final afferent nerve fiber response (as the signal propagates toward the central nervous system) can be measured. The system must therefore be treated as a series of black boxes for which we only have access to the first input and the last output. Previous research has focused on one or another of these boxes and related them to the final output, despite the fact that the components act together to produce the response and cannot be treated in isolation. Here we examine the system as a whole, with the goal of attributing different aspects of the final nerve fiber response to the various components of the system. Our approach is to determine the components which are necessary and sufficient to describe this overall system response.

Previous Work. Johnson and his colleagues have most extensively developed models of the various components of mechanoreception. Freeman and Johnson [10, 11] developed a four parameter model, consisting of a resting membrane time constant, a variable membrane conductance, the fraction of each sinusoidal stimulus cycle producing depolarization and a noise level for the impulse threshold, to explain the temporal response of the mechanoreceptive units. As a result of the model fit, they derived the relationship between the membrane conductance of their model and the stimulus input amplitude (as a function of frequency) although they did not explicitly model this component of transduction.

Phillips and Johnson [43] developed a mechanical model of skin as a homogeneous elastic medium to examine the discharge of the SAI and FAI units to spatial gratings applied to the fingerpad. They examined various strain components proportionally to the mean rate of firing, and found that the response of the SAI units could best be explained by the local maximum compressive strain and the FAI units by the maximum horizontal strain. However, Johnson and his colleagues did not further combine their models to consider the system as a whole.

As mentioned previously (in Chapter 3), Dandekar [6] developed a detailed 3-D finite element model of the fingerpad which took into account the precise geometry of the fingertip, as well as the layered structure of the skin. He compared his model to the SAI unit response to various spatial stimuli, although he did not consider the contribution of the end organs or the nerve fiber itself.

Only Nemoto and his colleagues [39] have considered the relationship between the Hodgkin-Huxley equations and mechanoreceptor responses. Although they noted the ability of the Hodgkin-Huxley equations to exhibit phase locking similar to the mechanoreceptors, they proceeded to attribute the differences between the SA and FA units to differences in a d.c. bias of the nerve membrane on which the input signal is superposed. None of the above models specifically considered the contribution of the mechanics of the end organ.

Several researchers have, though, considered modeling the Pacinian corpuscle and its

associated nerve fiber (i.e., the FAII type units) *in vitro*. This is presumably due to the relatively large size of the Pacinian corpuscle (1 mm long and 0.5 mm in diameter [34]), and the considerable amount of experimental work directly on the mechanics of the end organ and the nerve fiber response. (The other three types of mechanoreceptors are too small to experimentally manipulate.) These end organs were first considered by Loewenstein [34] who developed a lumped parameter model to explain the mechanical filtering effects of the layered structure of the Pacinian corpuscle. In addition he considered a spatial representation of the neural component to explain the spatial summation of the generator current. However, he did not formulate a quantitative model nor relate it to the final neural action potential response.

Grandori and Pedotti [14] developed a transfer function representation of the mechanical capsule, the mechanical to neural transduction and the neural impulse initiation consisting of a pole-zero filter representation, which included a nonlinearity in the mechanical to neural transduction and a thresholding mechanism in the neural transduction. More recently Bell and Holmes [2] have developed a more complex model of the capsule, consisting of alternating layers of fluid and elastic shells. They have related the mechanics to the neural response using the hoop strain imposed by the capsule on a dendritic cable model, which included strain-activated channels. In contrast to these models which attempted to capture the details of the transduction process, we are only interested in those components which are necessary and sufficient to describe the final nerve fiber response as the signal proceeds toward the brain.

Our Approach. Our general modeling approach is to develop the most parsimonious model which encompasses the general engineering principles seemingly involved. Although this can be considered a higher level model, its development will be made consistent with the known morphology and physiology of the human hand. For example, a group of structures will be modeled together as a lumped spring only if it is plausible that together they achieve

a "spring-like" characteristic.[1]

The models that we present are primarily based on the frequency response of the four types of mechanoreceptors experimentally obtained by Johansson and colleagues [26]. The nerve impulses of individual afferent fibers were measured using microneurography in alert human subjects. The test stimuli were sinusoidal displacements applied perpendicular to the skin varying in amplitude (0.002 - 1.0 mm) and frequency (0.5 - 1024 Hz). The measured frequency response for each receptor type is given in Figure 4-1. As shown in the figure, the responses of the mechanoreceptive units are highly nonlinear, with the frequency at which the peak output occurs shifting to higher frequencies at lower stimulus amplitudes.

In modeling the mechanoreceptive units, the data fit is only intended to be qualitative because of the large variation in response of units of the same type (see Figure 4-2). More quantitatively, we performed a one-way analysis of variance on the sinusoidal displacement data of Johansson and his colleagues [26], in which individual fiber responses were also given at some input amplitudes. The ANOVA revealed that although differences between the four types of receptive units was relatively significant ($p \approx 0.20$), only about half of the square root of the variance in the data could be accounted for by these differences ($\eta = 0.49$). In addition, for these data, there was statistically no difference between the SAI and SAII units, and between the FAI and FAII units. Therefore, we will develop a single model for the SA type units and another for the FA type units.

4.2 Preliminary Models and Simulation Results

4.2.1 Neural Model

As the basis for the neural component of our models we wanted to choose a basic model of neural conduction. Although there has been no analysis of the kinetics of the mechanoreceptor nerve fibers in humans, all axons which have been studied (ranging across several Phyla)

---

[1]Note that internally the details of the system may be very complex to achieve this "spring-like" behavior.

have been found to be qualitatively similar to the Hodgkin-Huxley equations [18]. Since there was no initial reason to believe that the mechanoreceptor nerve fibers are an exception and since currently we are only interested in the qualitative analysis of the mechanoreceptors' responses (due to the high variability within each receptor type), we chose to model the impulse initiation component by the Hodgkin-Huxley equations. For our initial models we used the equations at their measured temperature of 6.3°C (see Appendix B.1.1). Alternatively, it may have been possible to use simpler models (e.g., a leaky integrator model), however the receptors have a relatively low firing rate which suggested that the nonlinearities in the membrane kinetics may be important.

Due to the growing evidence for mechanically sensitive ion channels (e.g., [8, 45, 20, 3]), it is presumed that the generator current is created directly by the application of a mechanical input rather than through some chemical intermediary. However, as there is yet no consensus as to a standard model, we will assume for simplicity that the generator current is linearly proportional to the displacement applied to the membrane.

It follows from incorporating the concept of mechanically sensitive ion channels that the generator current must be restricted to positive values: channels can open and close to gate the movement of ions but they cannot control the direction of movement. Additionally we must consider whether this implies that the mechanical signal is half-wave or full-wave rectified. Typically when mechanically sensitive ion channels are patched-clamped suction is used to examine them (e.g., [8]). Technically this only implies that the channels are sensitive to tension. However, it is hard not to believe that the receptors are sensitive to compression, given that it is their typical mode of excitation. In addition, one would expect that both tension and compression have a similar effect of stretching the nerve membrane, which is presumably the mechanism opening the mechanically sensitive ion channels. From this reasoning we would conclude that the signal should be full-wave rectified.

However, it is also important to consider the mode of coupling between the various mechanical components of the system to consider whether the mechanical signal should be

half-wave or full-wave rectified. In order for the nerve fiber to be sensitive to tension, the outer components of the system (i.e., the end organ and then the skin) would have to be firmly coupled to the inner elements (i.e., the nerve fiber and end organ, respectively). This would allow the outer elements, when in tension, to "pull" on the inner elements rather than detaching. We are unaware of any evidence that the nerve fiber is firmly coupled to the end organ structure, and there is only evidence that some of the end organs are coupled to the skin. Therefore, from these morphological considerations, we would conclude that the nerve fiber cannot respond to tension in the outer elements and that the signal should be half-wave rectified.

Nevertheless, if we assume incompressibility of the skin, we must consider the possibility that tension applied vertically to the surface of the skin may compress the corpuscle in the horizontal direction (as the skin 'decreases in width' to preserve constant volume). However, this mode of compression would typically be in the direction perpendicular to the long axis of the nerve fiber and to which it has been shown that at least the FAII units are very insensitive [24]. In contrast, sensitivity to vertically applied compression can easily be explained by the sandwiching of the components between the indentor applied at the surface of the skin and the rigid bone underneath. We have therefore assumed that the generator current is half-wave rectified.

We will further assume that all of the different types of mechanoreceptors share a common type of nerve fiber and mechano-electrical transduction mechanism. This implies that any differences between the receptor types can be attributed to the mechanical components.

4.2.2 Simulations with Simple Mechanical Components

Because of uncertainty about the contribution of the highly nonlinear neural impulse initiation component to the response characteristic of any mechanoreceptor model, very simple models were initially examined. The initial approach uses one-dimensional, lumped parameter models. The goal of these models is to capture the experimental results shown in

Figure 4-1 with physically plausible representations of each of the constituent elements.[2]

The first such model is shown in Figure 4-4a. Although we know from our biomechanical analysis in Chapters 2 and 3 that the skin is highly nonlinear and viscoelastic, we will assume for simplicity that it can be modeled as a linear spring. We will further assume that the end organ and the nerve membrane can be modeled as simple springs as well. As mentioned above, the generator potential is made linearly proportional to the nerve membrane displacement, and the impulse initiation is modeled by the Hodgkin-Huxley equations. Note that in this model the mechanical components contribute essentially nothing to the form of the output signal. This is because they form a simple proportionality factor which only affects the input range to which the model responds.

The equations were solved using a fourth order Runge-Kutta integrator with adaptive step-size [44], and with the parameters given by Hodgkin and Huxley for squid axon (see Appendix B). The input to the model is the displacement of the skin surface and the output is the time history of the nerve impulses initiated. The model was simulated for sinusoidal displacement inputs varying in amplitude (over the entire range which produced a nerve impulse train) and frequency (0.5-512 Hz). The form of the input was the same as that used by Johansson and his colleagues [26] superposed on their pre-adapted indentation

$$x_{in}(t) = A[cos\omega t + 1] \qquad (4.1)$$

We have assumed a pre-indentation of zero as our model does not take into account adaptation.

The latter half of a typical simulation is shown in Figure 4-3. An intracellular potential was considered a spike if the peak was more than 40 mV and it retained a 'characteristic form'. In reference to the latter measure: as the inputs were increased beyond a reasonable

---

[2]The effect of the nerve fiber branching structure, which exists for some types of units, is assumed negligible in these initial models as the stimulus probe for the given data was a relatively flat indentor.

amplitude, the voltage would plateau until the input was removed. This was considered to be not of characteristic form and beyond the input range to be considered. Although this could easily have been fixed by a saturation nonlinearity, there was no reason to assume from the data of Johansson and his colleagues [26] that a saturation limit had been reached (at least for the low frequencies).

The frequency response is shown in Figure 4-4b. The amplitude levels are presented in decibels, where 0 dB corresponds to the maximum input level; this non-dimensionalizes the input range and enables the model to be viewed independently of the proportionality constants. Note that the output is in terms of nerve impulses per input frequency cycle to facilitate the comparison with the experimental results in Figure 4-1.

The shape of the frequency response function (Figure 4-4b) is similar to those experimentally obtained for both SA type units: at large amplitudes the response is hyperbolic and at lower amplitudes it is an inverted U-shape. In addition, the variation of the response as a function of the input amplitude (not shown) is also similar, being logarithmic in both cases. The results also suggest that the shifting of the 'peak' of the frequency response with amplitude, most apparent in the responses of the FA type units, is an inherent property of the nerve membrane rather than due to nonlinearities in the skin mechanics.

However, there are two major discrepancies between this model and the SA type units:

1. the nerve impulse rate in the model is over an order of magnitude larger than the afferent units, and

2. the input range to which the model responds is smaller than the range for all the receptors except the SAII units.

The addition of a simple mechanical high-pass filter (i.e., a single zero in the transfer function of the mechanical components) alleviates both of these discrepancies. In this second model (Figure 4-5a), the simple springs used to model the skin, end organ and nerve membrane are replaced with dampers. For simplicity we will also allow the generator

73

potential to become proportional to the derivative of the nerve membrane displacement (although this is not expected to be physically realistic). The model then results in a derivative relationship between the displacement of the skin surface and the input current of the nerve fiber equations. This emphasizes the viscous properties of these viscoelastic materials.

The model was simulated for sinusoidal displacement inputs of varying amplitude and frequency, as above for the 'spring' model. The frequency response is shown in Figure 4-5b. Both the magnitude of the nerve impulse rate and the decibel input range are comparable to the mechanoreceptive units. More specifically, the results are also similar to the FA type units in their general form and exhibition of 'shifting peaks' with amplitude.

The results from both the spring model and the damper model suggest that modeling the mechanical components with carefully placed simple zeros and poles coupled with the Hodgkin-Huxley equations will explain the frequency responses of the mechanoreceptive units. A further significant aspect of the experimental results which is important to consider is the portion of the sinusoidal indentation cycle to which the different types of mechanoreceptive units respond (i.e., the phase response). Qualitatively, the SAI and SAII units respond principally to the indentation portion; the FAI units respond to both the indentation and the retraction, but much less to the retraction portion; and the FAII units also respond to both portions, but more to the retraction [26]. These experimental results can be compared to simulations of models using simple mechanical components, as above.

The simulation results showed that for a mechanical component consisting of:

1. a simple gain (e.g., the spring model), the response occurs over the entire input cycle;

2. a simple derivative $\frac{dx}{dt}$ (e.g., the damper model), the response occurs only on the indentation; and

3. a second derivative $\frac{d^2x}{dt^2}$, the response occurs primarily on the retraction, but to some degree on the indentation.

74

These results suggest that the SAI and SAII units can be modeled by first order systems, and the FAI and FAII units by second order systems (with the poles placed at much lower frequencies for the FAI units than for the FAII units).

4.3 Determination of the Mechanoreceptor Models

4.3.1 System Analysis

From the insight gained in analyzing these initial models, we proposed slightly more elaborate models to explain the experimental results. These models were chosen based on whether they were the simplest models which could:

1. produce the desired overall shape of the frequency responses, including phase characteristics;

2. meet the constraint that all types of units must share the same model of skin and the same model of the nerve fiber; and

3. be morphologically plausible based on the known structure of the individual components and their connectivity.

In examining the first two requirements, more insight can be gained if we first make a simple approximation to the Hodgkin-Huxley equations, such as with a simple integrate-and-fire model. This implies that the mean rate of firing (per second) is approximately equal to the mean input value. Consequently, the response of the neural component is not expected to vary with frequency for the same input amplitude. As a result, any variations in the mean firing rate with input frequency can primarily be attributed to the mechanical components of the mechanoreceptive system.

We can then use this result to examine the response of the mechanoreceptors in terms of their mean firing rate *per second*. Figure 4-6a shows the response of the SAI units obtained by Johansson and his colleagues [26] replotted in terms of impulses/sec. Comparison of

75

the slopes of the response, which primarily depend on frequency, with that for a direct proportionality factor and a first derivative suggested that the SAI units can be modeled by a first order system. Our previous analysis of the phase response also suggested that the system is first order. After considering any further constraints, we proposed to represent the SAI units as shown in Figure 4-6b. Similar results can be obtained for the SAII units.

It should be remarked that the result of our analysis of the SA units suggested that the skin should be modeled as a simple spring. This was not due to an arbitrary assignment of the model components to the different morphological constituents. It is based on the fact that in our statistical analysis (see Section 4.1) we found no statistical significance of depth on receptor response. Since the receptors are found at very different depths (some within the subcutaneous tissue), we have therefore concluded that the skin and subcutaneous tissue should be treated as approximately homogeneous. If we were then to assume that the skin was viscoelastic, the minimum order of the system would be second order (i.e., due to a viscoelastic component on either side of the end organ). As the response of the SA units appear to be only a first order system, this suggests that the skin should only be modeled by a simple spring. This result is of relevance in our consideration of the FA type units.

We also examined the response of the FAI and FAII units in terms of mean number of impulses per second. Figure 4-7a shows the response of the FAII units obtained by Johansson and his colleagues [26] replotted in terms of impulses/sec. Comparison of the slopes of the response with that for a direct proportionality factor, a first derivative and a second derivative suggested that the FAII units can be modeled by a second order system. Our previous analysis of the phase response also suggested that the system is second order. After considering the further constraint that the skin must be considered as a simple spring, we proposed to represent the FAII units as shown in Figure 4-7b. Similar results can be obtained for the FAI units, although they suggest that the poles be placed at lower frequencies than for the FAII units.

The resulting models can then be compared to the known morphology. For example, the end organs of the SAI units can be described as fluid-filled sacs, with the afferent nerve terminal entering along the bottom surface (Figure 4-6c). It is plausible that the fluid in the sac corresponds to the damper in our model, whereas the membrane of the sac corresponds to its parallel spring. Both presumably apply forces on the nerve ending to cause mechanosensitive channels to open, represented by the spring and proportionality constant in the generator current.

The end organ of the FAII units, in contrast, can be described as a series of fluid filled lamellae in the form of an onion, with weak interconnections between the layers. It is plausible that the lamellae can be modeled as simple springs, the lamellar spaces as a parallel damper (for the fluid) and spring (for the interconnections), and the entire corpuscle by a network of these structures as in [34]. We have assumed that each of the spring-damper networks on each side of the end organ can be approximated by a single spring-damper pair in parallel. The lamellae-fluid structure also presumably applies forces on the nerve ending to cause mechanosensitive channels to open (see Figure 4-7c).

4.3.2 Modification of the Hodgkin-Huxley Equations

There was unfortunately a problem with our formulation due to the Hodgkin-Huxley equations themselves: the input amplitude range at 0.5 Hz for which the equation simulations had an output response below 20 impulses/cycle was extremely small. As a result, no element could be added in front of the equations to produce the type of response and range observed in the SA units at low frequencies. However, this is not necessarily surprising as many encoding membranes, such as sensory terminals, fire at a rate much slower than the Hodgkin-Huxley equations [18].

It was therefore necessary to decrease the rate of the channel kinetics. One method by which some encoding membranes achieve this is by the presence of a fast transient K^+ channel that is activated in the subthreshold range of membrane potentials [18, 5]. However,

we have chosen instead to decrease the rates of the existing channels in the equations themselves. This also achieves a lower firing rate. The rates were decreased by a factor of approximately 6. We did not adjust the rates for temperature as there is effectively only one rate parameter; adjusting for temperature would only contribute an additional scaling factor for which we would have to adjust the overall rate parameter again to obtain realistic firing rates.

It should be emphasized that modifying the rates of the Hodgkin-Huxley equations did not change their fundamental nature. The qualitative form of the frequency responses from simulations with different rates were very similar to that with the original equations.

4.3.3 Preliminary Models Revisited

In order to verify that the modification to the Hodgkin-Huxley equations did not effect the conclusions we obtained from our preliminary models, we repeated our simulations with the modified nerve fiber equations.

We first simulated the response of the spring model (Figure 4-4a) which, as previously stated, was essentially the response of the nerve equations themselves. The equations were solved using a fourth order Runge-Kutta integrator with adaptive step-size, and with the parameters given in Appendix B.1. The model was simulated for sinusoidal displacement inputs of the form

$$x_{in}(t) = A[cos\omega t + 1] \tag{4.2}$$

Frequencies were varied between 0.5-512 Hz. Amplitudes were varied over a range that produced outputs comparable in magnitude to the SA units.

The frequency response of the spring model is shown in Figure 4-8. It is qualitatively very similar to that of the original model (Figure 4-4b): at large amplitudes the response is hyperbolic and at lower amplitudes it is an inverted U-shape. In addition, the phase

response behaved similar to the original model. These results verify our assertion that our modification of the rates and temperature did not change the fundamental nature of the Hodgkin-Huxley equations.

The response of this simple model also agrees very well with the responses of both the SAI and SAII units (refer to Figure 4-1). It is very similar both in the shape and in the magnitude of the response, and spans a similar input range. The minor differences in the magnitude of the response could be accounted for by optimizing the scaling of the rate parameters. However, as we are interested in understanding the underlying mechanism rather than obtaining precise values we will ignore this discrepancy. Unfortunately there was one noticeable difference between the model response and the actual receptors: the model tended to respond over most of the input cycle in contrast to the receptors which responded primarily to the indentation phase. As the phase can have an important effect on the time response of the model, we will need to consider a more complex model, such as the one we have proposed in Section 4.3.1.

We also examined the response of the damper model using the modified Hodgkin-Huxley equations. The model was simulated for sinusoidal displacement inputs of varying amplitude and frequency, as above for the 'spring' model. Frequencies were varied between 0.125-512 Hz. Amplitudes were varied over a range that produced output mean rates comparable in magnitude to the FA units. It should be noted that in determining the input range, unrealistically high output voltages were tolerated for larger input amplitudes at higher frequency. This problem could easily be eliminated with a saturation nonlinearity. In fact, adding a simple pole (between $10 - 100$ Hz) to the mechanical component could significantly reduce this problem while maintaining a very similar response to the pure derivative in terms of the magnitude response, the input range and the general phase of the indentation trajectory to which it responded.

The frequency response of the damper model is shown in Figure 4-9. It is qualitatively very similar to the original damper model (Figure 4-5) in both the magnitude and phase

79

response. This modified model also agrees very well with the responses of both the FAI and FAII units (refer to Figure 4-1). It is very similar in both the general shape and magnitude of the response, including the shifting of the 'peak' of the frequency response with amplitude. It also has a comparable input range. Unfortunately, as with the comparison between the spring model and the SA units, the model and the FA units deviated in terms of their phase response. The modified 'damper' model was similar to the original damper model in only responding to the indentation phase of the response. This result disagrees with the qualitative phase information for the FAI and FAII units.

4.3.4 Model Parameterization

As the modified nerve fiber equations combined with the preliminary models were insufficient to explain the results, we more closely examined the response of our slightly more complicated models proposed in Section 4.3.1. The models describing the SA type units (Figure 4-6) and the FA type units (Figure 4-7) were simulated as described in Appendix B: rather than varying each parameter specifically, we examined the models in terms of placing the poles and zeros of an equivalent filter. This reduced the number of unknowns to an amount that could be constrained.

The model of the SA type units can then be reduced to the determination of a single pole and zero

$$\frac{X_{out}}{X_{in}} = \frac{M(s+z)}{(s+p)}.$$

(4.3)

However, we are restricted by the model to place the zero below the pole as

$$z = \frac{K_e}{b_e}$$

(4.4)

and

$$p = \frac{K_e}{b_e} + \frac{K_s K_n}{b_e(K_s + K_n)} \qquad (4.5)$$

where,

K_s = combined stiffness of the skin and subcutaneous tissue

K_e = stiffness of the end organ

K_n = stiffness of the nerve fiber

b_e = damping of the end organ.

This is expected from our previous analysis (Section 4.3.1) to give rise to the desirable magnitude and phase characteristics.

As with our preliminary models, we simulated the response to sinusoidal displacement inputs of varying amplitude and frequency. For the most part, varying the location of the zero and pole did not change the magnitude of the frequency response very much. The shape was very similar as long as the basic requirement that there was a d.c. response (for comparable amplitudes as for other frequencies) was fulfilled. However, the phase response did change noticeable and was the primary determinate for selecting filter parameters. We therefore chose filter values for the SAI model to have a response primarily during the indentation phase ($f_z = 0.1$ and $f_p = 1.0$); whereas the SAII model was allowed to have a bit of a response on the retraction phase as well ($f_z = 0.5$ and $f_p = 5.0$).

The frequency responses of the model of the two SA type units, using the chosen parameters, are shown in Figure 4-10. Both responses look similar to the actual response of the SAI and SAII units (Figure 4-1). As with our simple spring model, the response is very similar in shape to the receptor responses: at large amplitudes the response is hyperbolic and at lower amplitudes it is an inverted U-shape. In addition, as with the modified spring model, the neural impulse rate is comparable to that of the actual receptors. Although one may question the use of a more complex model due to the similarity of the magnitude

81

responses, we will show in Section 4.3.5 the merit of our phase analysis.

The model of the FA units can equivalently be considered as a filter consisting of two zeros and two poles

$$\frac{X_{out}}{X_{in}} = \frac{M(s + z_1)(s + z_2)}{(s + p_1)(s + p_2)}.$$

(4.6)

It is not clear from the transfer function what should be the relationship between the poles and zeros. However, we know from our previous analysis (Section 4.3.1) that we want to place both zeros below the poles.

Similar to the SA model, we varied the placement of the zeros and poles, and examined the simulated response of the FA model to sinusoidal displacement inputs of varying amplitude and frequency. As long as both zeros were placed below the poles and at least one was placed at zero (or very close to it, to ensure that there was no d.c. response at comparable amplitudes to those at other frequencies), the magnitude of the response did not change much with variations in the parameters. However, as the poles were placed increasingly higher in frequency, the response range increased significantly and there was an increasing lead in the phase. As with the SA model, the phase response was the primary determinate for selecting the filter parameters. We, therefore, chose filter values for the FAI model to have more of a response, for the most part, to the indentation phase than to the retraction phase ($f_{z1} = f_{z2} = 0$, $f_{p1} = 1.0$ and $f_{p2} = 10.0$); whereas the FAII model was chosen to have more of a response to the retraction phase, which was more characteristic of that type of unit ($f_{z1} = f_{z2} = 0$, $f_{p1} = 100.0$ and $f_{p2} = 1000.0$).

The frequency responses of the model of the two FA type units, using the chosen parameters, are shown in Figure 4-11. Both responses look similar to the actual response of the FAI and FAII units (Figure 4-1). As with the simpler damper models, the response is very similar in shape and magnitude to the receptor responses, including the exhibition of the shifting of the 'peak' frequency. In addition, the given model for the FAII units can

finally encompass the large input range to which the actual receptors respond. Once again, though, the essential differences between these models and the simpler damper models is that they are able to account for the phase response.

There are two brief comments that should be made before continuing. As with the modified damper model, unreasonably high voltages were tolerated when simulating the higher frequencies of the FA type units. Adding a saturation nonlinearity could easily fix this problem and does not seem unreasonable given the convergence of the FAII units, in particular, at higher amplitudes to a single output value for high frequencies. In addition, there was also a tendency for the nerve fiber equations to converge to 1 impulse/cycle between 4 − 16 Hz. This limited our ability to match the specific shape of the frequency responses for all receptor types. These issues are discussed further in Section 4.4.

4.3.5 Comparison of the Models to Time Series Data

In order to test the predictive power of our models, we examined their responses to ramp and hold position inputs. We were then able to compare our results to preliminary data provided by Roland Johansson's group (Umeå University, Sweden). This allowed us to achieve two important objectives:

1. test our models using inputs very different than those used to develop them; and

2. examine a new and more complex dimension of the response (i.e., the actual time series response of the impulse train).

The data which were provided consisted of the responses of one of each type of receptor. Two of the units were stimulated directly above the center of the receptive field (the FAI and SAII units), and two of the units were stimulated further away from the center (the FAII and SAI units). The skin was indented normal to the surface in a trajectory consisting of a constant velocity to a given displacement, followed by a constant hold at the given position,

83

and then by a retraction at the same speed. The speeds used were 2, 8, and 32 mm/sec, and the position was held at a point between 2 − 3 mm for a duration of 1 sec.

Simulations of our models were performed using analytical approximations to the given experimental displacement trajectories. This was done rather than using the actual displacement input trajectory itself to ensure that the differential equations were well-behaved. As we are interested in a qualitative comparison, due to the large variation between receptors of the same type (see Section 4.1), the exact trajectory was not necessary. The ramp-hold-and retraction was represented by a trapezoidal displacement trajectory with 'rounded corners' 10 msec in duration. The rounded corners were required to avoid infinite accelerations.

From the responses of our simulations we generated similar diagrams to that provided by Johansson. The gain scaling of the receptors was estimated from the previous sinusoidal input data. In order to determine the instantaneous frequency, spikes were generated by marking the point where the intracellular potential first past 40 mV. The instantaneous frequency was calculated as the inverse of the time between two spikes.

The neurophysiological responses of both SA type receptors are shown in Figure 4-12 to ramp and holds at 8 mm/sec. As would be predicted from our models, and which underlie the basic characteristic of these receptors, both have a static response. However, it also should be noted that both show a higher firing rate to the initial ramp portion of the input, despite the fact the indentor is not as deep as during the hold phase. The firing rate during the ramp portion of the input also appears to increase for increasing indentation velocity. These observations are expected from our model, due the contribution of the mechanical damping component. The fact that neither show a parallel increase upon retraction is anticipated by the phase characteristics of our models, which only responded to the indentation component of the sinusoidal inputs used previously. Note that it is difficult to compare the receptors quantitatively as the stimuli were slightly different and were applied at different distances away from the center of the receptive fields.

In order to verify the effective contribution of the damping component, we first simulated the response of our simple 'spring' model, which had a similar frequency response to our SA models but differed in phase (due to the lack of a damper). The response of the simple 'spring' model showed a gradual increase in firing rate until the steady state input was reached, upon which it remained constant (Figure 4-13). It also continued to respond well into the retraction phase. This is clearly in contrast to the response of the SA type units and shows that the nerve fiber alone cannot explain the response of these receptors. We then simulated the response of our SAI and SAII models using the parameter values chosen in the previous section. These models showed very high qualitative agreement with the neurophysiolgical data (Figure 4-14): both showed a higher firing rate during the initial ramp portion of the input which increased with increasing indentation velocity, and neither continued to respond into the retraction phase.

The neurophysiological responses of both FA type receptors are shown in Figure 4-15, also to ramp and holds at 8 mm/sec. The basic characteristic of these receptors not having a static response is clearly shown in the data, and is predicted from our models due to the zeros being chosen at 0 Hz. The firing rate upon indentation can also be observed to increase with increasing indentation velocity. This is also expected due to the damping components in our models. The responses that the receptors show upon retraction are more difficult to explain. For slower ramps, composed only of low frequency components, the models would not have a response on the retraction as they would be expected to act similar to an accelerometer which is half-wave rectified (the input velocity and acceleration are both negative on retraction). For much faster ramps, the poles of the models would act as a simple gain for the *high* frequency components: this may produce action potentials on the retraction (since the input position is positive), although it is not clear. The FAI unit also exhibited an unexpected characteristic in consistently having a double peak in the instantaneous frequency response on the indentation ramp. The latter peak, as well as the responses to the retraction phase, may be due to components of the input not captured in

our analytical representation of the ramp and hold (i.e., small indentor vibrations or shear forces).

For comparison to the neurophysiological data, we first examined the response of our simple 'damper' model. The response of even this simple model clearly captures the basic characteristic of these receptors in not having a static response (Figure 4-16). In addition it does show an increase in the firing rate to increases in indentation velocity. However, it does not respond to the retraction phase. The response of the FAI model (Figure 4-17) also shows similar characteristics. In addition, the response of the model correlates very well with the first peak of the instantaneous frequency response of the experimentally measured FAI unit. The response of the models to actual experimental inputs (which may contain small variations detectable by these very sensitive units) and the response of the FAII model remains to be investigated.

It is also interesting to note that the instantaneous frequencies of the neurophysiological data are noticeably higher than the models. This suggests that we possibly decreased the rates of the Hodgkin-Huxley equations a little more than we needed. However, this is not expected to qualitatively change our results.

4.4 Further Considerations

4.4.1 Consideration of Force Inputs

One significant prediction of our models is that, because mechanically they consist of serial chains, all units (both SA and FA) would respond similarly to force inputs. Furthermore, the response would be that of the "bare" nerve fiber. This is because the force applied to the surface of the nerve fiber is expected to be the same force applied to the surface of the skin due to the serial chain. Unfortunately, preliminary data made available by Roland Johansson's group (Umeå University, Sweden) clearly show that this is not the case. The FA type units clearly do not respond to a constant *force* input, as would be predicted from

86

our model.

We now propose new models to explain these results (Figure 4-18). The basic concept behind these models is the addition of a spring in parallel with our current models. Consequently, when displacements are applied to the surface of the skin, the parallel spring does not have an effect and the system acts like our serial chain models. When forces are applied to the surface of the skin, the parallel spring shares the load and produces a filtering effect. These models need to be analyzed in more detail to see if they can be expected to explain the physiological data.

4.4.2 Addition of a Fast Transient K^+ Channel

As discussed in Section 4.3.2 it may be more appropriate to produce a slower firing rate by adding a fast transient K^+ channel rather than decreasing the rates of the Hodgkin-Huxley equations. One subtle point this is expected to solve is that there is a tendency for the output response to converge to the same mean rate of firing (at 1 impulse/cycle) between a frequency of $4 - 16$ Hz independent of the input amplitude (above some threshold). This does not appear to occur for the actual neurophysiology data [26], even when examining individual receptors. Increasing the temperature in the standard Hodgkin-Huxley equations (i.e., with the values for squid axon) eliminates this problem by shifting this convergence point higher in frequency: at 37°C this problem no longer exists within the frequency range considered. However, the predicted mean rate of firing is extremely high (i.e., over a thousand impulses/cycle cf. a few at 0.5 Hz). The benefit of adding a fast K^+ channel is expected to be:

1. the pulse generating dynamics are at the rate of the standard Hodgkin-Huxley equations at 37°C, thereby avoiding the convergence problem; and

2. the fast K^+ channel acts to decrease the mean firing rate.

4.4.3 Addition of a Mechano-sensitive Ion Channel

In developing our model, given the limited knowledge about mechano-sensitve ion channels and our desire for simplicity, we have chosen a simple linear approximation between the displacement applied to the nerve fiber and the generator current. For compatibility with other models of excitable membranes, it would be desirable to incorporate an actual mechano-sensitive ion channel into the model. This would also alleviate problems with the current model in its response to overly large inputs by its natural inclusion of a saturation effect. However, until more is known about these channels, it is simpler to only add a saturation nonlinearity directly to the existing component.

4.5 Discussion

We have shown that the Hodgkin-Huxley equations coupled with simple mechanical components capture the essential properties of the experimental frequency responses. Furthermore, we have developed slightly more complex models which appear to capture more of the behavior of the different mechanoreceptors. The simplicity of the models should facilitate further examination of mechanoreception, including models of branching afferent fibers and of population responses.
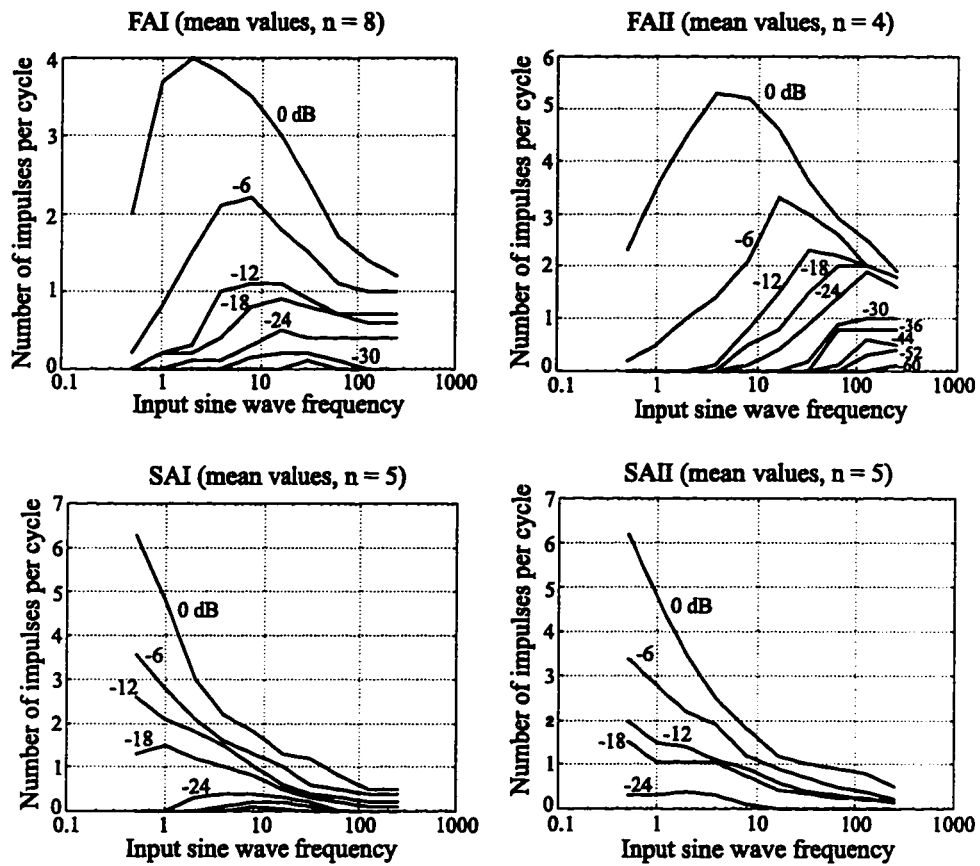
Figure 4-1: Frequency response functions of the four different types of mechanoreceptors. The inputs applied to the surface of the skin were displacement indentations of the form $A(coswt+1)$ superposed on a pre-indentation of 0.5 mm to which the receptors were allowed to adapt. Note that the vertical axis units are in terms of nerve impulses per input frequency cycle and that 0 dB corresponds to an amplitude of 1 mm. Adapted from [26].

89
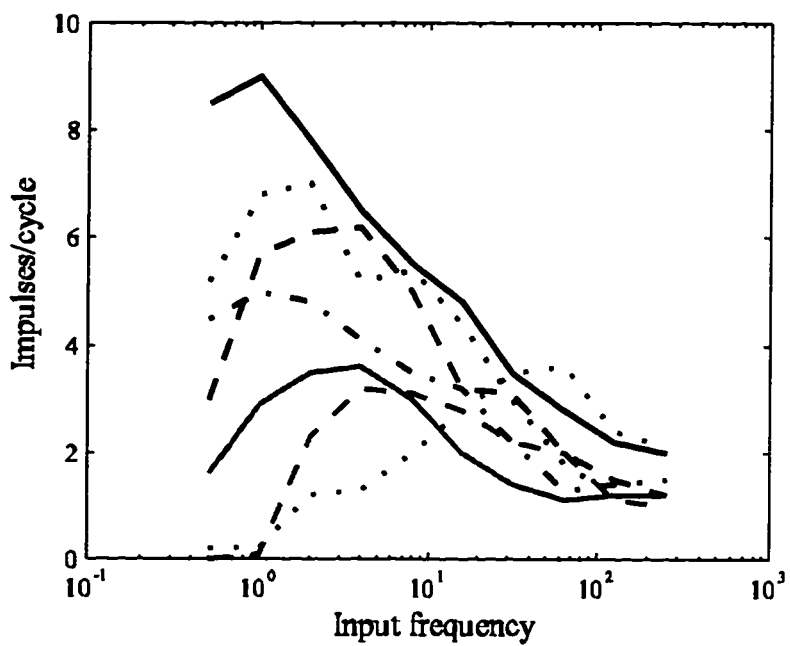
Figure 4-2: Variability within a receptor type. Response of 7 different FAI Units to 1 mm peak-to-peak sinusoidal displacements as a function of frequency. Adapted from [26].
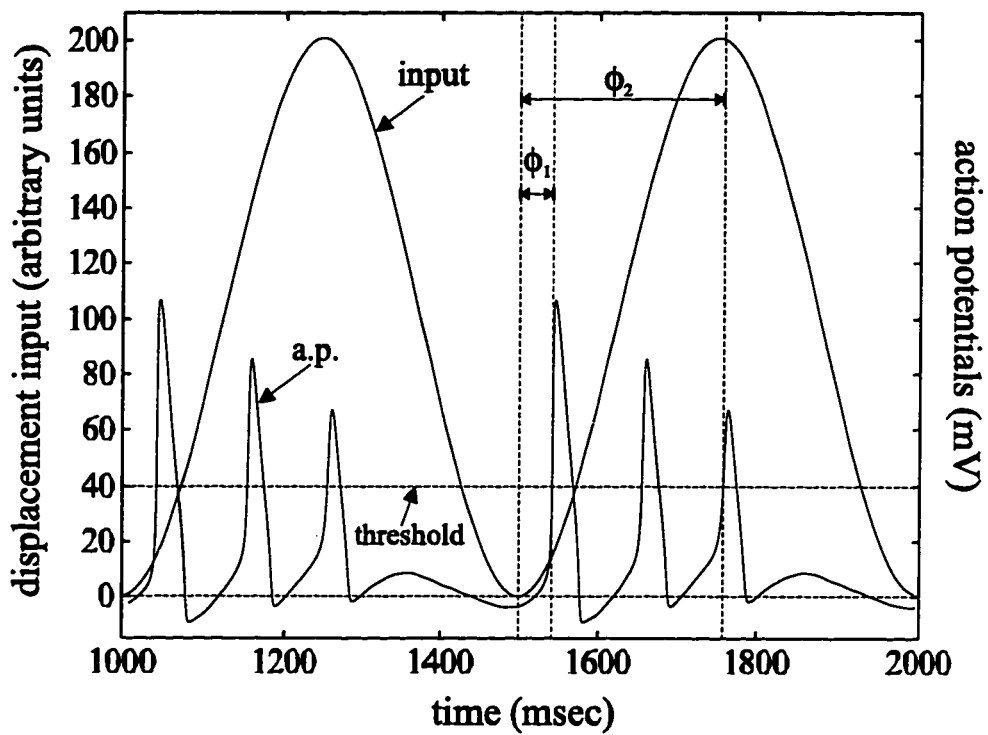
Figure 4-3: Latter half of the simulation of the 'spring' model to a sinusoidal input with a peak-to-peak amplitude of 200 and a frequency of 2 Hz. The intracellular potential was considered a spike if the peak was greater than 40 mV. The phase over which there was a response, bounded by ϕ_1 and ϕ_2, is referenced with respect to the zero value of an input cycle.

91
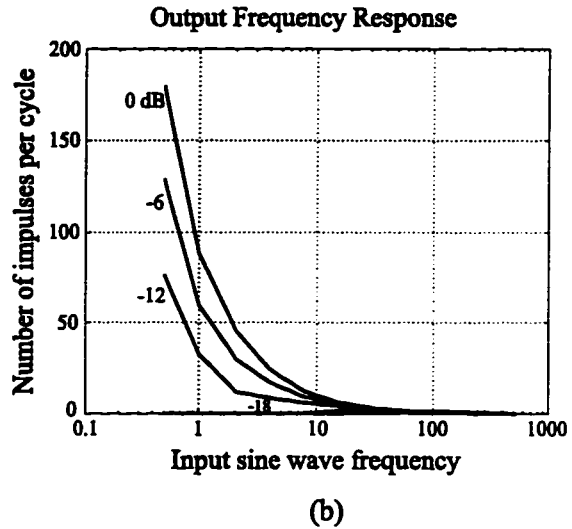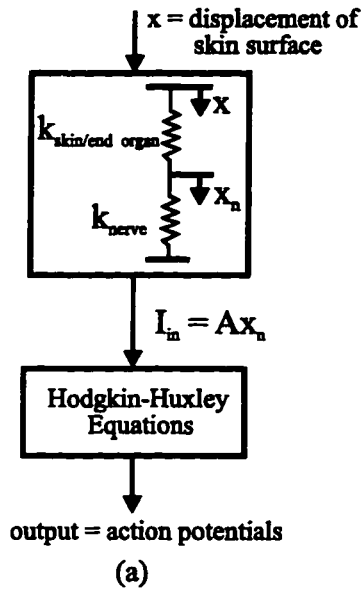
Figure 4-4: (a) Spring model of the skin, end organ and nerve membrane proportionally coupled to the Hodgkin-Huxley equations. (b) Frequency response function of the 'spring' model. 0 dB corresponds to the maximum input level.
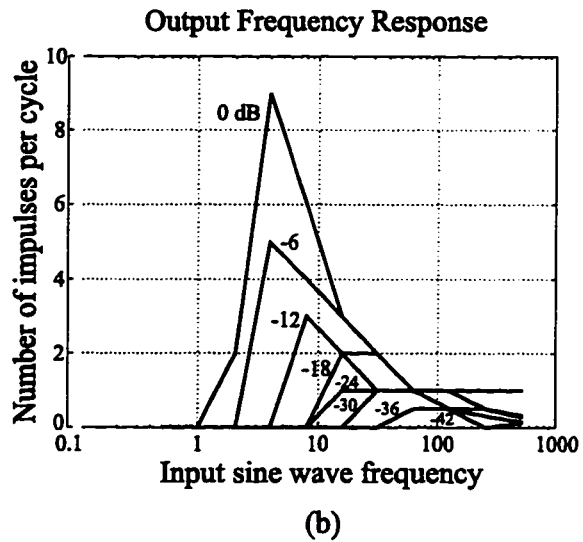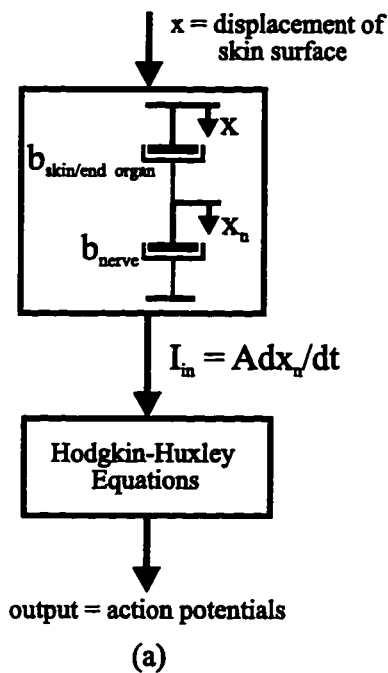
Figure 4-5: (a) Damper model of the skin, end organ and nerve membrane coupled by its derivative to the Hodgkin-Huxley equations. (b) Frequency response function of the 'damper' model. 0 dB corresponds to the maximum input level.
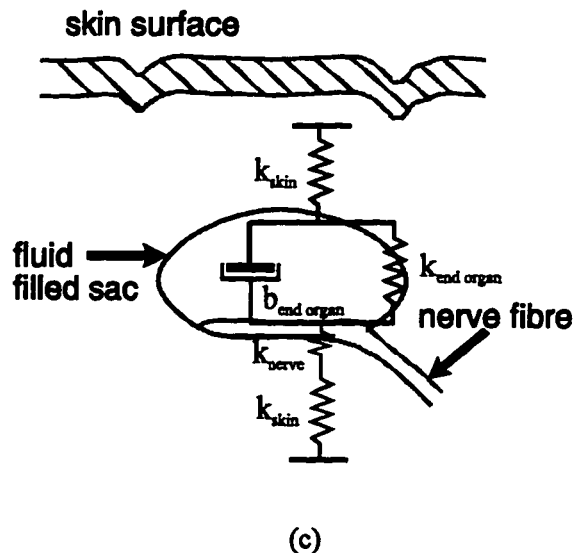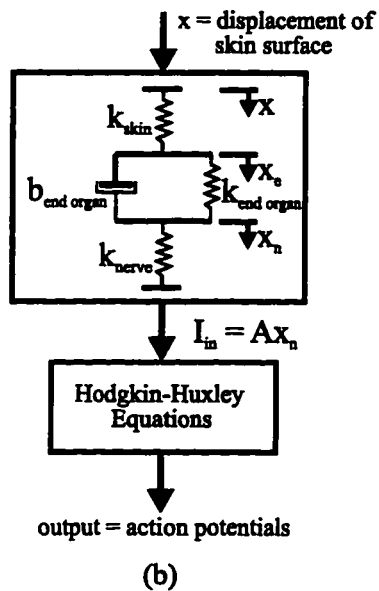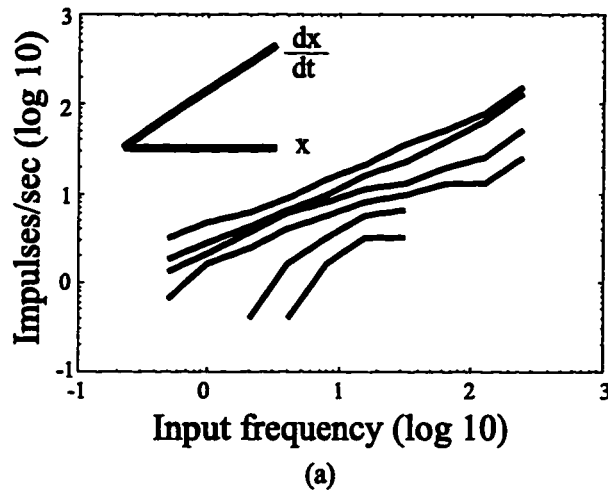
Figure 4-6: (a) Frequency response of the SAI units replotted in terms of impulses/sec. Adapted from [26]. (b) Model of the SAI and SAII units. Same parameters for the skin and nerve fiber for all four types of mechanoreceptors. Different parameters for the end organs of each of the types of receptors. (c) Correspondence between the morphology of the SAI units [23] and the proposed model; the end organ is not to scale and structural details are omitted.
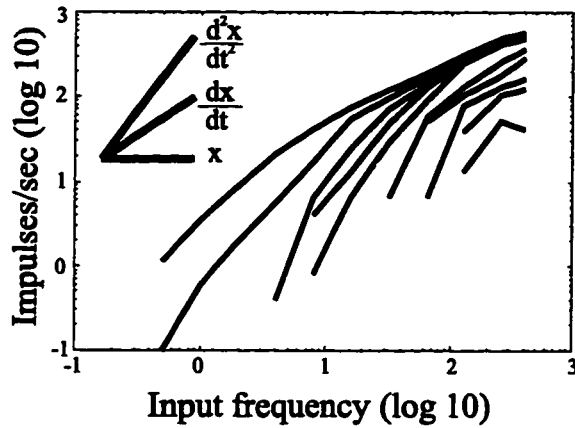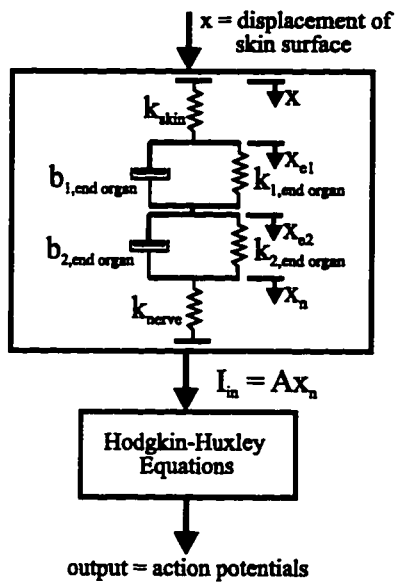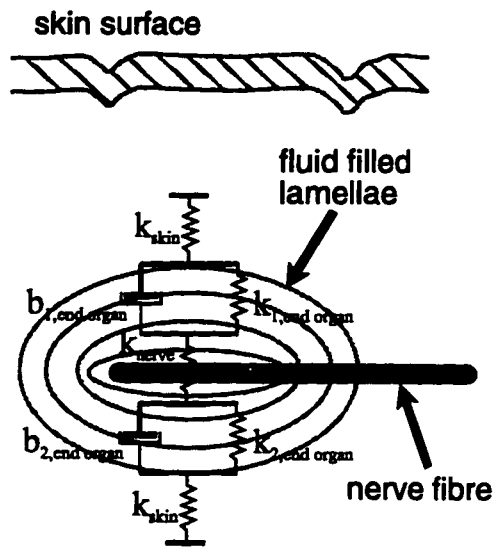
Figure 4-7: (a) Frequency response of the FAII units replotted in terms of impulses/sec. Adapted from [26]. (b) Model of the FAI and FAII units. Same parameters for the skin and nerve fiber for all four types of mechanoreceptors. Different parameters for the end organs of each of the types of receptors. (c) Correspondence between the morphology of the FAII units [34] and the proposed model; the end organ is not to scale and structural details are omitted.
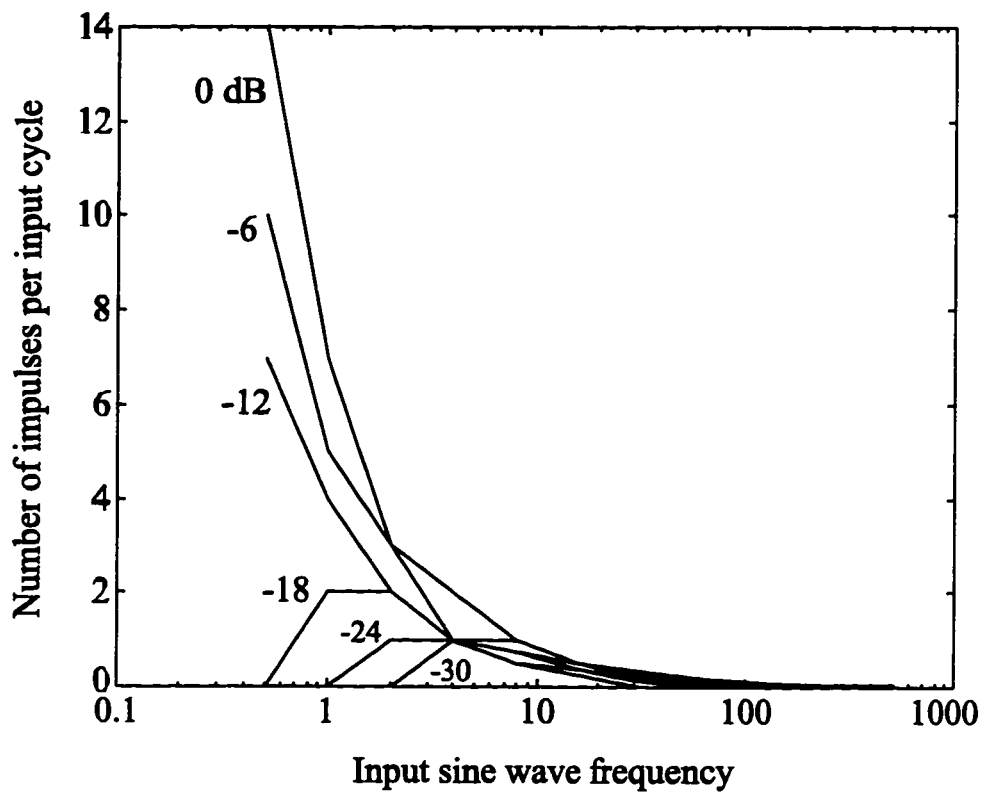
Figure 4-8: Frequency response function of the 'spring' model using the modified version of the Hodgkin-Huxley equations (see text for details). 0 dB corresponds to the maximum input amplitude considered.
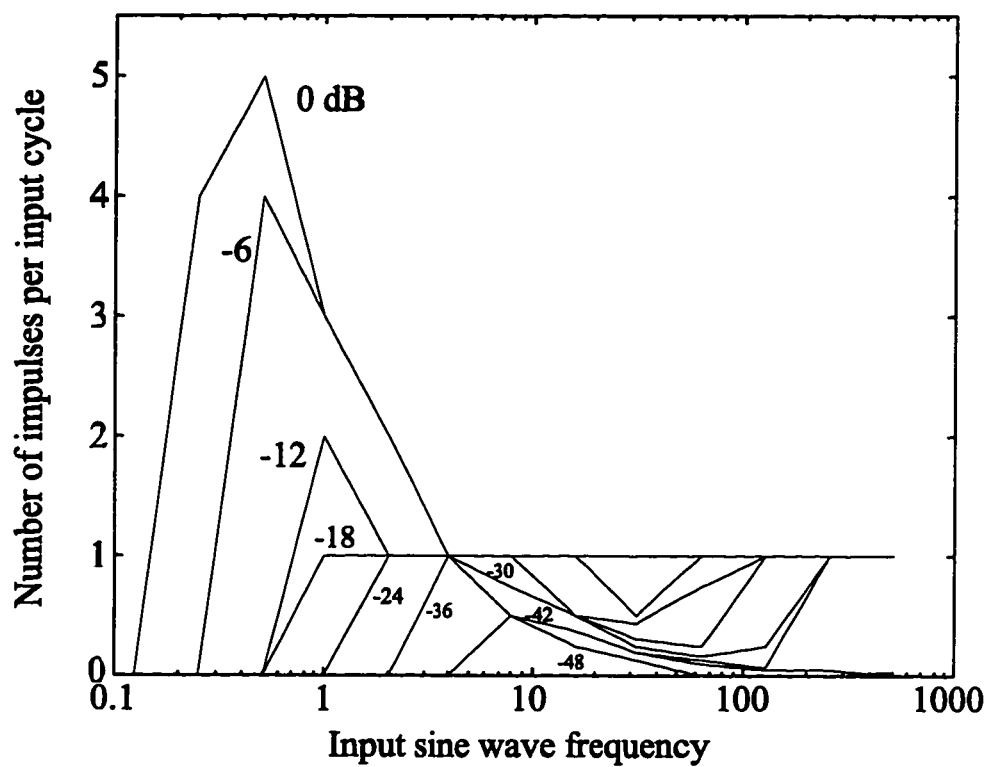
Figure 4-9: Frequency response function of the 'damper' model using the modified version of the Hodgkin-Huxley equations (see text for details). 0 dB corresponds to the maximum input amplitude considered.
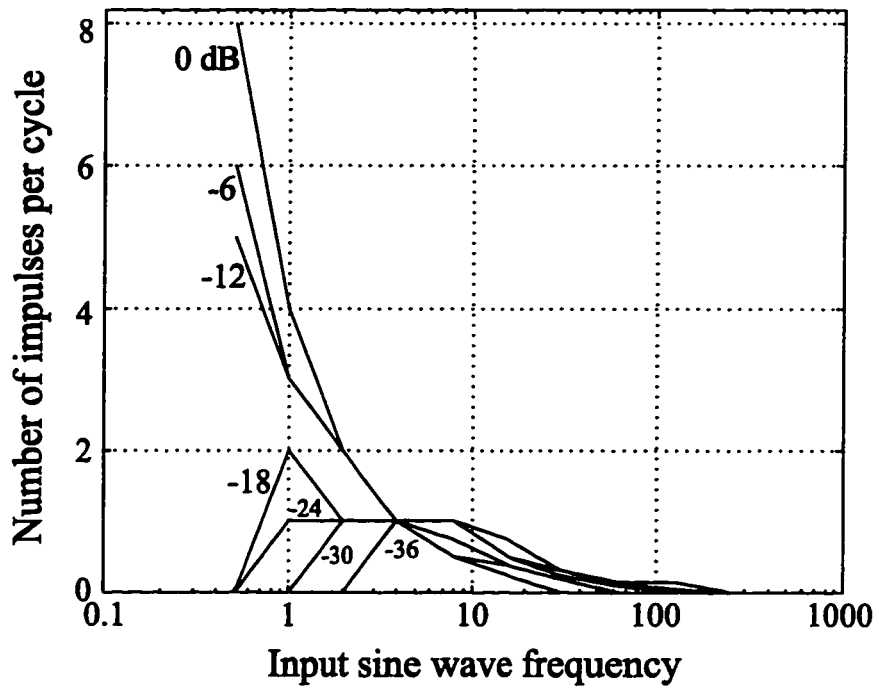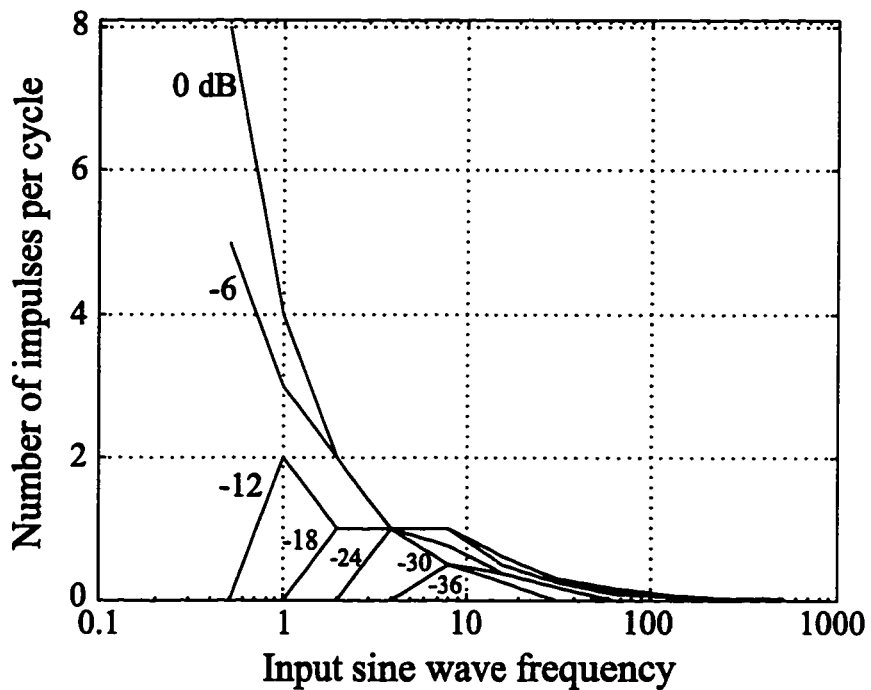
Figure 4-10: Frequency response function of the SA models. (a) SAI model. (b) SAII model. 0 dB corresponds to the maximum input amplitude considered.
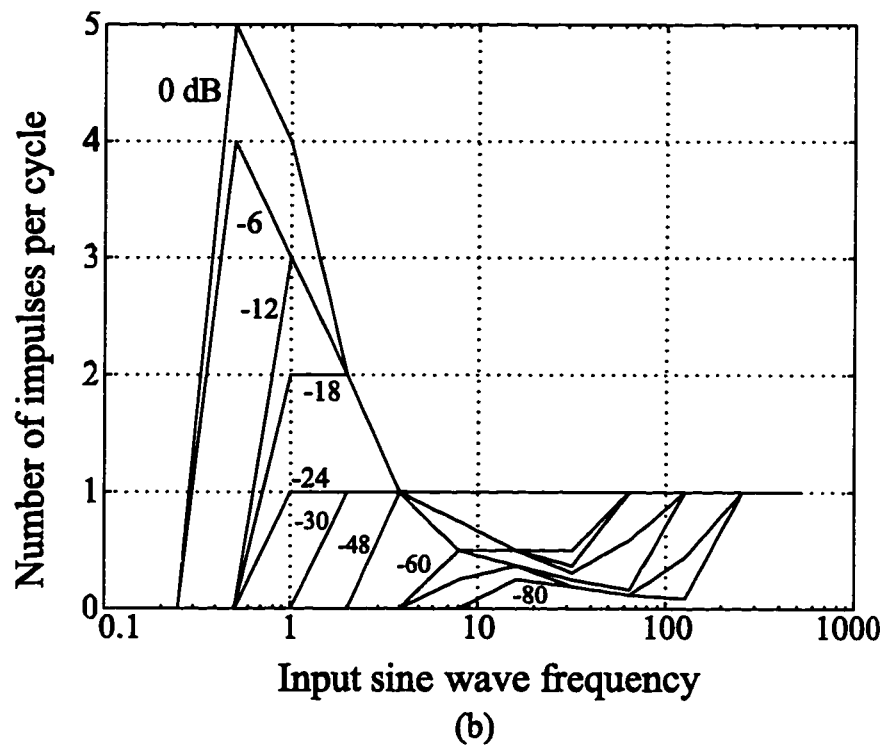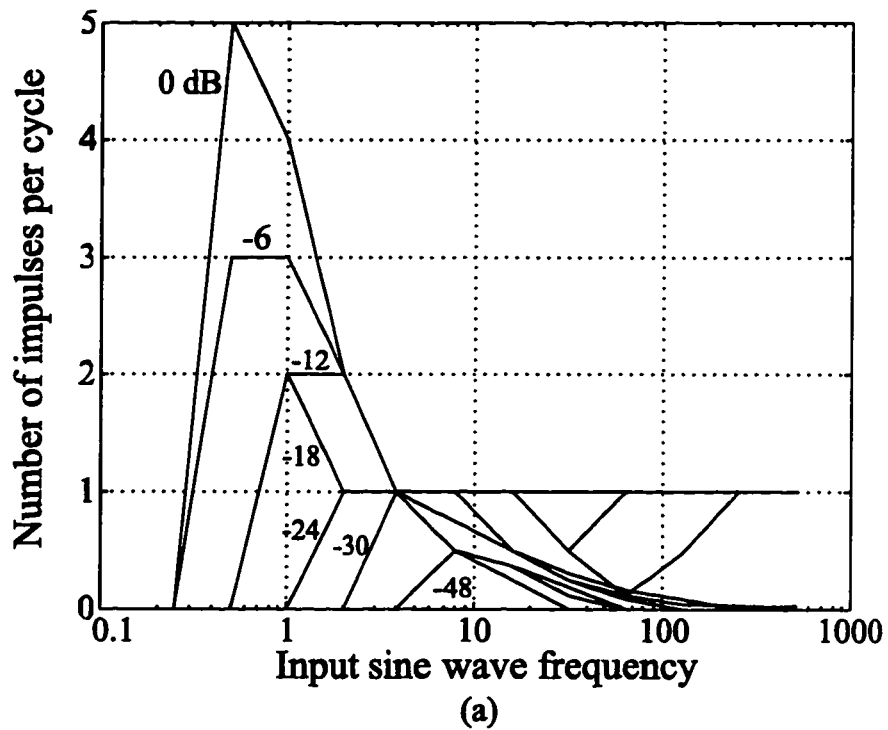
Figure 4-11: Frequency response function of the FA models. (a) FAI model. (b) FAII model. 0 dB corresponds to the maximum input amplitude considered.

98
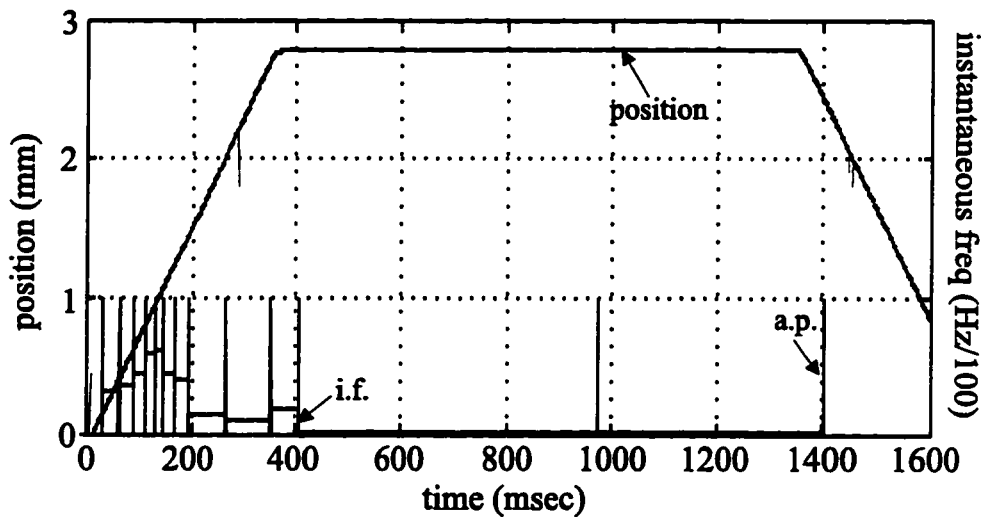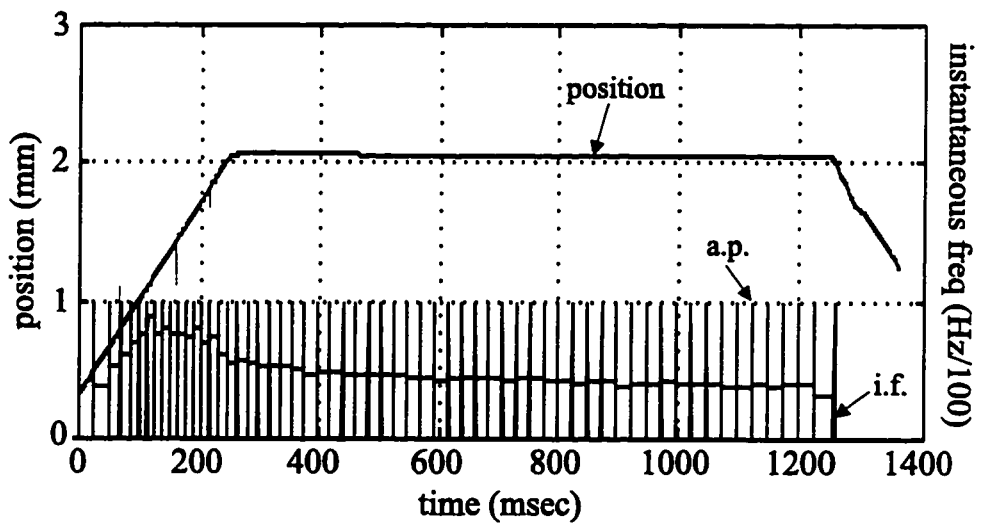
Figure 4-12: Typical neurophysiological response of SA type units at a ramp speed of 8 mm/sec. Position, appearance of an action potential (indicated by a vertical line of constant height) and instantaneous frequency are shown. Only that portion of the position trajectory in contact with the skin is displayed. (a) Response of a SAI unit; the stimulus was applied adjacent to the center of the receptive field. (b) Response of a SAII unit; the stimulus was applied at the center of the receptive field. Unpublished data from Roland Johansson's group (Umeå University, Sweden).
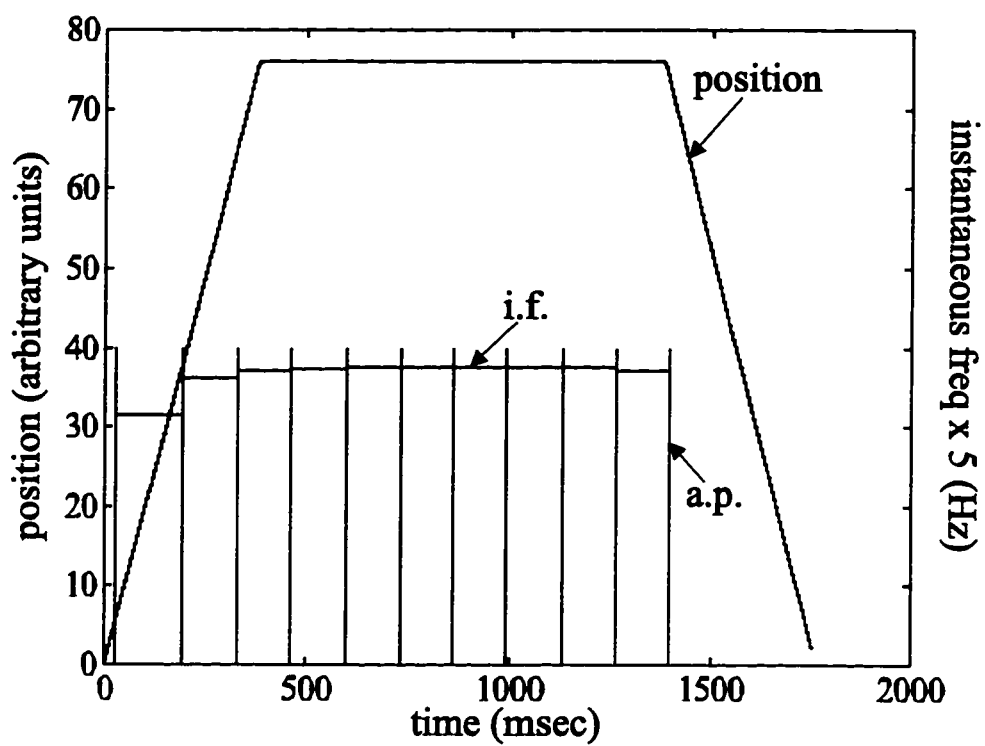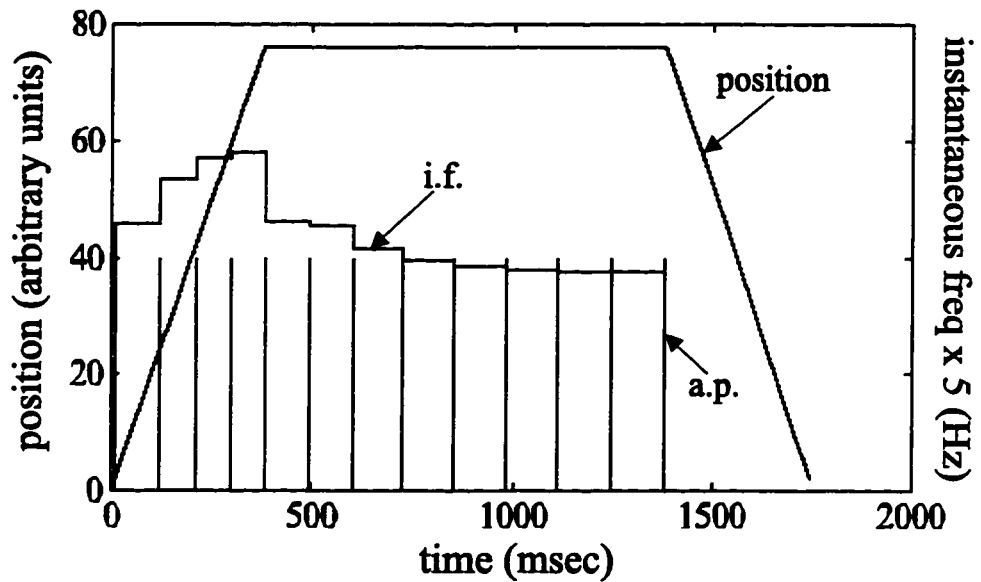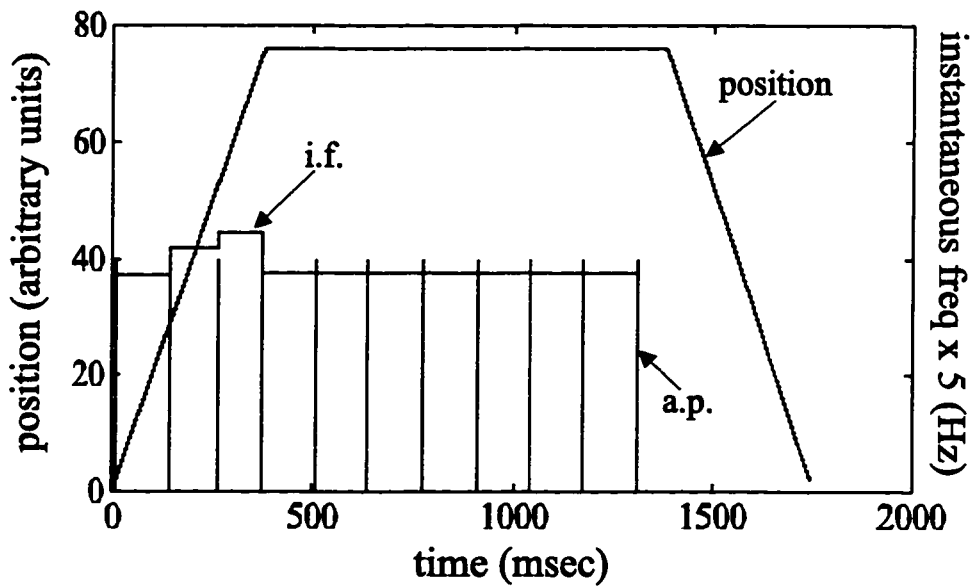
Figure 4-13: Simulation response of the modified Hodgkin-Huxley equations (i.e., our simple spring model) to a ramp and hold. Position, appearance of an action potential (indicated by a vertical line of constant height) and instantaneous frequency are shown.
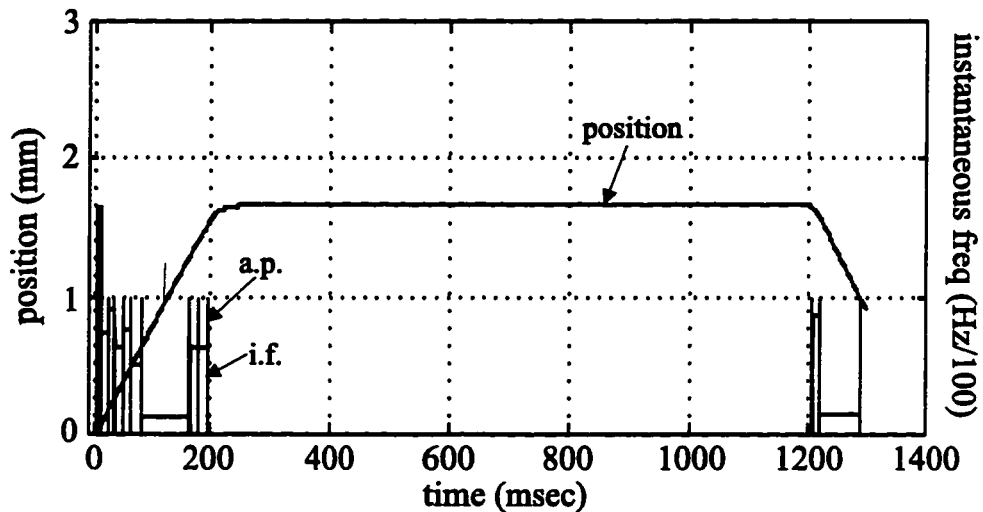
Figure 4-14: Simulation response of SA models to a ramp and hold. Position, appearance of an action potential (indicated by a vertical line of constant height) and instantaneous frequency are shown. (a) Response of the SAI model. (b) Response of the SAII model.
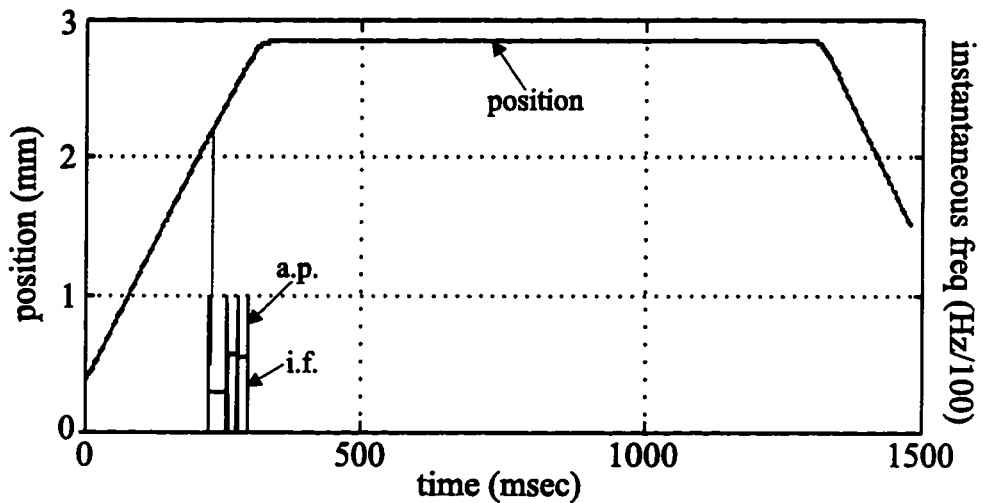
Figure 4-15: Typical neurophysiological response of FA type units at a ramp speed of 8 mm/sec. Position, appearance of an action potential (indicated by a vertical line of constant height) and instantaneous frequency are shown. Only that portion of the position trajectory in contact with the skin is displayed. (a) Response of a FAI unit; the stimulus was applied at the center of the receptive field. (b) Response of a FAII unit; the stimulus was applied further away from the center of the receptive field. Unpublished data from Roland Johansson's group (Umeå University, Sweden).
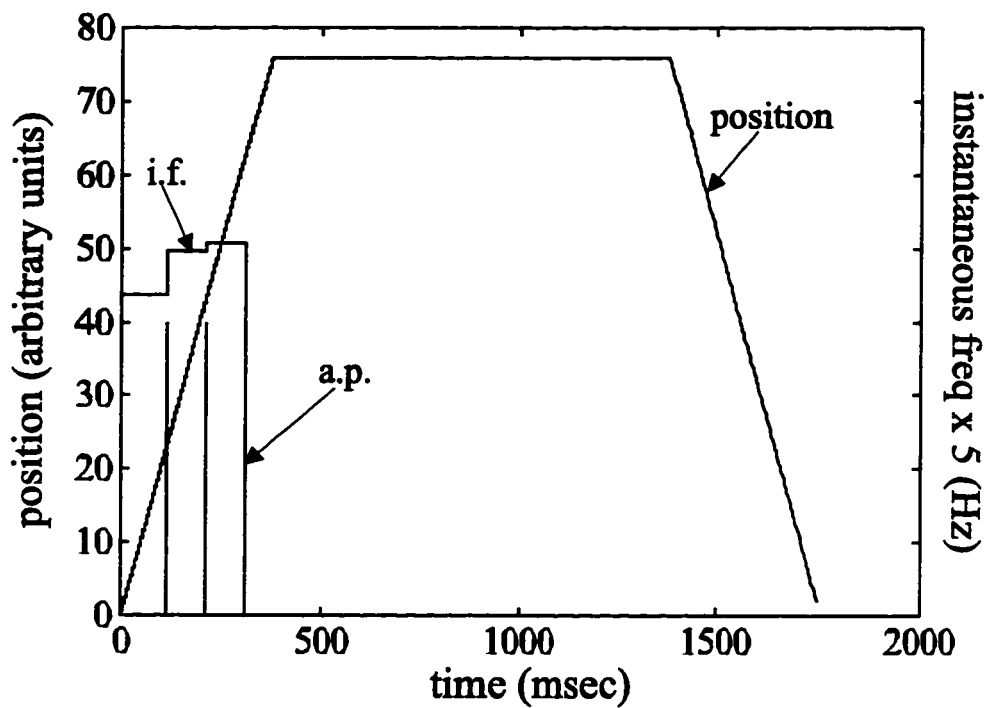
Figure 4-16: Simulation response of the simple 'damper' model to a ramp and hold. Position, appearance of an action potential (indicated by a vertical line of constant height) and instantaneous frequency are shown.
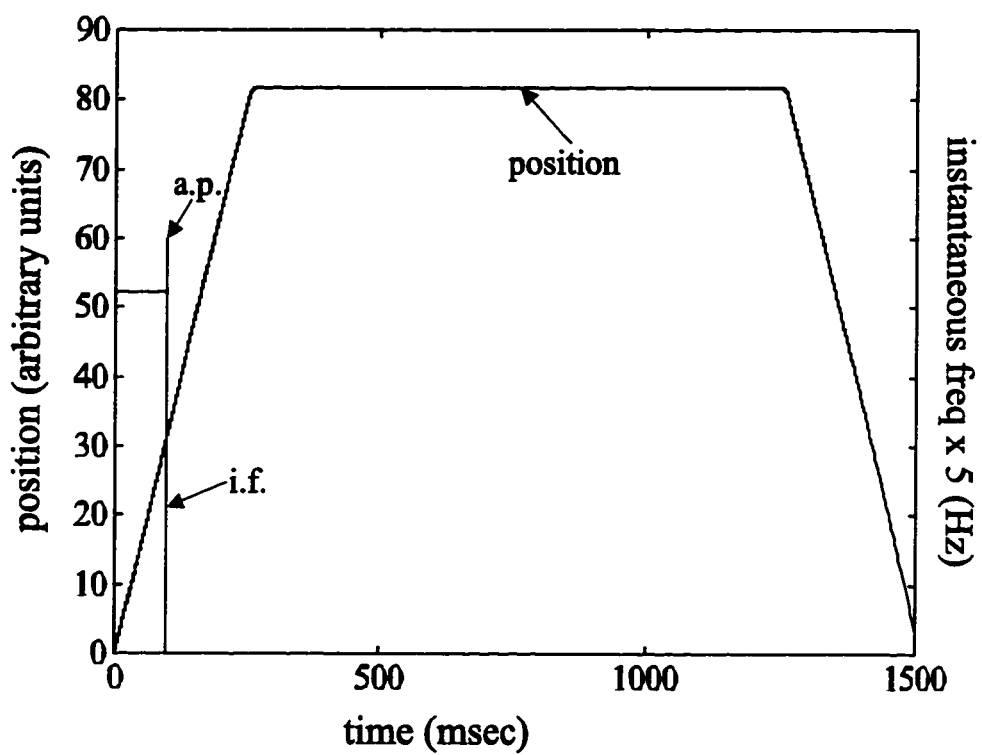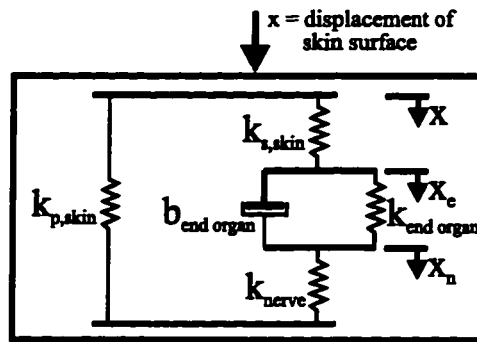
Figure 4-17: Simulation response of the FAI model to a ramp and hold. Position, appearance of an action potential (indicated by a vertical line of constant height) and instantaneous frequency are shown.
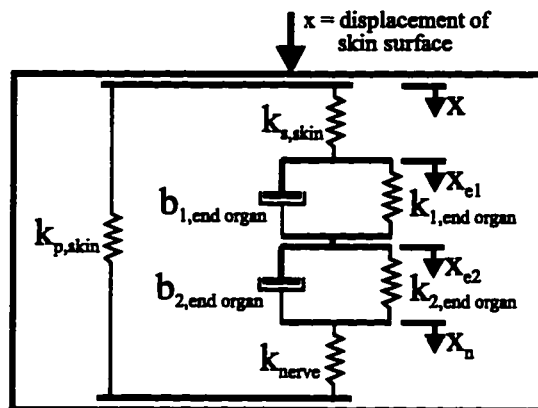
Figure 4-18: Proposed models to account for the response to force inputs as well as displacement inputs. (a) Model of the SAI and SAII units. (b) Model of the FAI and FAII units. When displacements are applied to the surface of the skin, the parallel spring does not have an effect and the response is as before. When forces are applied to the surface of the skin, the parallel spring does have an effect.

Chapter 5

Discussion

In this thesis we considered the modeling of the two major components of the peripheral tactile system separately. First we considered the dynamic interaction between the fingerpad and a flat object upon contact. The bulk response of the fingerpad was found to consist of an exponentially increasing stiffness component and an exponentially increasing damping component, as a function of indentation displacement. Both of these components appeared to increase in parallel. This allowed the force response of the fingerpad to be described by a nonlinear instantaneous elastic response combined linearly with a linear force relaxation, similar to other soft tissues [12, 55].

Examining the distributed pressure response of the fingerpad using a distributed pressure array sensor suggested that locally, a small area of the fingerpad also consisted of an exponentially increasing stiffness component and an exponentially increasing damping component. This was perhaps not too surprising given that Fung's original model was for isolated tissues of constant cross-sectional area. However, it was not expected that the resulting bulk fingerpad response could also be explainable by this type of model given the significant change in contact area upon indentation. Combining Fung's quasi-linear viscoelastic model for tissues of constant cross-sectional area with a Hertzian contact model appeared to adequately explain the distributed pressure data. It was also shown why this

106

model was consistent with the previously developed model of the lumped fingerpad response.

We then considered what was happening beneath the surface of the skin. Here we restricted our analysis to a one dimensional model, only considering the response of the peripheral tactile system to vibrating stimuli applied by a flat probe covering most, if not all, of the receptive field. Considering the system as a whole, we found that simple linear models of the skin and end organ mechanics combined with the Hodgkin-Huxley equations could capture the essential properties of the frequency responses of the four different types of receptors to displacement sinusoids. In light of additional data, particularly the response of the mechanoreceptors to force inputs [25], modifications to the models have been proposed.

5.1 Relation Between the Two Models

One result of our holistic model of the temporal response of the peripheral tactile system is the suggestion that the skin can be modeled as a simple linear spring. This was unexpected given that our biomechanical results showed noticeable velocity dependence (i.e., damping) and significant nonlinearities with indentation depth (see Figure 5-1).

One possible explanation of why the nonlinearities of the skin do not affect the response is based on observations about the mechanical components of the model. First, let us consider the SA model for displacement inputs (Figure 5-2) ignoring the damping component of the end organ for now. If we assume that both the skin and the end organ can be modeled as typical soft tissues then we can model the stiffness of each of these components as a linear function of applied force:

$$k_{skin} = m_{skin} F_{skin} + b_{skin} \tag{5.1}$$

and

$$k_{end\,organ} = m_{end\,organ} F_{end\,organ} + b_{end\,organ} \tag{5.2}$$

where k_i is the stiffness of the tissue, F_i is the force applied, and m_i and b_i are parameters of the linear relation. The ratio between these two stiffnesses is

$$\frac{k_{skin}}{k_{end\,organ}} = \frac{m_{skin}F_{skin} + b_{skin}}{m_{end\,organ}F_{end\,organ} + b_{end\,organ}} \tag{5.3}$$

Let us assume that the initial stiffness upon contact is approximately zero, i.e.,

$$b_{skin} \approx 0 \tag{5.4}$$

$$b_{end\,organ} \approx 0, \tag{5.5}$$

as was true for the fingerpad response; note that this still allows very different force-displacement relationships for the different components, although they will be qualitatively similar. For this simplified receptor model the springs are in series and therefore

$$F_{skin} = F_{end\,organ}, \tag{5.6}$$

resulting in

$$\frac{k_{skin}}{k_{end\,organ}} = \frac{m_{skin}}{m_{end\,organ}}. \tag{5.7}$$

Hence the ratio between these two components remains constant despite their nonlinear and different force-displacement curves.

In this model, the generator current is proportional to the displacement of the nerve membrane

$$x_{nerve} = \frac{k_{skin}k_{end\,organ}}{k_{nerve}(k_{skin} + k_{end\,organ})}x_{in} \tag{5.8}$$

If we further assume that the stiffness of the nerve membrane also linearly increases with

108

force then the ratio relating x_{in} to x_{nerve} is a constant. Consequently, the nonlinearities of the individual mechanical components have no effect on the model's neural response.

We then can consider any *nonlinear effect* of the damping component by noting that typically for soft tissues the damping appears to increase in parallel with the stiffness, maintaining a fixed time constant. If we assume that this is also true for the end organ, then it follows that the ratio of all the mechanical components remains constant despite the nonlinearities. A similar analysis can be performed for the FA Unit model.

We acknowledge that the mechanoreceptor end organs may not be adequately modeled by a bulk tissue model and that more complicated models may be needed (in particular, taking into account the membrane structure). In addition, it may not be appropriate to model the nerve membrane as a nonlinear spring. This is only offered as a possible explanation of why the nonlinear stiffness of the skin does not appear to be important for the mechanoreceptors' responses to displacement inputs. However, it does predict that the nonlinearity of the skin (in particular the parallel element in our proposed models) will affect the response of the mechanoreceptive units to force inputs applied to the surface of the skin. This remains to be confirmed in further analysis of the response of the receptors to force inputs.

There may be additional reasons why the nonlinearities of the skin do not appear to be important for the temporal response of the mechanoreceptors. Furthermore, the above reasoning cannot explain why the viscosity of the skin (which is significant) does not appear to be a necessary component as well. One potential contributing factor is suggested by the analysis of our models to variations in input amplitude for sinusoidal inputs. For this analysis we determined how much we could vary the input amplitude for our simulations in Chapter 4 and still produce the same mean firing rate as for the points examined in our simulations (i.e., amplitudes decreasing by factors of 2, and frequencies varying from 0.5 Hz to 512 Hz).

The results of this analysis considering only the neural component (i.e., assuming the

mechanical component is only composed of springs) are shown in Figure 5-3. The amount by which the input amplitude can vary and still produce the same mean firing rate can be quite large, particularly at higher amplitudes.[1] This suggests that it may be possible for nonlinearities and damping effects of the skin to be obscured in the final output measure.

One interesting issue which this latter consideration raises is whether the nonlinearities and damping effects of the skin are really insignificant or whether measuring the mean rate is an insufficient measure of the response. An additional parameter, such as phase may be appropriate to consider. One way to test whether the mean rate is insufficient is suggested by the experimental neurophysiology data. As previously mentioned, the responses tended to converge to the same number of impulses per cycle regardless of the input amplitude at higher frequencies. If mean rate was the only code used, then we would predict that relative differences in the amplitude of vibrational stimuli at high frequency are poorly perceived. For example, we would not expect people to be able to discriminate between a 1 mm peak-to-peak, 256 Hz sinusoid and a 0.25 mm peak-to-peak, 256 Hz sinusoid.

5.2 Future Work

The next logical step is to connect these two models together to examine the complete response of the peripheral tactile system to a spatiotemporal input, such as contact with a flat side of a box. This is very exciting as it will allow us to examine the population responses of the tactile receptors which are densely distributed in the fingertip. Experimentally, this can only be approximated by serially scanning an object across the receptive field of a single tactile receptor, due to the difficulty in locating receptors on the same fingerpad from which to record. However, the contact location does not remain constant, which potentially can

---

[1]For 128 Hz and higher frequency, the amount by which the input amplitude could change to produce the same mean firing rate was quite small, even at higher amplitudes. However, the signal itself is essentially zero if we are to put it in a form comparable to the experimental data of Johansson and his colleagues [26], i.e., in impulses/cycle. We have therefore not included higher frequencies in our analysis. For the FA units, where the signal is significant at higher frequencies, both the model and the data show a convergence of the response to the same mean rate regardless of the input amplitude.

change the mechanics of interaction. With our model we should be able to make predictions that can be verified with relatively sparse data (from receptors at different locations on the same fingerpad); therefore, the contact location could be held fixed.

In addition, we can consider the response of the combined model using the general form of the distributed biomechanics model. This would allow us to make predictions for the responses of the mechanoreceptor populations to changes in curvature (i.e., variations in the spherical radius) and compliance of an object, two important object properties in tactile sensing and manipulation.
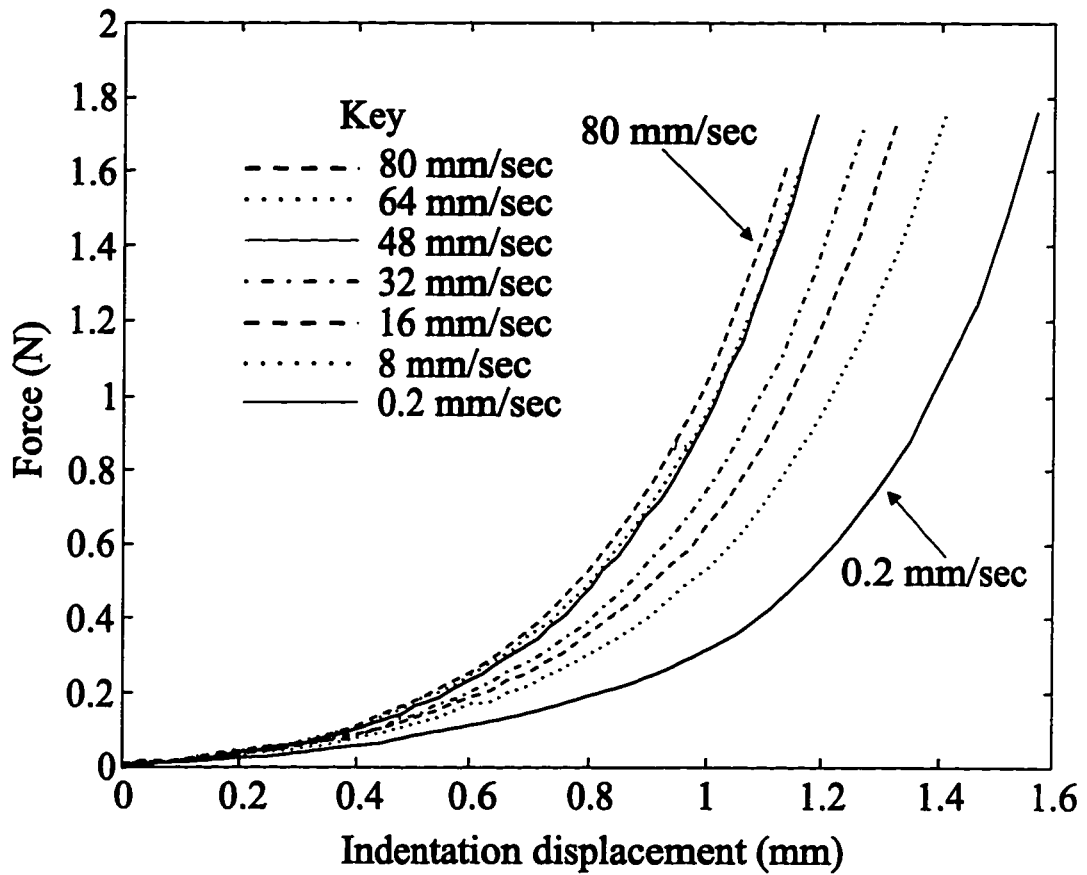
Figure 5-1: Response of the fingerpad of a typical subject to indentations of constant velocities. Data at each speed are from four trials which were geometrically averaged.
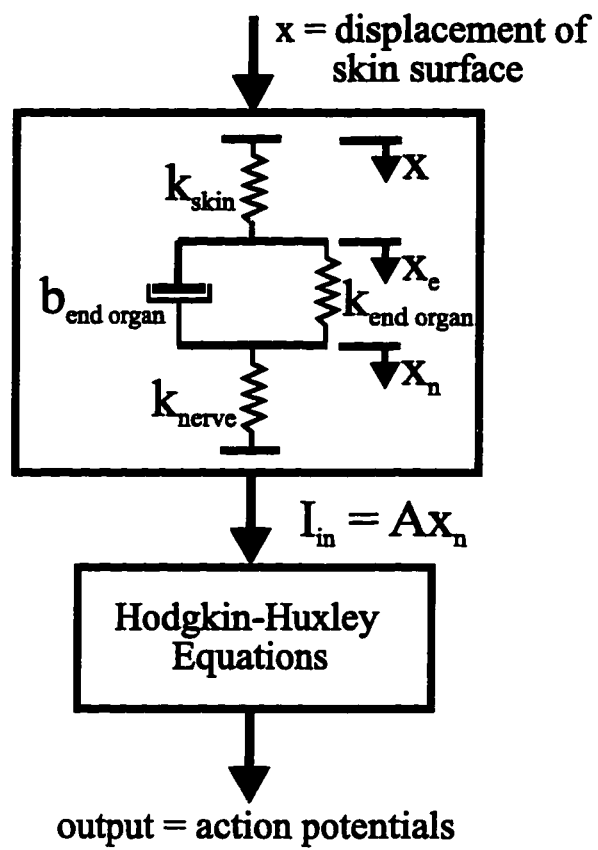
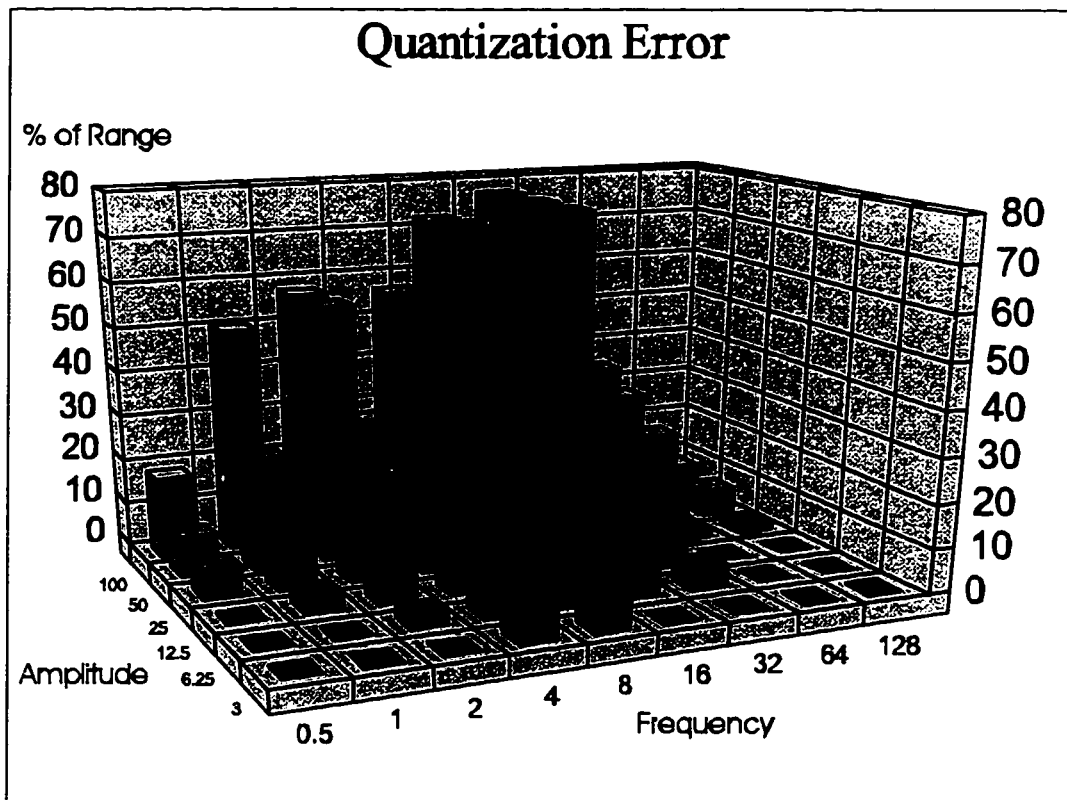Figure 5-2: Model of the SA Units in response to displacement inputs.

Figure 5-3: Amount by which the input amplitude can vary and still produce the same mean rate. Values for which there was no response are set to zero. Above 64 Hz the firing rate was very low per input cycle (less than 1 in 16); therefore, only 128 Hz was examined above this frequency.

Appendix A

Pressure Sensor Calibration

The tactile sensor used to measure the distributed response was designed and constructed by J.S. Son, P.S. Wellman and W.J. Peine. In order to use this sensor to make biomechanical measurements, we thoroughly calibrated its response. Here we briefly describe the sensor's construction and then provide the details of the calibration procedures.

A.1 Device Design

The design is based on capacitive tactile array sensors developed for robotic applications. These sensors consist of orthogonal layers of copper strips separated by a dielectric. Applying pressure to the sensor's upper surface forces the copper strips closer together, increasing the capacitance at the cross-points, each of which forms one array element. The change in the measured capacitance of the element is closely proportional to the local pressure above it [9]. Using a linear and nonhysteretic dielectric and decreasing its height can significantly increase the sensitivity of the sensor.

The device which was used is a flat 8 element by 8 element sensor array with an elemental spacing of 2 mm (see Figure A-1). This design uses thin strips of silicone rubber to separate the layers of copper strips, with air as the dielectric. The array was covered with a 2.0 mm

layer of elastomer (GE RTV 110 Silicone Rubber Adhesive Sealant) to protect it from mechanical damage. It was electrically shielded by grounding the rigid back plane on which it was mounted, and by embedding a thin layer of gold foil in the elastomer which was also grounded. The sensor is characterized assuming both the rigid back plane and protective elastomer as integral components of the device.

The sensing electronics are based on a design by Fearing [9]. The elements are serially scanned by applying a 200 kHz sine wave to the column of an element and demodulating the output from the corresponding row. All unused rows and columns are grounded to reduce cross talk. For the tests reported here, as well as the biomechanical experiments, the entire array was scanned at 200 Hz (corresponding to an inter-element sampling rate of 13.5 kHz), although rates of up to 400 Hz can be used.

A.2 Sensor Performance

The key performance parameters for a distributed pressure sensor for biomechanical applications are the time response, the spatial response and the absolute sensitivity, usually limited by noise, hysteresis and linearity [21]. Low noise is particularly important when examining fingers as the pressures of interest are often small ($\leq$ 50 kPa). The noise of the sensing elements was gaussian with a standard deviation of 0.5 kPa ($\approx$ 1.2 g per element). Resolutions below this noise level can be achieved by integration.

Low hysteresis is essential for accurate measurements and linearity is desirable for ease of calibration and data analysis. Performance was evaluated by examining the correspondence between the capacitance of each element and the local pressure using a pneumatic static pressure chamber. Pressure was increased from 0 to 60 kPa in steps of 10 kPa, then decreased in the same manner. A silicon pressure transducer (SenSym 142SC15D: maximum deviation from linearity of 0.75%, typical repeatability and hysteresis of 0.2%) recorded the chamber pressure. The responses of the elements fit a linear response (see Figure A-2) with a worst

case element mean squared error (m.s.e.) of 0.4% and a maximum deviation from linearity of 4%. Hysteresis was below the noise level. Figure A-2 also shows that any hysteresis is below the noise level of the sensor. As a verification of the gain calibration procedure, the sum of the calibrated pressure measurements during a contact experiment was compared to the net force measured with a separate force sensor with a resulting m.s.e. = 0.2% (see Figure A-5).

Viscoelastic properties can limit the time response of the sensor, even with fast electronics. The response time was measured by rapidly removing a brass weight from the surface of the sensor using a lever mechanism. A typical resulting temporal response for a pressure element is shown in Figure A-3. The response for all of the elements is within 80% of its final value in less than a single sample (i.e., 5 msec).

The spatial resolution of a sensor may be limited by coupling between the array elements and the spatial summation across an element. The spatial impulse response function for a single element was obtained by indenting the array sensor with a rounded 1.5 mm diameter probe to a constant depth at increments of 0.25 mm in the x and y directions (five trials at each position). A typical impulse response of one of the elements along the x-axis of the sensor is shown in Figure A-4; the y-axis response is similar.

This response data may be closely approximated by a gaussian:

$$f_{spatial}(x) = \frac{A}{\sqrt{2\pi}\sigma}e^{-x^2/2\sigma^2} \tag{A.1}$$

where A is the gain, σ describes the width of the response function, and x corresponds to the distance from the center of the element; for the given data, $A = 80$ and $\sigma = 0.96$ mm. The proportion of the signal applied to a given element which is coupled into an adjacent element in the same row and column is less than 8% and in the diagonal directions is less than 1%. The spatial response, including the degree of coupling, can be changed with the thickness of the top layer [9].

117

The linearity of the spatial response was confirmed by the invariance of the inter-element coupling with load and successful superposition of two indentations applied to adjacent elements. Since the response is uniform and linear, the spatial impulse response can be used to deconvolve the signal, limited by noise. This can correct the measured pressures for spatial coupling between elements and spatial summation within an element, improving the accuracy of the measurements. Alternatively, if a model of the measured pressures is available, the predicted response can be convolved with the spatial impulse response (as in the following section) to account for spatial effects.

A.3   Verification of Sensor Response

As an independent verification of our sensor calibration, we verified the overall array sensor response by experimentally measuring the quasi-static pressure distribution generated by contact with a rubber ball ($R_b = 31$ mm, $E_b = 540$ kPa). For small, static displacements the response is expected to be linearly elastic and predicted by the Hertz theory of elastic contact for solids of revolution [29]. This theory predicts the radial symmetric distributed pressure response, $p(r)$, as a function of indentation depth, δ, and radial distance from the center of contact, r:

$$p_{Hertz}(r) \;\; = \;\; \frac{2E^*}{\pi R}(R\delta - r^2)^{\frac{1}{2}} \tag{A.2}$$

where

$$\frac{1}{E^*} = \frac{1 - \nu_b^2}{E_b} + \frac{1 - \nu_a^2}{E_a}. \tag{A.3}$$

The modulus of elasticity of the array sensor, E_a, was 1 MPa, and both the ball and the array sensor were assumed incompressible ($\nu_b = \nu_a = 0.5$). The fraction $\frac{1}{R}$ is a constant describing the relative curvature of the two surfaces. Since, in our case, the array sensor is

118

flat, the relative curvature is defined by the radius of the rubber ball.

Experimentally, the ball was mounted rigidly in a machinist's vise and a flat tipped, motorized indentor applied controlled indentations normal to the ball surface. A force sensor on the tip (maximum noise $\approx$ 0.1 N) measured the net force, and a magneto-resistive position sensor (maximum noise $\approx$ 0.02 mm) located on the motor shaft measured the indentation distance. The tactile array sensor described above was mounted in front of the force sensor and measured the pressure distribution.

The sensor was indented into the rubber ball at a rate of 0.2 mm/sec to emulate static conditions (four trials). The center of contact, to which all element positions were referenced, was calculated as the pressure centroid at a net force of about 2.5 N. The pressure distribution at one force level from one trial is shown in Figure A-5. Since the response was radially symmetric about the center of contact (as predicted by the theory), the pressure distribution is shown as a function of the radial distance from the center of contact. It is readily apparent from the data that the experimental response is qualitatively very similar to the parabolic shape characteristic of Hertz contact. However, it should also be noted that the data exhibits 'tails' towards the edges of contact which are not predicted by the theory. This is not unexpected given the spatial impulse response of the array sensor elements.

We fit the data to the predicted response, taking into account the spatial impulse response of an array sensor element:

$$p_{predicted}(r, \theta) = p_{Hertz}(r) * f_{spatial}(r, \theta) \qquad (A.4)$$

where $p_{Hertz}(r)$ is defined in Equation A.2 and $f_{spatial}(r, \theta)$ is the 2-D representation of Equation A.1. The least squares error was minimized using a simplex search on R and E_b for all δ. The resulting fit had a m.s.e. of 5.5% with $R = 32.6$ mm and $E_b = 570$ kPa. The fit to the distributed response as well as to the net force response (m.s.e. = 3%) is shown in Figure A-5. The actual response is very similar to the filtered Hertz contact model, including

119

the presence of 'tails' towards the edges. In addition, the parameter values determined for

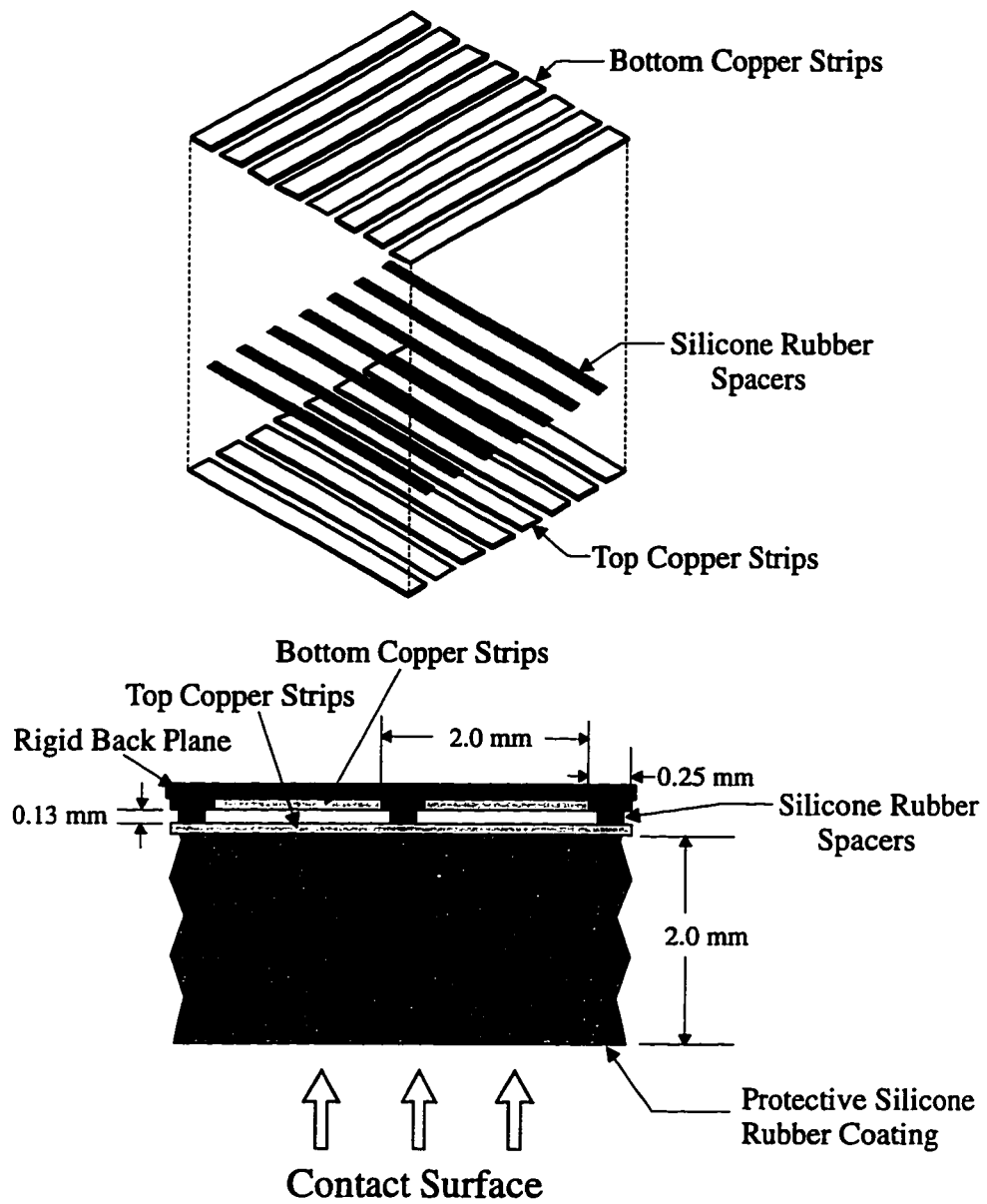R and E_b were within 6% of their actual values.

Figure A-1: Tactile array sensor. Top: exploded view showing sensor construction. Bottom: side view showing the crossed layers of copper strips separated by silicone rubber spacers. A protective rubber coating is added on the contact surface.
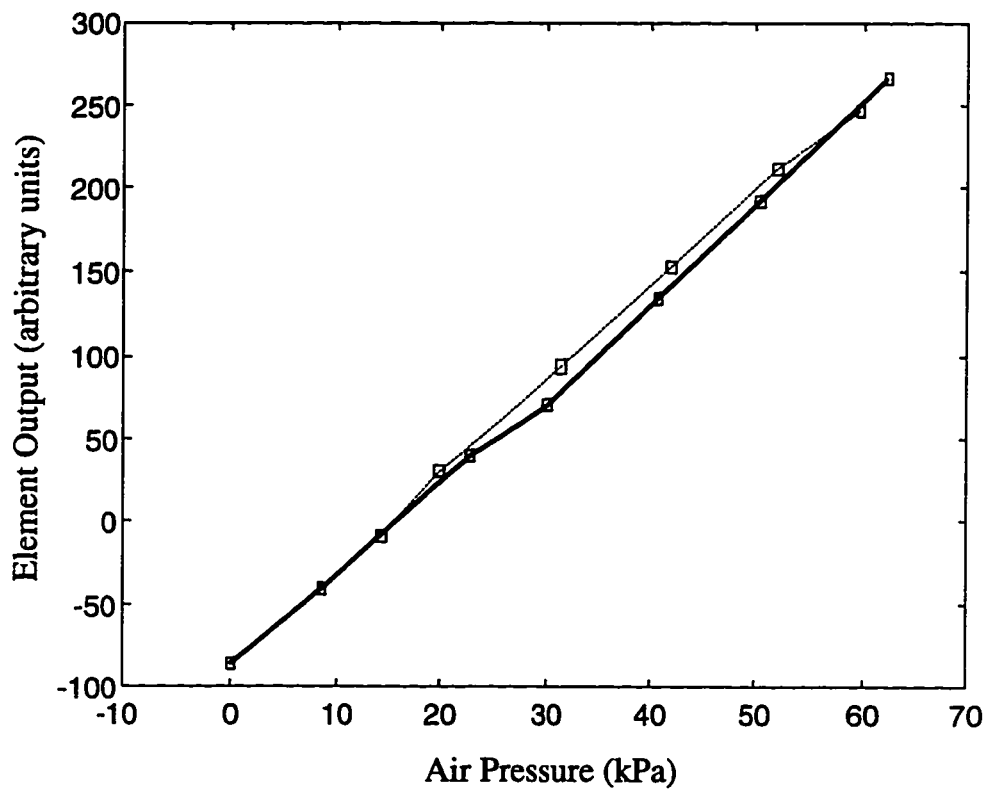
Figure A-2: Linearity and hysteresis. Correspondence between pressure applied and element value measured. Solid line shows ascending values. Dotted line shows descending values. The size of each box indicates the error at each sampling point.
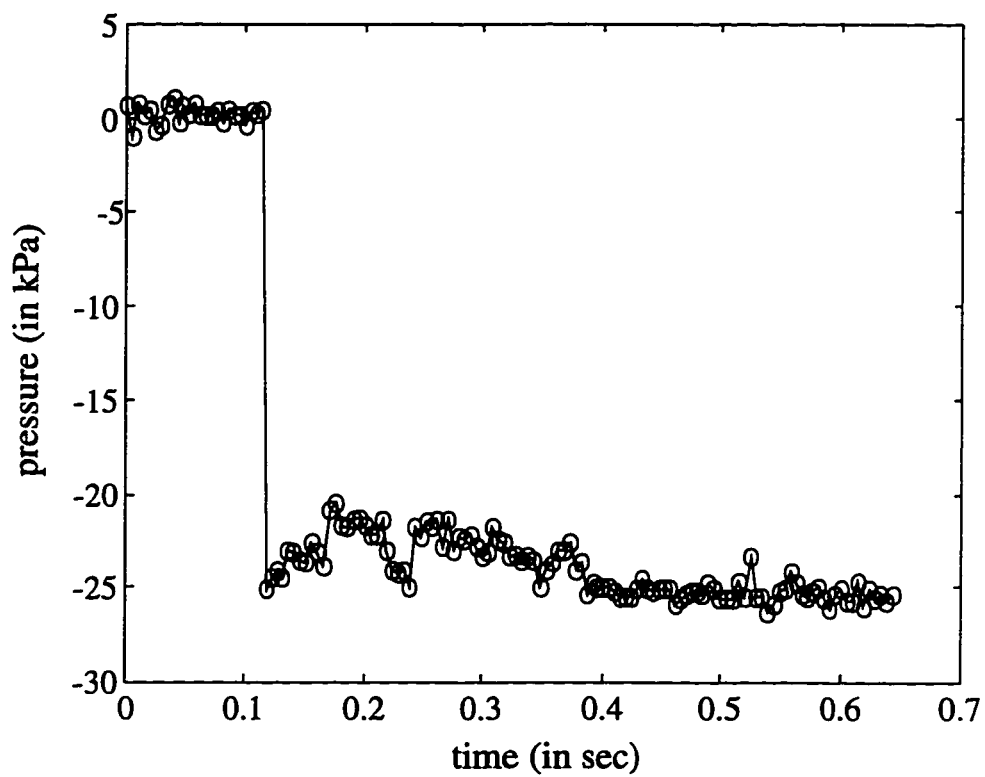
Figure A-3: Typical temporal response of an individual pressure element. Results are from the rapid removal of a load from the array sensor. Pressure values are referenced with respect to the load condition. Circles indicate individual sample points.
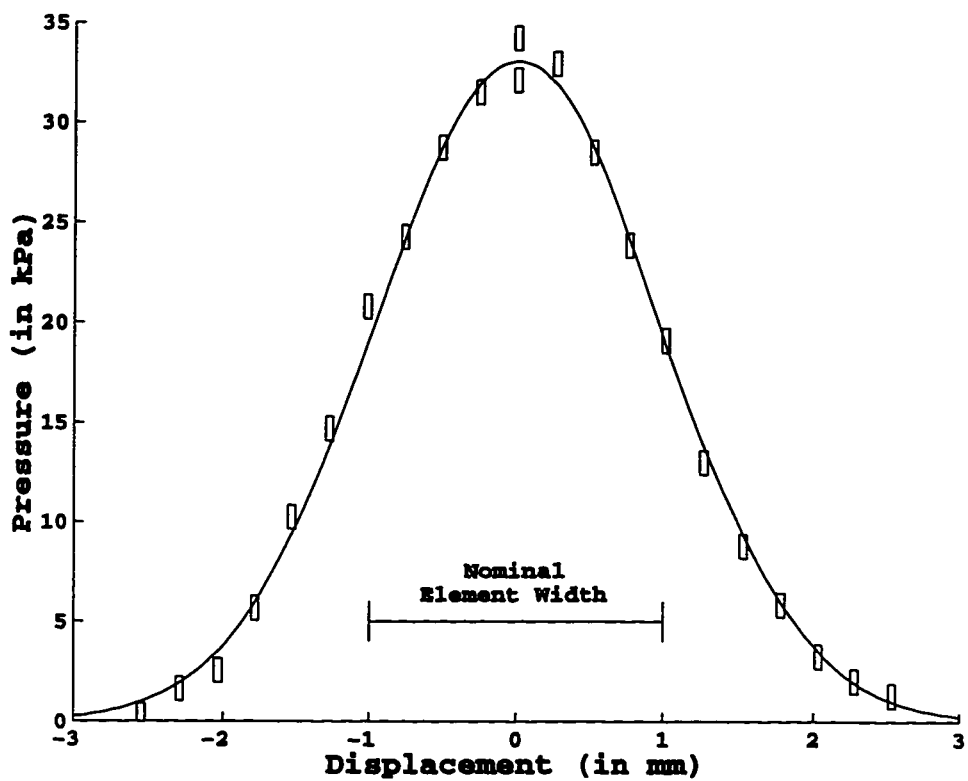
Figure A-4: Typical spatial impulse response of one element. Lateral displacements of the indentor are referenced from the center of the element. The size of the boxes indicates the error at each sampling point. The solid line shows a least squares fit of a gaussian function to the data, $\sigma = 0.96$ mm.
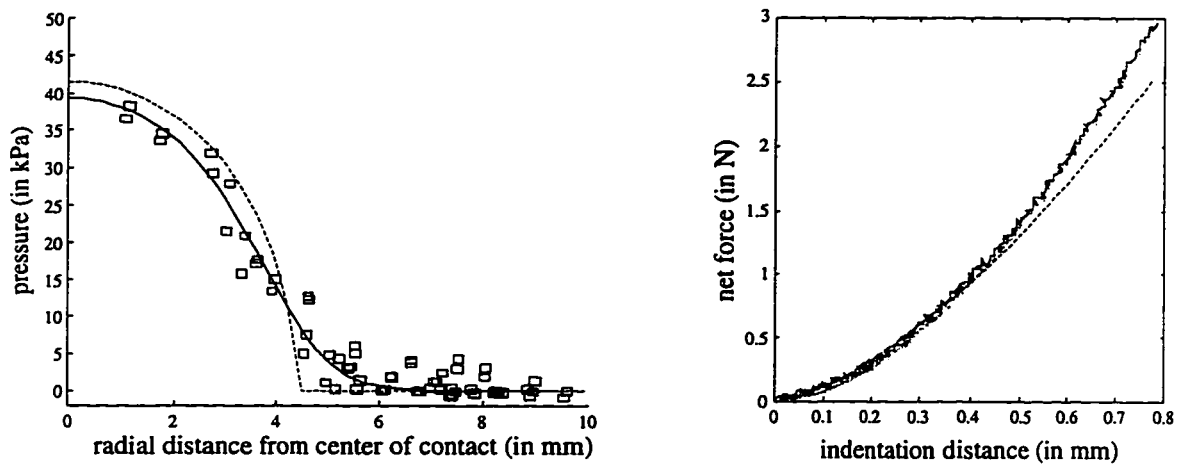
Figure A-5: Quasi-static contact with a rubber ball (radius = 31.0 mm). Left: distributed pressure response at one indentation depth (0.59 mm, corresponding to a net force of 1.8 N); the size of the boxes indicates the error. The solid line shows the least squares fit of a Hertz contact function taking into account the spatial response of the array sensor. The dashed line shows the corresponding unfiltered Hertz contact response. Right: net force response. The solid and dotted lines compare the sum of the response of the pressure elements to the net force measured with the force sensor. The dashed line shows the response predicted by Hertz theory for the estimated parameters.

Appendix B

Equations for the Holistic Models

This appendix contains the equations used for the simulation of the holistic models of mechanoreception (Chapter 4).

B.1 Neural Equations

B.1.1 Initial Model

The models of the nerve fibers were based on the Hodgkin-Huxley equations [19]. The initial model used for the preliminary mechanoreceptor models (see Section 4.2) was the standard Hodgkin-Huxley equations at 6.3°C. These are given by:

$$I_{in} = C_M \frac{dV}{dt} + \bar{g}_K n^4 (V - V_K) + \bar{g}_{Na} m^3 h (V - V_{Na}) + \bar{g}_l (V - V_l) \tag{B.1}$$

$$\frac{dn}{dt} = \alpha_n (1 - n) - \beta_n n \tag{B.2}$$

$$\frac{dm}{dt} = \alpha_m (1 - m) - \beta_m m \tag{B.3}$$

$$\frac{dh}{dt} = \alpha_h (1 - h) - \beta_h h \tag{B.4}$$

$$\alpha_n = 0.01(V+10)/(exp(\frac{V+10}{10})-1) \qquad \text{(B.5)}$$

$$\beta_n = 0.125exp(\frac{V}{80}) \qquad \text{(B.6)}$$

$$\alpha_m = 0.1(V+25)/(exp(\frac{V+25}{10})-1) \qquad \text{(B.7)}$$

$$\beta_m = 4exp(\frac{V}{18}) \qquad \text{(B.8)}$$

$$\alpha_h = 0.07exp(\frac{V}{20}) \qquad \text{(B.9)}$$

$$\beta_h = 1/(exp(\frac{V+30}{10})+1) \qquad \text{(B.10)}$$

where V is the membrane potential (depolarzation positive) (mV), I is the membrane current density (μA/cm^2) and t is time (msec).

Parameters

$$C_M(\mu F/cm^2) = 1.0 \qquad \text{(B.11)}$$

$$V_{Na}(mV) = +115 \qquad \text{(B.12)}$$

$$V_K(mV) = -12 \qquad \text{(B.13)}$$

$$V_l(mV) = +10.613 \qquad \text{(B.14)}$$

$$\bar{g}_{Na}(mmho/cm^2) = 120 \qquad \text{(B.15)}$$

$$\bar{g}_K(mmho/cm^2) = 36 \qquad \text{(B.16)}$$

$$\bar{g}_l(mmho/cm^2) = 0.3 \qquad \text{(B.17)}$$

The correctness of the implementation was verified with the results of Hodgkin and Huxley for single action potentials [19] and the results of Stein for constant current inputs [51].

The generator current, I_{in}, was assumed to be linearly related to the displacement of the nerve membrane (see text for details, Section 4.2.1)

$$I_{in} = A x_{nerve} \qquad \text{(B.18)}$$

Furthermore, as discussed in the text, the input current was assumed to be half-wave rectified, that is to say for

$$x_{nerve} \quad < \quad 0 \qquad \text{(B.19)}$$

$$\Rightarrow I_{in} \quad = \quad 0 \qquad \text{(B.20)}$$

B.1.2 Modified Model

For the modified mechanoreceptor models (Section 4.3) we decreased the rate parameters of Equations B.3-B.5 by a factor of approximately 6 to produce more realistic firing rates for the receptors (see Section 4.3.2). No adjustments were made for temperature as this would only contribute a scaling factor which we would have to adjust to again obtain realistic firing rates.

B.2 Mechanical Components of the Modified Models

B.2.1 SA Unit: Mechanical Component

The transfer function of the mechanical component of the modified SA model given in Section 4.3.1 is given by

$$\frac{X_{out}}{X_{in}} = \frac{K_s[K_e + sb_e]}{sb_e(K_s + K_n) + K_e K_n + K_s K_e + K_s K_n} \qquad \text{(B.21)}$$

where,

K_s = combined stiffness of the skin and subcutaneous tissue

K_e = stiffness of the end organ

K_n = stiffness of the nerve fiber

b_e = damping of the end organ.

This can be simplified to

$$\frac{X_{out}}{X_{in}} = \frac{M(s + z)}{(s + p)} \qquad \text{(B.22)}$$

which can be simulated by

$$\frac{dx_{out}}{dt} = M\frac{dx_{in}}{dt} + Mzx_{in} - px_{out}. \qquad \text{(B.23)}$$

For the displacement input, $A(1 - cos(wt))$, the initial condition is

$$x_{out} = 0. \qquad \text{(B.24)}$$

For the ramp and hold input, the initial condition is also

$$x_{out} = 0. \qquad \text{(B.25)}$$

The correctness of the implementation was verified by examining the response of the simulation of this component in isolation and comparing it to analytical results.

B.2.2 FA Unit: Mechanical Component

The transfer function of the mechanical component of the modified FA model given in Section 4.3.1 is given by

$$\frac{X_{out}}{X_{in}} = \tag{B.26}$$

$$\frac{K_s(K_{e2}+sb_{e2})(K_{e1}+sb_{e1})}{K_s[(K_{e2}+sb_{e2})(K_n+K_{e1}+sb_{e1})+K_n(K_{e1}+sb_{e1})]+K_n(K_{e2}+sb_{e2})(K_{e1}+sb_{e1})} \tag{B.27}$$

where,

K_s = combined stiffness of the skin and subcutaneous tissue

K_{e1} = stiffness of part of the end organ

K_{e2} = stiffness of part of the end organ

K_n = stiffness of the nerve fiber

b_{e1} = damping of part of the end organ

b_{e2} = damping of part of the end organ.

This can be simplified to

$$\frac{X_{out}}{X_{in}} = \frac{M(s+z_1)(s+z_2)}{(s+p_1)(s+p_2)} \tag{B.28}$$

which can be simulated by

$$\frac{dx_{out}}{dt} = M(\frac{d^2x_{in}}{dt^2} + (z_1+z_2)\frac{dx_{in}}{dt} + (z_1z_2)x_{in}) - (p_1+p_2)\frac{dx_{out}}{dt} + p_1p_2x_{out} \tag{B.29}$$

For the input $A(1 - cos(wt))$, the initial conditions are

$$x_{out} = 0 \qquad \text{(B.30)}$$

$$\frac{dx_{out}}{dt} = 0. \qquad \text{(B.31)}$$

For the ramp and hold input, the initial conditions are

$$x_{out} = 0 \qquad \text{(B.32)}$$

$$\frac{dx_{out}}{dt} = \frac{Mv}{1000.0} \qquad \text{(B.33)}$$

where v is the velocity of the ramp.

The correctness of the implementation was verified by examining the response of the simulation of this component in isolation and comparing it to analytical results.

Bibliography

[1] K.E. Atkinson. *An Introduction To Numerical Analysis*. John Wiley and Sons, 1989.

[2] J. Bell and M. Holmes. Model of the dynamics of receptor potential in a mechanoreceptor. *Mathematical Biosciences*, 110:139–174, 1992.

[3] J. Bell and M.H. Holmes. A note on modeling mechano-chemical transduction with an application to a skin receptor. *Journal of Mathematical Biology*, 32:275–285, 1994.

[4] J.C. Cohen, J.C. Maous, B.W. Pietras, and S.J. Boanowski. Do the stimulator and skin decouple under sinusoidal vibrations? Abstracts of the Society for Neuroscience Annual Meeting, 1996.

[5] J.A. Connor, D. Walkter, and R. McKown. Neural repetitive firing. modifications of the hodgkin-huxley axon suggested by experimental results from crustacean axons. *Biophysical Journal*, 18:81–102, 1977.

[6] K. Dandekar. *Role of Mechanics in Tactile Sensing of Shape*. PhD thesis, MIT, 1995.

[7] C.L. Van Doren. *Measurement and Modelling of Spatiotemporal Tactile Sensitivity*. PhD thesis, Syracuse University, 1987.

[8] C. Erxleben. Stretch-activated current through single ion channels in the abdominal stretch receptor organ of the crayfish. *J. Gen. Physiol.*, 94:1071–1083, 1989.

[9] R.S. Fearing. Tactile sensing mechanisms. *International Journal of Robotics Research*, 9:3–23, 1990.

[10] A.W. Freeman and K.O. Johnson. Cutaneous mechanoreceptors in macaque monkey: Temporal discharge patterns evoked by vibration, and a receptor model. *J. Physiology*, 323:21–41, 1982.

[11] A.W. Freeman and K.O. Johnson. A model accounting for effects of vibratory amplitude on responses of cutaneous mechanoreceptors in macaque monkey. *J. Physiology*, 323:43–64, 1982.

[12] Y.C. Fung. *Biomechanics: Mechanical Properties of Living Tissue*. Springer-Verlag, New York, 1993.

[13] A.W. Goodwin, A.S. Browning, and H.E. Wheat. Representation of curved surfaces in responses of mechanoreceptive afferent fibers innervating the monkey's fingerpad. *The Journal of Neuroscience*, 15:798-810, 1995.

[14] F. Grandori and A. Pedotti. A mathematical model of the pacinian corpuscle. *Biol. Cybern.*, 46:7-16, 1982.

[15] R.J. Gulati. Determination of mechanical properties of the human fingerpad in vivo, using a tactile stimulator. Master's thesis, Boston University, 1995.

[16] R.J. Gulati and M.A. Srinivasan. Human fingerpad under indentation i: Static and dynamic force response. In *ASME Bioengineering Conference*, volume BED-29, 1995.

[17] A.Z. Hajian and R.D. Howe. Identification of the mechanical impedance at the human finger tip. *ASME Journal of Biomechanical Engineering*, 119:109-114, 1997.

[18] B. Hille. *Ionic Channels of Excitable Membranes*. Sinauer Associates Inc., 1992.

[19] A.L. Hodgkin and A.F. Huxley. A quantitative description of membrane current and its application to conduction and excitation in nerve. *J. Physiology*, 117:500-544, 1952.

[20] J. Howard, W.M. Roberts, and A.J. Hudspeth. Mechanical transduction by hair cells. *Annual Review of Biophysics and Biophysical Chemistry*, 17:99-124, 1988.

[21] R.D. Howe and M.R. Cutkosky. Touch sensing for robotic manipulation and recognition. In O. Khatib, J.J. Craig, and T. Lozano-Perez, editors, *The Robotics Review 2*. MIT Press, 1992.

[22] R.D. Howe and M.R. Cutkosky. Practical force-motion models for sliding manipuation. *International Journal of Robotics Research*, 15:557-572, 1996.

[23] A. Iggo and A.R. Muir. The structure and function of a slowly adapting touch corpuscle in hairy skin. *J. Physiology*, 200:763-796, 1969.

[24] O.B. Ilyinsky, N.K. Volkova, V.L. Cherepnov, and B.V. Krylov. Morphofunctional properties of pacinian corpuscles.

[25] R.S. Johansson. Personal communication, 1997.

[26] R.S. Johansson, U. Landström, and Lundström. Response of mechanoreceptive afferent units in the glabrous skin of the humand hnad to sinusoidal skin displacements. *Brain Research*, 244:17-25, 1982.

[27] R.S. Johansson and A.B. Vallbo. Tactile sensory coding in the glabrous skin of the human hand. *TINS*, pages 27-32, 1983.

[28] R.S. Johansson and G. Westling. Roles of glabrous skin receptors and sensorimotor memory in automatic control of precision grip when lifting rougher or more slippery objects. *Experimental Brain Research*, 56:550-564, 1984.

[29] K.L. Johnson. *Contact Mechanics*. Cambridge University Press, Great Britain, 1985.

[30] K.O. Johnson, J.R. Phillips, and A.W. Freeman. Mechanisms underlying the spatiotemporal response properties of cutaneous mechanoreceptive afferents. In *Development, Organization and Processing in Somatosensory Pathways*. Alan R. Liss, Inc., 1985.

[31] Y. Lanir, S. Dikstein, A. Hartzshtark, and V. Manny. In-vivo indentation of human skin. *Journal of Biomechanical Engineering*, 112:63–69, 1990.

[32] Y. Lanir and Y.C. Fung. Two-dimension mechanical properties of rabbit skin i. experimental results. *Journal of Biomechanics*, 7:171–182, 1974.

[33] S.J. Lederman and R.A. Browse. The physiology and psychophysics of touch. In P. Dario, editor, *Sensors and Sensory Systems for Advanced Robots*. Springer-Verlag, 1988.

[34] W.R. Loewenstein. Mechano-electric transduction in the pacinian corpuscle. initiation of sensory impulses in mechanoreceptors. In *Handbook of Sensory Phsiology, Vol I. Principles of Receptor Physiology*. Springer-Verlag, 1971.

[35] R. Lundström. Local vibrations - mechanical impedance of the human hand's glabrous skin. *Journal of Biomechanics*, 17:137–144, 1984.

[36] J.F.M. Manschot and A.J.M Brakee. The measurement and modelling of the mechanical properties of human skin in vivo i. the measurement. *Journal of Biomechanics*, 19:511–516, 1986.

[37] J.F.M. Manschot and A.J.M Brakee. The measurement and modelling of the mechanical properties of human skin in vivo ii. the measurement. *Journal of Biomechanics*, 19:517–521, 1986.

[38] L. Moss-Salentijn. The human tactile system. In H.R Nicholls, editor, *Advanced Tactile Sensing for Robotics*. World Scientific, 1992.

[39] I. Nemoto, S. Miyazaki, M. Saito, and T. Utsunomiya. Behavior of solutions of the hodgkin-huxley equations and its relation to properties of mechanoreceptors. *Biophysicial Journal*, 15:469–479, 1975.

[40] D.T.V. Pawluk, W.J. Peine, P.S. Wellman, and R.D. Howe. Simulating soft tissue with a tactile shape display. Submitted to IMECE97, November 1997.

[41] W.J. Peine. Personal communication, 1997.

[42] W.J. Peine, D.A. Kontarinis, and R.D. Howe. A tactile sensing and display system for surgical applications. In R.M. Satava et al., editor, *Interactive Technology and the New Paradigm for Healthcare*. IOS Press, 1995.

[43] J.R. Phillips and K.O. Johnson. Tactile spatial resolution iii. a continuum mechanics model of skin predicting mechanoreceptor responses to bars, edges, and gratings. *J. Neurohysiology*, 46:1204–1225, 1981.

[44] W.H. Press, B.P. Flannery, S.A. Teukolsky, and W.T. Vetterling. *Numerical Recipes in C*. Cambridge University Press, 1989.

[45] F. Sachs. Mechanical transduction in biological systems. *CRC Critical Reviews in Biomedical Engineering*, 16:141–169, 1988.

[46] E. Serina and D. Rempel. Stiffness of *in vitro* fingertip soft tissue in compression. In *Second World Congress of Biomechanics*, Amsterdam, The Netherlands, July 1994.

[47] E.R. Serina. *Characterization and Modeling of the Fingertip Pulp Under Repeated Loading*. PhD thesis, University of California, Berkeley, 1996.

[48] E.R. Serina, Jr. C.D. Mote, and D.M. Rempel. Mechanical properties of the fingertip pulp under repeated, dynamic, compressive loading. In *ASME Winter Annual Meeting*, 1995.

[49] E.R. Serina and D.M. Rempel. Fingertip pulp response during keystrikes. In *ASB Conference*, Atlanta, 1996.

[50] M.A. Srinivasan. Surface deflection of primate fingertip under line load. *Journal of Biomechanics*, 22:343–349, 1989.

[51] R.B. Stein. The frequency of nerve action ptentials generated by applied currents. *Proc. Royal Society of London B.*, 167:64–86, 1967.

[52] D.E. Thompson, H.Mg. Hussein, and R.Q. Perritt. Point impedance characterization of soft tissues in vivo. In R. Marks and P.A. Payne, editors, *Bioengineering and the Skin*. MTP Press, 1981.

[53] P. Tong and Y.C. Fung. The stress-strain relationship for the skin. *Journal of Biomechanics*, 9:649–657, 1976.

[54] G. Westling and R.S. Johansson. Responses of glabrous skin mechanoreceptors during precision grip in humans. *Experimental Brain Research*, 66:128–140, 1987.

[55] S.L.-Y. Woo. Biomechanics of tendons and ligaments. In S.L.-Y. Woo G.W. Schmid-Schönbein and B.W. Zweifach, editors, *Frontiers in Biomechanics*. Springer-Verlag, 1986.